Advances in Civil Engineering

Employing Smart Power Generation in Buildings

Lead Guest Editor: Aritra Ghosh
Guest Editors: Dong Li and Padmanaban Sanjeevikumar

Employing Smart Power Generation in Buildings

Advances in Civil Engineering

Employing Smart Power Generation in Buildings

Lead Guest Editor: Aritra Ghosh
Guest Editors: Dong Li and Padmanaban Sanjeevikumar

Contents

A New Environmentally Friendly Utilization of Energy Piles into Geotechnical Engineering in Northern China
Jianguo Peng, Qingwen Li, and Chungho Huang
Review Article (13 pages), Article ID 4689062, Volume 2021 (2021)

Research on Photovoltaic Grid-Connected Control Strategy Based on Active Disturbance Rejection of Adaptive Extended State Observer
Dejun Liu, Jinfei Xu, Ruonan Xue, Chao Song, and Zhenxiong Zhou
Research Article (9 pages), Article ID 9241867, Volume 2021 (2021)

A Systematic Review on Indoor Environmental Quality in Naturally Ventilated School Classrooms: A Way Forward
Nishant Raj Kapoor, Ashok Kumar, Chandan Swaroop Meena, Anuj Kumar, Tabish Alam, Nagesh Babu Balam, and Aritra Ghosh
Review Article (19 pages), Article ID 8851685, Volume 2021 (2021)

Thermal Behaviour Analysis and Cost-Saving Opportunities of PCM-Integrated Terracotta Brick Buildings
A. Chelliah, Shaik Saboor, Aritra Ghosh, and Karolos J. Kontoleon
Research Article (15 pages), Article ID 6670930, Volume 2021 (2021)

Energy and Daylighting Evaluation of Integrated Semitransparent Photovoltaic Windows with Internal Light Shelves in Open-Office Buildings
Abdelhakim Mesloub, Artira Ghosh, Ghazy Abdullah Albaqawy, Emad Noaime, and Badr M Alsolami
Research Article (21 pages), Article ID 8867558, Volume 2020 (2020)

Hindawi
Advances in Civil Engineering
Volume 2021, Article ID 4689062, 13 pages
https://doi.org/10.1155/2021/4689062

Review Article

A New Environmentally Friendly Utilization of Energy Piles into Geotechnical Engineering in Northern China

Jianguo Peng,[1] Qingwen Li ,[1] and Chungho Huang [2]

[1]*Department of Civil Engineering, University of Science and Technology Beijing, Beijing 100083, China*
[2]*Department of Civil Engineering, National Taipei University of Technology, Taipei 10608, Taiwan*

Correspondence should be addressed to Qingwen Li; qingwenli@ustb.edu.cn and Chungho Huang; cdewsx.hch@gmail.com

Received 18 August 2021; Revised 17 October 2021; Accepted 23 October 2021; Published 23 November 2021

Academic Editor: Dong Li

In the past 30 years, because of built-in advantages, energy saving, pollution control, and sustainability, the energy pile system has had a rapid development around the world. Many scholars did numerous researches on the parameters' optimization, heat exchange efficiency, and structure-soil response. Also, the researches of evolutional GSHP system using high temperature in deep mine and lager collection surface of tunnel lining were learned. At present, most of researchers are discussing the geothermal collection for the heating or cooling the building, and plenteous and significant research achievements have been obtained. It is a novel attempt to apply energy pile to geotechnical engineering, and good results have been achieved in engineering practice in Northern China. The area of northern China is a typical seasonal frozen region: the high temperature in summer and the cold weather and accumulated snow in winter will result in huge challenge and resource consumption of maintaince on highway tunnel, pavement, and other geotechnical engineering facilities. In this paper, taking example of using the geothermal heat exchanger to melt snow, the novel idea of using energy piles to prevent track in summer and crack in winter of pavement, and guaranteeing the safety of frost crack on tunnel lining were discussed. Also, through simulation research, we propose a buried pipe form with good heat transfer uniformity-spiral buried pipe, which has better engineering applicability. This shows us that the application of energy pile in geotechnical engineering will provide solutions to geotechnical problems, which will have a brilliant future.

1. Introduction

In the background of the global energy crisis, energy pile is a form of green and sustainable energy utilization, or one of the solutions to energy problems. At present, a large number of scholars have conducted scientific research on energy piles and formed a large number of research results.

1.1. The Development of Energy Pile. At present, the coal, petroleum, natural gas, and other nonrenewable energy forms are consumed rapidly, and energy crisis has become a worldwide problem. Due to the more unreasonable energy structure, this problem is more serious in China. Meanwhile, in order to realize the social sustainable development, harmonious development between the energy exploitation and environmental protection and ecological balance are required. So far, the clean energy system and energy-saving system are becoming the direction of the world's energy development strategy. And as everyone knows, comparing with the air temperature, the soil temperature is more stable the whole year, and the changing of soil temperature with depth in Beijing area is shown in Figure 1. As it can be seen, when the soil temperature is within 6 m, the monthly temperature dispersion of soil is very large. When the soil depth exceeds 6 m, the monthly temperature of the soil tends to be close to 18°C. In the 1980s, considering the stable temperature characteristic of soil, geotechnical engineers in Austria and Switzerland creatively utilized building foundations (concrete pile [1], CFG pile [2], and underground diaphragm [3–5]) placed by the heat exchanger, to process the heat exchange between fundamental components and its host soil. This new geotechnical structure, which can achieve the function of heat complementation between summer and

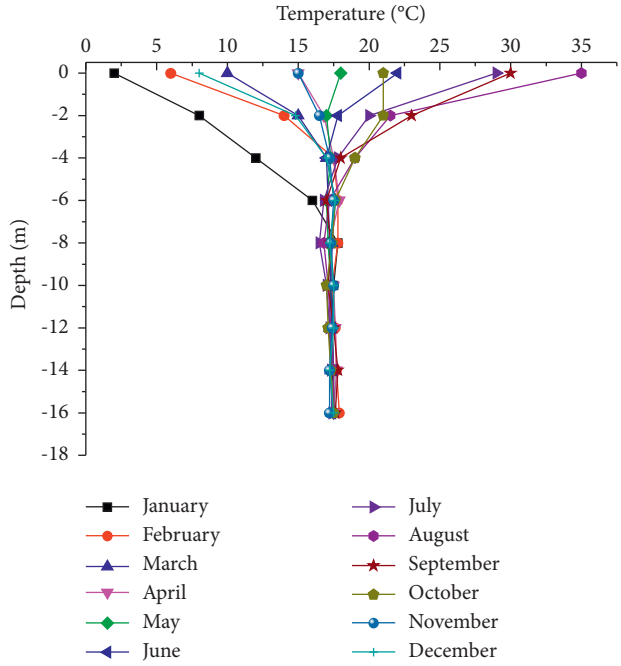

Figure 1: Change rule of soil temperature along with the depth.

winter, is the energy pile system. It is due to the preferable heat conduction properties of concrete and larger heat exchange surface of foundation structure that the energy pile has the better heat exchange efficiency than the traditional geothermal heat exchanger. Research results showed that the energy pile system could save more than 30% energy than air conditioning system. Meanwhile, the heat exchanger pipe is surrounded closely by pile foundation, the stability and durability could be guaranteed, and the cost of energy pile is also much lower than the traditional geothermal heat exchange system. Because of the built-in advantages, the energy pile system has achieved fast development around the world.

1.2. Research Status of Energy Pile System. In the interest of improving the heat exchange efficiency, many scholars did numerous researches on the parameters' optimization. Bozis et al. evaluated the effects of design parameters on the heat transfer efficiency and developed a methodology for comparative estimation of design alternatives of cast-in-place of energy piles [6]. Bandos et al. presented a finite cylinder-source model for simulating the energy pile heat exchangers and studied the effects of thermal storage and vertical temperature variations [7]. Moon and Choi contrastively analyzed the heating performance characteristics of the ground-source heat pump system with energy piles and energy slabs [8]. In addition, there are also many other scholars who did the parameters' optimization to improve the heat exchange efficiency [9–12]. Meanwhile, a number of scholars have already did research on the thermal performance of different coil types, and the research achievements were listed in Table 1.

As shown in Table 1, the latest studies show that spiral coil with the largest heat exchange surface of the fluid tube is the optimal type of heat exchanger cast-in-place energy pile. For the thermal efficiency analysis results, the spiral coils type has the best heating and cooling performance, accounting for near 150% thermal efficiency compared to double U type [25].

Usually, concrete energy pile systems are comprised of exchange fluid, metal pipe, concrete, and host soil, and the structural diagram is exhibited in Figure 2 [27]. It is easy to know that the thermal parameters of heat exchange medium (mainly concrete and soil) would be the important impact factor of thermal efficiency. So, many scholars begin to research the backfill material with high thermal parameters for replacing the soils with lower thermal parameters. Delaleux et al. adopted the bentonite-graphite composites as the backfill material to enhance the geothermal borehole heat exchangers performances [28]. Coccia et al. considered municipal solid waste landfills as a potential source of heat for GSHP (Ground-Source Heat Pumps) [29]. Indacoechea-Vega et al. analyzed the different behaviors of different grouting materials (bentonite-based grouts and cement-based grouts) for GSHP, by contrastively proceeding the thermal conductivity, water/solid ratios, permeability, mechanical strength, and other tests [30]. Ocłoń et al. simulated the heat dissipation processes in underground power cable system situated in thermal backfill and buried in a multilayered soil [31]. Li et al. researched the heat transfer performance of the U-tube heat exchangers with different backfill materials (shape-stabilized phase change materials and crushed stone concrete) [32]. To achieve improvement of the heat exchange efficiency, scholars have discussed the parameters' optimization, types of heat exchangers cast-in-place energy piles, and the backfill material with high

Table 1: Research achievements on different types of heat exchangers cast-in-place energy piles.

Reference	U-shaped	Double U-shaped	Triple U-shaped	W-shaped	Double W-shaped	Spiral type
Park et al. [13]						★
Zarrella et al. [14]			▼			★
Go et al. [15]						★
Zhang et al. [16]						★
Xiang et al. [17]						★
Go et al. [18]						★
Lee et al. [19]						★
Yoon et al. [20]				◆		★
Wang et al. [21]						★
Wang et al. [22]						★
Park et al. [23]						★
Zhao et al. [24]	■			◆		★
Luo et al. [25]		▲	▼		●	★
Zarrella et al. [26]	■					

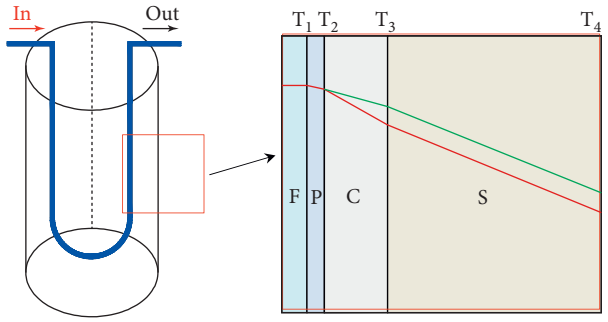

Figure 2: Energy pile with U tube and its heat transfer medium diagram.

thermal parameters. A series of mature and applicable achievements were obtained.

For the energy pile, it is not only a heat-exchanging system, but also a foundation structure, so it should meet the double requirement of heat exchanging and supporting. The research on different mechanical property of pile under the cyclic action of cooling and heating is necessary. Suryatriyastuti et al. studied the the temperature-induced mechanical behavior of energy pile foundations [33]. Park et al. evaluated the thermal response and performance of precast-high strength concrete energy pile by taking results of field experiments and numerical simulation [34]. Besides, there are also abundant researches on structural response between pile and soil [35–44]. For the group of energy piles, scholars and professionals in many countries also did the corresponding research on the multiple interaction [45–47] and mechanical response [48–51]. By studying the above references, plenteous and significant achievements on the research of energy pile system were realized, and it has been widely used in green energy-saving buildings in China, European countries, Canada, Japan, and other countries.

2. Evolutional GSHP System Use with Geotechnical Engineering Structure

2.1. Geothermal Heat Extraction from Mines. With the development of mining depth, the high temperature problem is becoming more and more serious. In China, the temperature in working faces at more than 700 m mining depth are mostly larger than 35°C, the highest temperature is near 50°C, and the typical rock temperatures of deep mine are listed in Table 2.

It is easy to know that the working environment under high temperature not only has an effect on the mechanical property of host rock but also inflicts harm to the body health of worker. The high temperature environment would reduce their ability of attention and reaction; sometimes, these effects may lead to real accidents. According to the surveyed data by the former Soviet Union and Germany, the labor productivity will decline by 6%~8% when the working temperature is 1°C out of limit [52]. Based on the surveyed data of 7 mines in Hokkaido, Japan, the results show that the accident rate at working face under 37°C is 2.13 times that under 30°C [53]. So it is very important to research the technique of high temperature control and cooling. And many scholars have done some research on how to cool deep mine heat. He et al. adopted a high temperature exchange machinery system (HEMS) to cool the high temperature and control heat hazard in deep coal mines [54]. Plessis et al. analyzed the variable speed drives for cost-effective energy savings in South African mine cooling systems and found that an annual cost saving of USD 6,938,148 and CO_2 emissions reduction of 132 M ton are possible [55], and they further researched the development and integrated simulation of a variable water flow energy-saving strategy for deep mine cooling systems at 2015 [56]. Apel et al. simulated the effects of thermal insulating shotcrete on the energy consumption of ventilation and cooling systems at deep underground mines [57]. Chen et al. proposed a split-type vapor compression refrigerator for heat hazard control in deep mines [58]. With the developing and improving of the studying about heat hazard in deep mines, some people have realized that the high temperature is also an energy source and also can be utilized. Guo et al. used the HEMS technique to control the heat harm in Jiahe coal mine (Hunan province, China) and extracted the deep geothermal energy to replace the ground fired boiler for heating [59]. Ghoreishi-Madiseh and Abbasy did the numerical and experimental study of geothermal heat extraction from backfilled mine

Table 2: Rock temperatures of deep mine in Northern China.

Mines	Geographical location	Measuring depth (m)	Rock temperature (°C)
Dataigou iron mine	Liaoning province	1250	41.4~43.0
Linglong Gold mine	Shandong province	1095	42.0~44.0
Lingnan Gold mine	Shandong province	975	40.0
Xiadian Gold mine	Shandong province	850	35.2
Sanshandao Gold mine	Shandong province	825	38.5
Xincheng Gold mine	Shandong province	760	37.0~38.0

stopes [60]. Furthermore, Ramos et al. discussed the feasibility of using abandoned mines for geothermal heat recovery [61]. Guo et al. present a geothermal recycling system for parallel mine, where the collected heat can be used to supply heat for buildings and domestic hot water [62]. The schematic diagram of geothermal heat extraction from mines is shown in Figure 3. Driven by the circulation system, the heat exchange fluid circulates inside the mine, fully contacts the surrounding high temperature rock and soil, and extracts the heat for ground buildings.

2.2. Geothermal Heat Collection from Tunnel (Energy Tunnel). To extract the heat from mine is utilization of deeper geothermal resource, and for the shallow geothermal resource utilization, the researchers have noticed the tunnel. Mimouni and Laloui estimated the geothermal potential of heat exchanger anchors on a cut-and-cover tunnel, and the numerical simulation results showed that the extractable heat from the ground through the anchors ranges from 0.4 to 0.8 GWh per year and per kilometer of tunnel [63]. Barla et al. discussed the application of energy tunnels to an urban environment and investigated the possibility of thermal activation of a new section underground construction of the Metro Torino line 1 (Italy) to heat and cool adjacent buildings [64]. Lee et al. introduced development of energy textile to use geothermal energy in tunnels and conducted a test bed of six pilot energy textile modules with various configurations in an abandoned railroad tunnel in South Korea [65]. Buhmann et al. summarized the German experience with renewable energy concepts in tunnel projects [66]. López et al. evaluated energy consumption and sustainability of road tunnels [67]. The typical tunnel lining was equipped as ground heat exchanger as shown in Figure 4. Through the pipeline buried on the lining surface, the heat on the tunnel surface is collected to the heat collecting pipe to realize the efficient utilization of geothermal energy.

3. Geothermal Energy Resources in Northern China

China has rich geothermal resources accounting for 8% of total global geothermal energy reserve [68]. The distribution of geothermal resources in China was consulted as shown in Figure 5.

As shown in Figure 5, the main distribution of geothermal resources is in Northern China, including the Songliao Basin, Erlian Basin, North Basin, Ordos Basin, Qaidam Basin, and Tarim Basin. The shallow geothermal resource, which can be utilized by the energy piles, is also very abundant. According to the shallow depth data (within 200 m) provided by China Geological Survey, an evaluation on the shallow geothermal resources of 16 provinces in Northern China was performed [70, 71]. The shallow geothermal energy data in Northern China are listed in Table 3. It is easy to learn that the shallow geothermal resources in Northern China (16 calculated provinces) are about 31.32×10^{12} kWh, equal to 3752 million tons of standard coal. Considering the available shallow geothermal resource, the value is more than 1.17×10^{12} kWh, equal to 145 million tons of standard coal.

4. Energy Piles Utilized in Geotechnical Engineering

When solving geotechnical engineering problems, the traditional engineering technical measures have the characteristics of high pollution and high energy consumption. Under the background of carbon peak, carbon neutralization and green industrial revolution, huge green and clean geothermal energy reserves, and the great development of energy pile technology in the world, energy pile has been vigorously promoted and applied in Northern China. Combined with the geographical characteristics of seasonal freezing area in Northern China, specific application forms have been developed, such as snow melting and deicing, realization of wide temperature range of asphalt concrete pavement, and prevention and control of frost heave and frost crack of tunnel inlet and outlet lining.

In the northern China, there is a huge distance of air temperature between winter and summer; the daily variation of four seasons' temperature in Beijing area is shown in Figure 6. According to the Köppen classification, the climate types in Northern China are mainly Dwb (cold dry winter, warm summer) and Bsk (arid steppe, cold). In the past 30 years, the climate types in North China have changed significantly [72–74], which is of great value in the utilization of geothermal energy.

As shown in Figure 6, Beijing area is a typical seasonal frozen region in China, where the lowest air temperature in winter is about −15°C, the highest temperature in summer can reach more than 35°C, and the cold weather and accumulated snow in winter and the high temperature in summer will result in huge challenge and resource consumption of maintaince on highway tunnels, pavements, and other geotechnical engineering facilities.

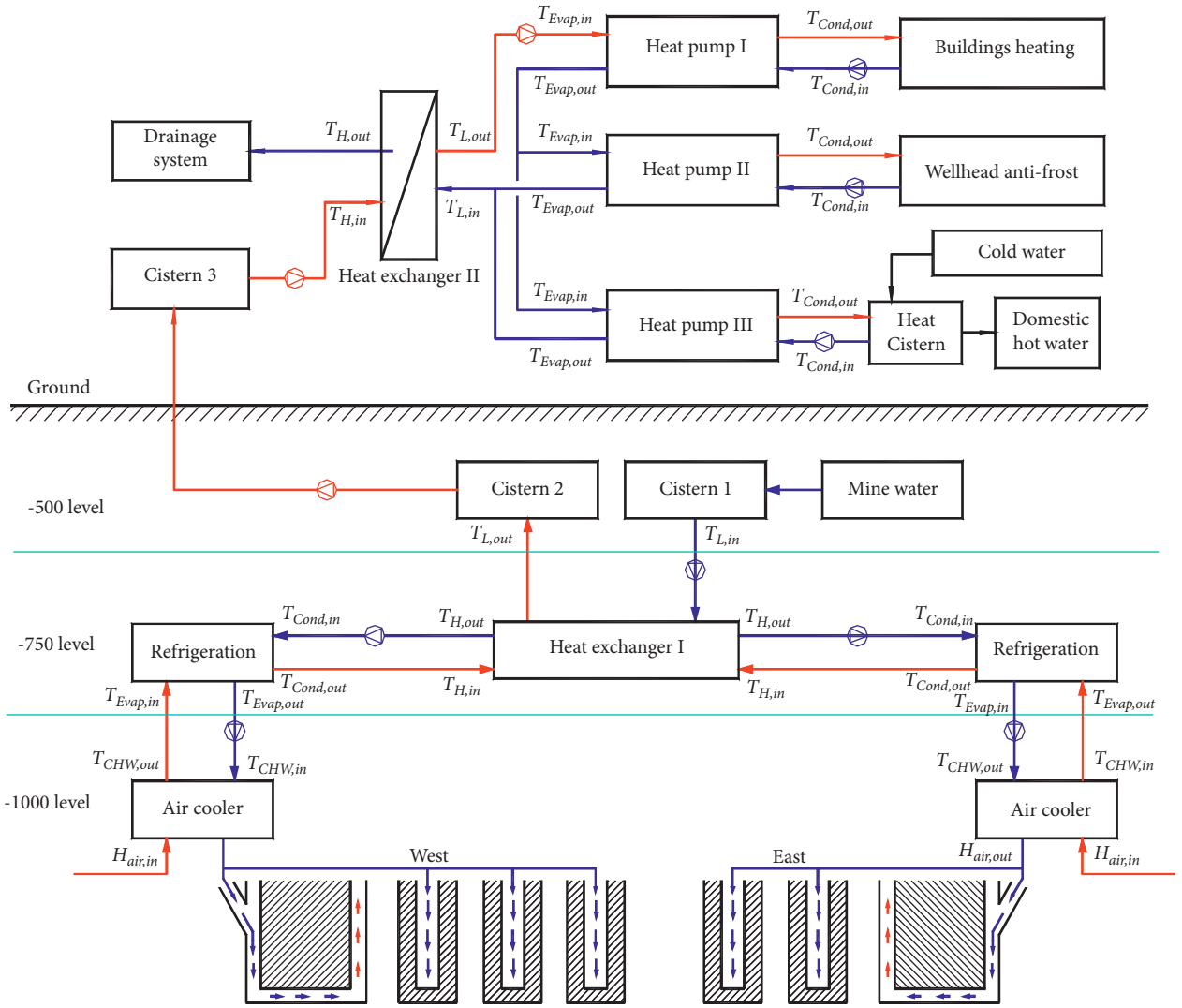

Figure 3: The schematic diagram of geothermal heat extraction in the Zhang Shuang-lou Mine [62].

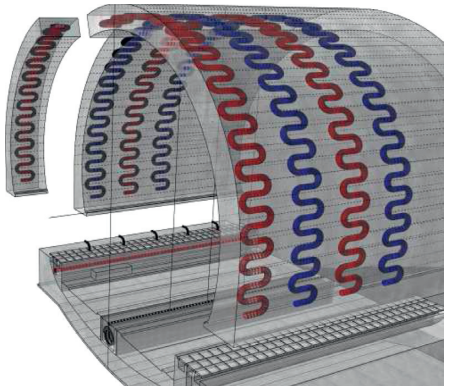

Figure 4: Schematic representation of a segmental tunnel lining equipped as heat exchanger [64].

4.1. GSHP System Used for Melting Snow. In Northern China, the continuous low temperature may bring about the accumulated snow for several months; usually, the pavement is icy. This accumulated snow and ice would cause the huge hidden danger for the motion of the vehicle safety. Now, for the snow and ice melting, numerous methods were proposed by scholars. All the common methods could be classified as chemical snow melting method and physical snow melting method. The chemical method uses salt-storage aggregates [75], sodium chloride [76], and other chemicals to melt the snow and ice on pavement; however, chemicals usually have a negative impact on the surround environment, and it is corrosive to vehicles and roadside structures. The physical method is utilization of natural heat or generated heat by employing a conductive asphalt solar collector [77], carbon fiber grille [78], copper plates [79], heating films [80], and electric heating pipes [81, 82], to remove the accumulated snow and ice. Although the above introduced methods could melt snow effectively, the low efficiency or huge electric energy consumption always restricts their wide application. With the development of GSHP system, some scholars have begun to study its practicability in melting of accumulated snow on pavement. Pan et al. summarized a review on hydronic asphalt pavement for energy harvesting and snow melting [83]. Yildirim and Hepbasli analyzed the

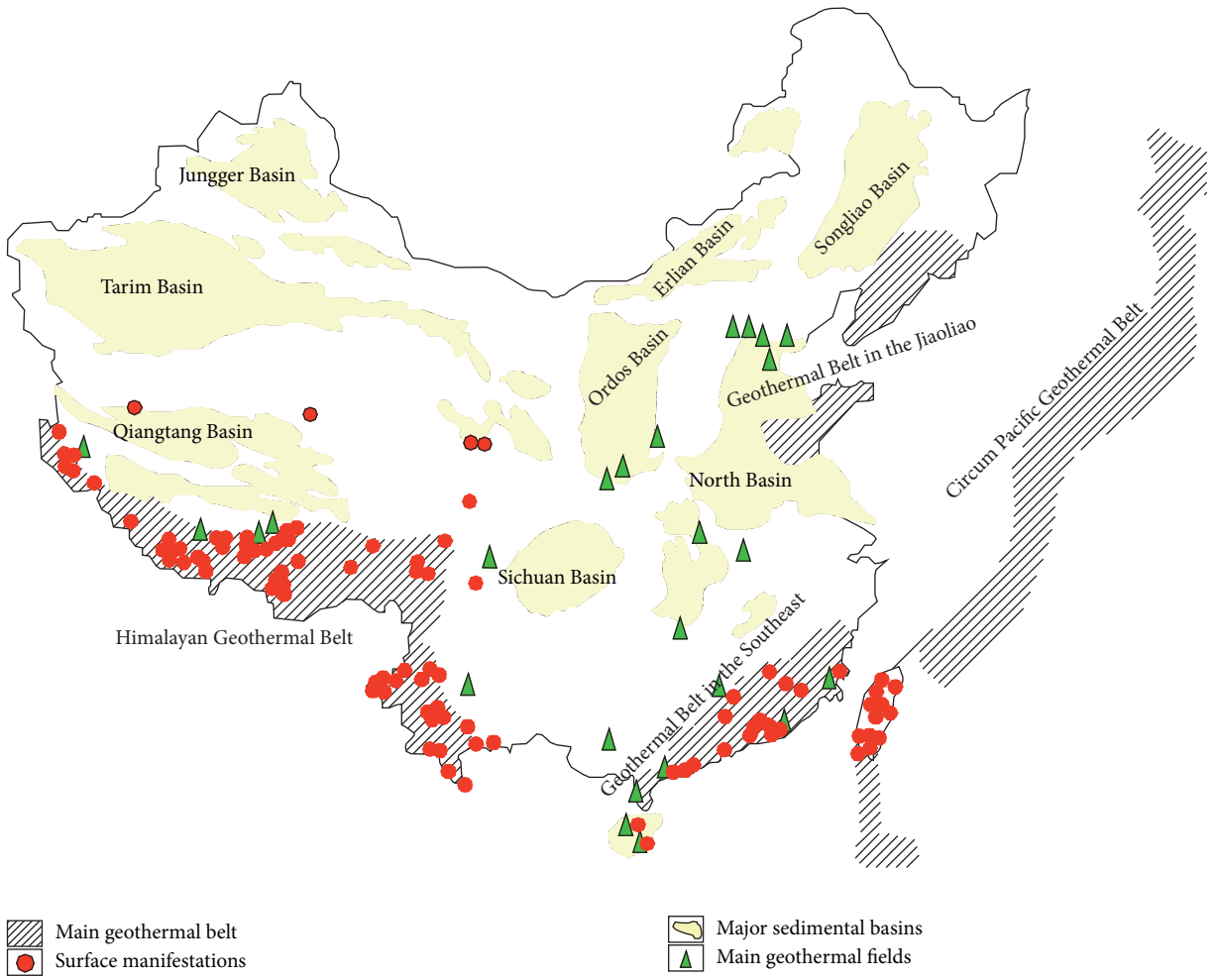

Figure 5: The geothermal resources distribution in China [69].

Table 3: Evaluation of the shallow geothermal resources in Northern China [71].

No.	Province or city	Total resource capacity		Available resource capacity		Benefit
		$\times 10^{12}$ kWh	Standard coal (Mt)	$\times 10^{9}$ kWh	Standard coal (Mt)	Reduction of CO_2 (Mt)
1	Heilongjiang	3.31	407	124	15	0.40
2	Jilin	1.84	226	69.1	9	0.22
3	Liaoning	3.30	406	124	15	0.40
4	Hebei	2.32	285	87.0	11	0.28
5	Beijing	3.01	270	113	14	0.36
6	Tianjin	1.75	215	65.6	8	0.21
7	Inner Mongolia	1.80	221	67.7	8	0.22
8	Shanxi	1.67	205	62.7	8	0.20
9	Shandong	3.47	427	130	16	0.42
10	Henan	3.45	424	129	16	0.42
11	Shanxi	2.24	276	84.2	10	0.27
12	Ningxia	0.974	120	36.5	4	0.12
13	Gansu	1.21	149	45.5	6	0.15
14	Qinghai	0.16	20	6.00	1	0.02
15	Xinjiang	0.486	60	18.2	2	0.06
16	Tibet	0.330	41	12.4	2	0.04
Total in Northern China		31.32	3752	1174.9	145	3.79

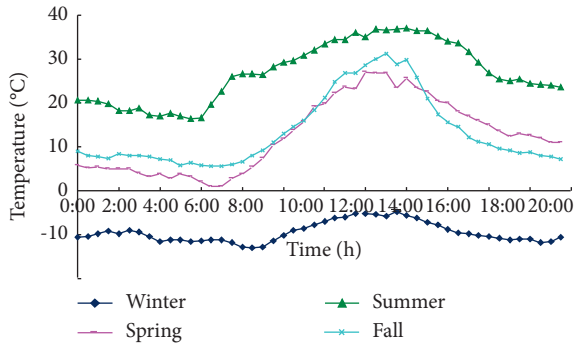

Figure 6: Daily variation of four seasons' temperature in Beijing area.

performance of snow melting using a GSHP system [84]. Xu and Tan simulated the pavement snow melting systems utilizing low temperature heating fluids [85]. Han and Yu discussed the feasibility of geothermal heat exchanger pile-based bridge deck snow melting system [86]. Wang et al. performed the thermal analysis and optimization of an ice and snow melting system using geothermal energy by superlong flexible heat pipes [87].

4.2. Guaranteeing Pavement Safety Using Energy Piles. The pavement asphalt is one of temperature sensitive materials; it will have different mechanical properties under different outer circumstance temperatures. In some regions of Northern China, due to the heat-trapping property of asphalt, the surface temperature of pavement can reach 50°C in summer, but this value is only −15°C in winter, and the temperature difference can reach 65°C. Researches show that dynamic modulus will reduce from 12,000 MPa to 100 MPa under 0.01 frequency when the environment temperature rises from −20°C to 54°C [88], as it can be seen in Figure 7. Hence, the contradictory issues between track in summer and crack of pavement asphalt in winter are especially serious, as shown in Figures 8 and 9, respectively.

For the purpose of dealing with the above contradictory problems, the traditional solving method is striving to develop wide temperature range asphalt material [89–92]. Although many efforts have been done, most of researches could solve the low temperature crack [93] and high temperature track [94] very well separately. It is really difficult to solve these contradictory problems uniformly. In the face of this bottleneck, the other new approach could be explored. Proceeding from that, taking example of GSHP system used for melting snow, and comprehensively considering mature and practical technique and higher thermal efficiency of energy pile and rich shallow geothermal resource in Northern China area, it is possible to implement the energy pile into roadbed structure, to solve the seasonal temperature-induced contradictory problems on pavement. The working schematic diagram of energy piles roadbed is shown in Figure 10. The temperature of the circulating liquid is increased through the vertical solenoid and then flows through the horizontal buried pipe to heat the road surface, so as to improve the road temperature and melt the snow in the road area.

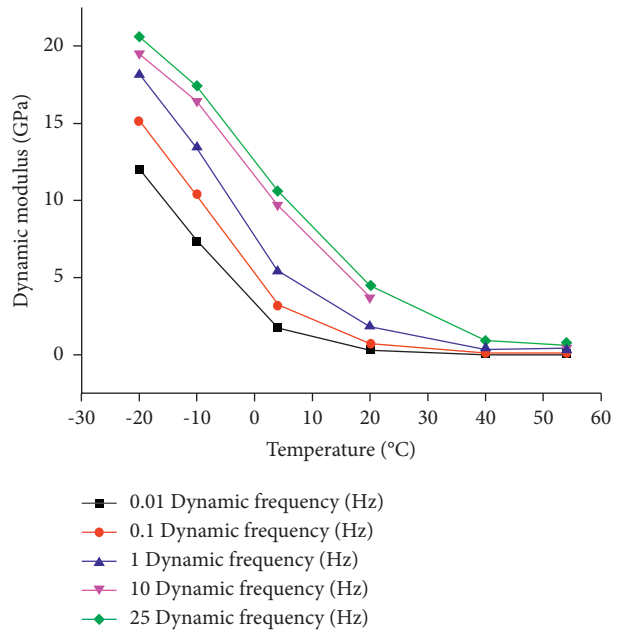

Figure 7: Relationships between dynamic modulus and temperature under different frequencies [85].

As shown in Figure 10, by using piles in composite road foundation, the spiral coil with the largest heat exchange surface of the fluid tube is the selected type of heat exchanger cast-in-place energy piles. And taking advantage of good thermal performance and protective layer, the pipes with multi-U type were installed in concrete roadbed. The dynamic modulus of asphalt material (as shown in Figure 7) has strong correlation with the environment temperature. And the soil temperature changing law (as shown in Figure 1) indicates that the soil temperature is stable at 18°C under more than 6 m depth. With utilizing the existing piles in roadbed, the energy pile system can be installed. If the energy piles system can change 30% of temperature differences, the pavement temperature will be about 40°C in summer and about −2°C in winter. So, under this situation, most of the existing asphalt material can meet the temperature requirements, which also means the energy pile system could solve the contradictory problem of track in summer and crack in winter on pavement.

4.3. Preventing Frost Crack Induced by Seepage Using Energy Piles. Such as Chengde area in Northern China, there is rich underground water in mountains, the low temperature will freeze the underground water around open surface in winter, and the lining at exit and entrance of tunnel will suffer the frost heave force continually with supply underground water. As time passes, a lot of tunnels' linings at position of exit and entrance are facing the water leakage problems. The more serious problem is that the leaked water will be freezing as the ice rapidly. A big block of ice will be hung and accumulated at the roof and road surface, respectively (as shown in Figure 11). It will be a huge potential safety hazard for traffic safety.

Figure 8: Pavement crack in winter.

Figure 9: Pavement track in summer.

Also, using the energy piles system to collect the heat from ground for heating the lining at both ends of tunnel, the frost heave phenomenon could be avoided. And then, the hanging and accumulating ice problem will be nonexistent. This system is the reverse utilization of energy tunnel, as shown in Figure 4: the heat collection structures are changed as the heat sink structure, and the schematic diagram is shown in Figure 12.

As shown in Figure 12, by using piles in tunnel lining, the spiral coil with the largest heat exchange surface of the fluid tube is the selected type of heat exchanger cast-in-place energy piles. And taking advantage of good thermal performance, the pipes with multi-U type were installed in concrete tunnel lining; also these multi-U type pipes could replace the steel in concrete tunnel lining. The soil temperature changing law (as shown in Figure 1) indicates that the soil temperature is stable at 18°C under more than 6 m depth. If the energy piles system can keep temperature above 0°C, the problem of frost crack induced by seepage could be avoided.

4.4. Simulation Study on Buried Pipe Form. Usually, we adopt the form of several shaped buried pipes. However, in engineering practice, we found that the heat transfer uniformity of several shaped buried pipes is poor. When the pipe spacing is large, the temperature at the center between pipes is low. When it is applied to road snow melting and deicing, it will cause uneven melting of ice and snow; when the pipe spacing is small, the temperature near

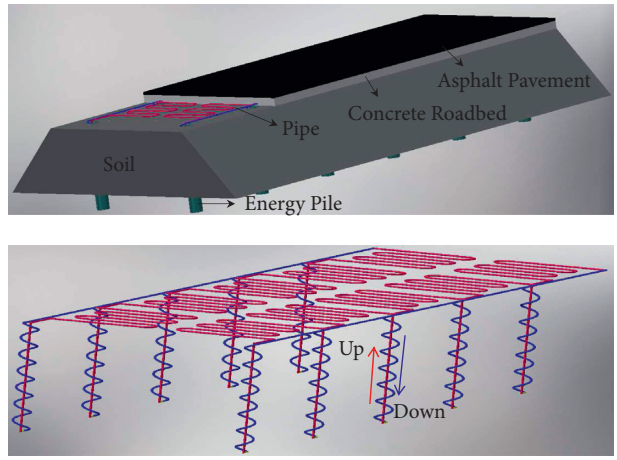

Figure 10: The working schematic diagram of energy piles roadbed and laying pipes.

(a)

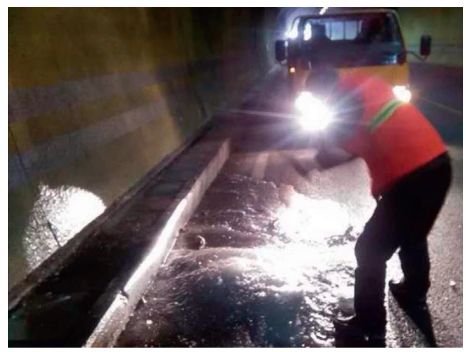

(b)

Figure 11: The hanging and accumulating ice at the roof and road surface.

the buried pipe is high, which wastes resources. After considering the above factors, the spiral buried pipe and zigzag buried pipe form are designed to discuss better heat transfer effect. The solid heat transfer and pipe heat transfer module in COMSOL is used for simulation, and the results are shown in Figure 13. The results show that the spiral buried pipe has better heat transfer uniformity and better engineering applicability compared with the zigzag buried pipe.

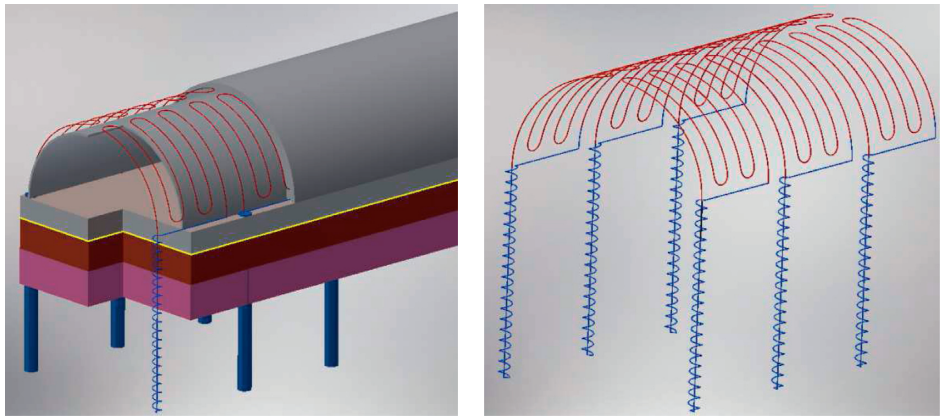

(a) (b)

Figure 12: The working schematic diagram of energy piles tunnel lining and laying pipes.

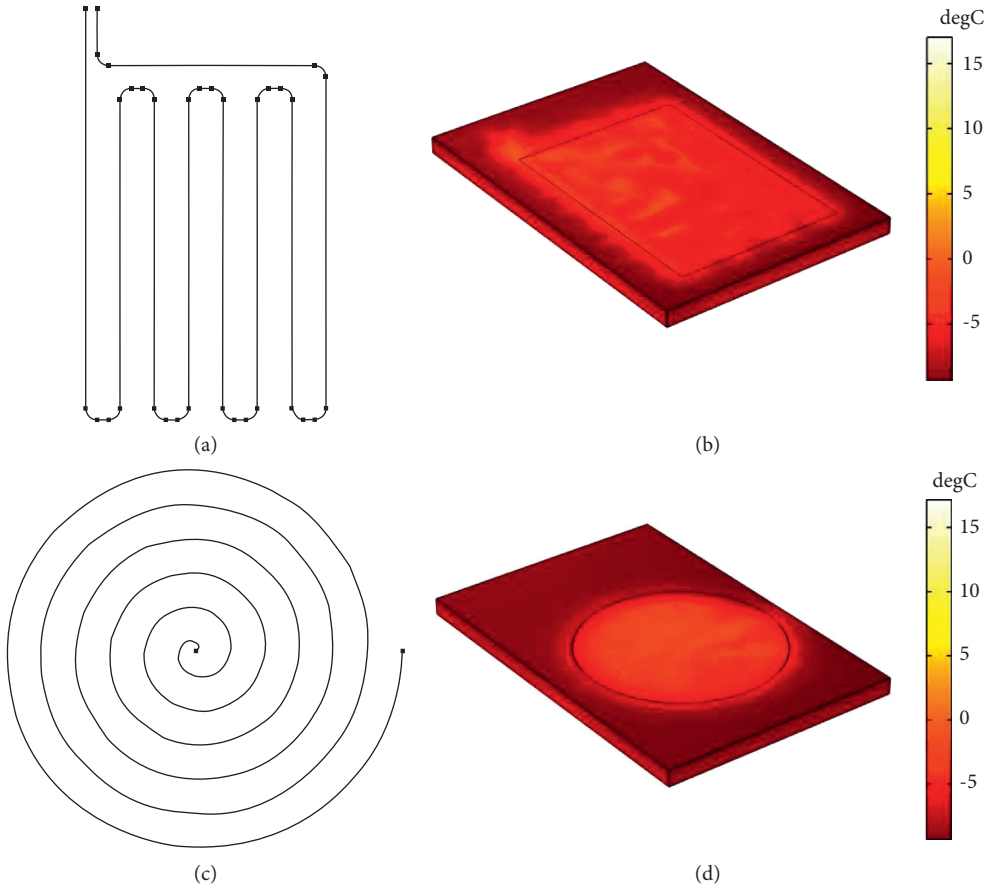

Figure 13: Pavement temperature distribution after 10 days of operation with buried depth of 0.5 m. (a) Zigzag buried pipe. (b) Heat exchange of zigzag buried pipe. (c) Spiral buried pipe. (d) Heat exchange of spiral buried pipe.

5. Conclusion and Discussion

In the recent 30 years, a large number of scholars have conducted extensive and in-depth research on the energy pile system. Through experimental research and numerical simulation, from parameter optimization and heat transfer efficiency to structure-soil response, they continuously promote the application of energy pile system from theory to engineering practice.

With the continuous development of ground-source heat pump system, researchers introduced it into geotechnical engineering from the field of building energy

conservation and applied it to deep mine geothermal collection and tunnel lining surface heat collection, which expanded the utilization forms of ground-source heat pump system.

The area of Northern China has abundant shallow geothermal resources. As a typical seasonal frozen soil area, it is high in summer and cold in winter. The application of ground-source heat pump system in geotechnical engineering has obvious popularization and application value. Hence, taking example of using the geothermal heat exchanger to melt snow, the novel idea of using energy piles to prevent track in summer and crack in winter of pavement and guarantee the safety of frost crack on tunnel lining was discussed, to develop implementation of the energy pile into geotechnical engineering. And through the simulation study, compared with the zigzag buried pipe, it is found that the arrangement form of spiral buried pipe has better heat transfer uniformity and engineering applicability.

Conflicts of Interest

The authors declare that they have no conflicts of interest.

Acknowledgments

This work was supported by the Opening Funds of State Key Laboratory of Building Safety and Built Environment (no. BSBE2015-06) and Joint Research Program between University of Science and Technology Beijing and National Taipei University of Technology (no. TW201703).

References

[1] S. Park, D. Lee, H.-J. Choi, K. Jung, and H. Choi, "Relative constructability and thermal performance of cast-in-place concrete energy pile: coil-type GHEX (ground heat exchanger)," *Energy*, vol. 81, pp. 56–66, 2015.

[2] S. You, X. Cheng, H. Guo, and Z. Yao, "Experimental study on structural response of CFG energy piles," *Applied Thermal Engineering*, vol. 96, pp. 640–651, 2016.

[3] C. Xia, M. Sun, G. Zhang, S. Xiao, and Y. Zou, "Experimental study on geothermal heat exchangers buried in diaphragm walls," *Energy and Buildings*, vol. 52, pp. 50–55, 2012.

[4] M. Sun, C. Xia, and G. Zhang, "Heat transfer model and design method for geothermal heat exchange tubes in diaphragm walls," *Energy and Buildings*, vol. 61, pp. 250–259, 2013.

[5] P. J. Bourne-Webb, T. M. Bodas Freitas, and R. A. da Costa Gonçalves, "Thermal and mechanical aspects of the response of embedded retaining walls used as shallow geothermal heat exchangers," *Energy and Buildings*, vol. 125, pp. 130–141, 2016.

[6] D. Bozis, K. Papakostas, and N. Kyriakis, "On the evaluation of design parameters effects on the heat transfer efficiency of energy piles," *Energy and Buildings*, vol. 43, no. 4, pp. 1020–1029, 2011.

[7] T. V. Bandos, Á. Campos-Celador, L. M. López-González, and J. M. Sala-Lizarraga, "Finite cylinder-source model for energy pile heat exchangers: effects of thermal storage and vertical temperature variations," *Energy*, vol. 78, pp. 639–648, 2014.

[8] C.-E. Moon and J. M. Choi, "Heating performance characteristics of the ground source heat pump system with energy-piles and energy-slabs," *Energy*, vol. 81, pp. 27–32, 2015.

[9] F. Cecinato and F. A. Loveridge, "Influences on the thermal efficiency of energy piles," *Energy*, vol. 82, pp. 1021–1033, 2015.

[10] A. A. Mehrizi, S. Porkhial, B. Bezyan, and H. Lotfizadeh, "Energy pile foundation simulation for different configurations of ground source heat exchanger," *International Communications in Heat and Mass Transfer*, vol. 70, pp. 105–114, 2016.

[11] R. Caulk, E. Ghazanfari, and J. S. McCartney, "Parameterization of a calibrated geothermal energy pile model," *Geomechanics for Energy and the Environment*, vol. 5, pp. 1–15, 2016.

[12] J. Fadejev, R. Simson, J. Kurnitski, and F. Haghighat, "A review on energy piles design, sizing and modelling," *Energy*, vol. 122, pp. 390–407, 2017.

[13] S. Park, S.-R. Lee, H. Park, S. Yoon, and J. Chung, "Characteristics of an analytical solution for a spiral coil type ground heat exchanger," *Computers and Geotechnics*, vol. 49, pp. 18–24, 2013.

[14] A. Zarrella, M. De Carli, and A. Galgaro, "Thermal performance of two types of energy foundation pile: helical pipe and triple U-tube," *Applied Thermal Engineering*, vol. 61, no. 2, pp. 301–310, 2013.

[15] G.-H. Go, S.-R. Lee, S. Yoon, and H.-b. Kang, "Design of spiral coil PHC energy pile considering effective borehole thermal resistance and groundwater advection effects," *Applied Energy*, vol. 125, pp. 165–178, 2014.

[16] W. Zhang, H. Yang, L. Lu, P. Cui, and Z. Fang, "The research on ring-coil heat transfer models of pile foundation ground heat exchangers in the case of groundwater seepage," *Energy and Buildings*, vol. 71, pp. 115–128, 2014.

[17] Y. Xiang, H. Su, W. Gou et al., "A new practical numerical model for the energy pile with spiral coils," *International Journal of Heat and Mass Transfer*, vol. 91, pp. 777–784, 2015.

[18] G.-H. Go, S.-R. Lee, H.-B. Kang, S. Yoon, and M.-J. Kim, "A novel hybrid design algorithm for spiral coil energy piles that considers groundwater advection," *Applied Thermal Engineering*, vol. 78, pp. 196–208, 2015.

[19] J.-U. Lee, T. Kim, and S.-B. Leigh, "Applications of building-integrated coil-type ground-coupled heat exchangers-Comparison of performances of vertical and horizontal installations," *Energy and Buildings*, vol. 93, pp. 99–109, 2015.

[20] S. Yoon, S.-R. Lee, J. Xue, K. Zosseder, G.-H. Go, and H. Park, "Evaluation of the thermal efficiency and a cost analysis of different types of ground heat exchangers in energy piles," *Energy Conversion and Management*, vol. 105, pp. 393–402, 2015.

[21] D. Wang, L. Lu, W. Zhang, and P. Cui, "Numerical and analytical analysis of groundwater influence on the pile geothermal heat exchanger with cast-in spiral coils," *Applied Energy*, vol. 160, pp. 705–714, 2015.

[22] D. Wang, L. Lu, and P. Cui, "A novel composite-medium solution for pile geothermal heat exchangers with spiral coils," *International Journal of Heat and Mass Transfer*, vol. 93, pp. 760–769, 2016.

[23] S. Park, S. Lee, D. Lee, S. S. Lee, and H. Choi, "Influence of coil pitch on thermal performance of coil-type cast-in-place energy piles," *Energy and Buildings*, vol. 129, pp. 344–356, 2016.

[24] Q. Zhao, B. Chen, and F. Liu, "Study on the thermal performance of several types of energy pile ground heat

exchangers: U-shaped, W-shaped and spiral-shaped," *Energy and Buildings*, vol. 133, pp. 335–344, 2016.

[25] J. Luo, H. Zhao, S. Gui, W. Xiang, J. Rohn, and P. Blum, "Thermo-economic analysis of four different types of ground heat exchangers in energy piles," *Applied Thermal Engineering*, vol. 108, pp. 11–19, 2016.

[26] A. Zarrella, G. Emmi, R. Zecchin, and M. De Carli, "An appropriate use of the thermal response test for the design of energy foundation piles with U-tube circuits," *Energy and Buildings*, vol. 134, pp. 259–270, 2017.

[27] M. Faizal, A. Bouazza, and R. M. Singh, "Heat transfer enhancement of geothermal energy piles," *Renewable and Sustainable Energy Reviews*, vol. 57, pp. 16–33, 2016.

[28] F. Delaleux, X. Py, R. Olives, and A. Dominguez, "Enhancement of geothermal borehole heat exchangers performances by improvement of bentonite grouts conductivity," *Applied Thermal Engineering*, vol. 33-34, pp. 92–99, 2012.

[29] C. J. R. Coccia, R. Gupta, J. Morris, and J. S. McCartney, "Municipal solid waste landfills as geothermal heat sources," *Renewable and Sustainable Energy Reviews*, vol. 19, pp. 463–474, 2013.

[30] I. Indacoechea-Vega, P. Pascual-Muñoz, D. Castro-Fresno, and M. A. Calzada-Pérez, "Experimental characterization and performance evaluation of geothermal grouting materials subjected to heating-cooling cycles," *Construction and Building Materials*, vol. 98, pp. 583–592, 2015.

[31] P. Ocłoń, P. Cisek, M. Pilarczyk, and D. Taler, "Numerical simulation of heat dissipation processes in underground power cable system situated in thermal backfill and buried in a multilayered soil," *Energy Conversion and Management*, vol. 95, pp. 352–370, 2015.

[32] X. Li, C. Tong, L. Duanmu, and L. Liu, "Research on U-tube heat exchanger with shape-stabilized phase change backfill material," *Procedia Engineering*, vol. 146, pp. 640–647, 2016.

[33] M. E. Suryatriyastuti, H. Mroueh, and S. Burlon, "Understanding the temperature-induced mechanical behaviour of energy pile foundations," *Renewable and Sustainable Energy Reviews*, vol. 16, no. 5, pp. 3344–3354, 2012.

[34] H. Park, S.-R. Lee, S. Yoon, and J.-C. Choi, "Evaluation of thermal response and performance of PHC energy pile: field experiments and numerical simulation," *Applied Energy*, vol. 103, pp. 12–24, 2013.

[35] P. Hu, J. Zha, F. Lei, N. Zhu, and T. Wu, "A composite cylindrical model and its application in analysis of thermal response and performance for energy pile," *Energy and Buildings*, vol. 84, pp. 324–332, 2014.

[36] N. Batini, A. F. Rotta Loria, P. Conti, D. Testi, W. Grassi, and L. Laloui, "Energy and geotechnical behaviour of energy piles for different design solutions," *Applied Thermal Engineering*, vol. 86, pp. 199–213, 2015.

[37] R. M. Singh, A. Bouazza, and B. Wang, "Near-field ground thermal response to heating of a geothermal energy pile: observations from a field test," *Soils and Foundations*, vol. 55, no. 6, pp. 1412–1426, 2015.

[38] G. A. Akrouch, M. Sánchez, and J.-L. Briaud, "An experimental, analytical and numerical study on the thermal efficiency of energy piles in unsaturated soils," *Computers and Geotechnics*, vol. 71, pp. 207–220, 2016.

[39] T. V. Bandos, Á. Campos-Celador, L. M. López-González, and J. M. Sala-Lizarraga, "Finite cylinder-source model for energy pile heat exchangers: effect of buried depth and heat load cyclic variations," *Applied Thermal Engineering*, vol. 96, pp. 130–136, 2016.

[40] W. Yang, P. Lu, and Y. Chen, "Laboratory investigations of the thermal performance of an energy pile with spiral coil ground heat exchanger," *Energy and Buildings*, vol. 128, pp. 491–502, 2016.

[41] A. Franco, R. Moffat, M. Toledo, and P. Herrera, "Numerical sensitivity analysis of thermal response tests (TRT) in energy piles," *Renewable Energy*, vol. 86, pp. 985–992, 2016.

[42] D. Perić, T. V. Tran, and M. Miletic, "Effects of soil anisotropy on a soil structure interaction in a heat exchanger pile," *Computers and Geotechnics*, vol. 86, pp. 193–202, 2017.

[43] S. Park, D. Lee, S. Lee, A. Chauchois, and H. Choi, "Experimental and numerical analysis on thermal performance of large-diameter cast-in-place energy pile constructed in soft ground," *Energy*, vol. 118, pp. 297–311, 2017.

[44] W. Zhang, H. Yang, L. Fang, P. Cui, and Z. Fang, "Study on heat transfer of pile foundation ground heat exchanger with three-dimensional groundwater seepage," *International Journal of Heat and Mass Transfer*, vol. 105, pp. 58–66, 2017.

[45] F. Loveridge and W. Powrie, "G-functions for multiple interacting pile heat exchangers," *Energy*, vol. 64, pp. 747–757, 2014.

[46] A. F. Rotta Loria and L. Laloui, "The interaction factor method for energy pile groups," *Computers and Geotechnics*, vol. 80, pp. 121–137, 2016.

[47] Y. Cui and J. Zhu, "3D transient heat transfer numerical analysis of multiple energy piles," *Energy and Buildings*, vol. 134, pp. 129–142, 2017.

[48] S. Jeong, H. Lim, J. K. Lee, and J. Kim, "Thermally induced mechanical response of energy piles in axially loaded pile groups," *Applied Thermal Engineering*, vol. 71, no. 1, pp. 608–615, 2014.

[49] J. Fadejev, R. Simson, J. Kurnitski, J. Kesti, T. Mononen, and P. Lautso, "Geothermal heat pump plant performance in a nearly zero-energy building," *Energy Procedia*, vol. 96, pp. 489–502, 2016.

[50] A. Di Donna, A. F. Rotta Loria, and L. Laloui, "Numerical study of the response of a group of energy piles under different combinations of thermo-mechanical loads," *Computers and Geotechnics*, vol. 72, pp. 126–142, 2016.

[51] A. F. Rotta Loria, A. Vadrot, and L. Laloui, "Effect of nonlinear soil deformation on the interaction among energy piles," *Computers and Geotechnics*, vol. 86, pp. 9–20, 2017.

[52] R. Ramsden, T. J. Sheer, and M. D. Buttrworth, "Design and simulation of ultra-deep mine cooling systems," in *Proceedings of the 7th International Mine Ventilation Congress*, pp. 755–760, Krakow, Poland, 2001.

[53] S. J. Biuhm, M. Biffi, and R. B. Wilson, "Optimized cooling systems for mining at extreme depths," *CIM Bulletin*, vol. 93, no. 1, pp. 146–150, 2000.

[54] M.-c. He, "Application of HEMS cooling technology in deep mine heat hazard control," *Mining Science and Technology*, vol. 19, no. 3, pp. 269–275, 2009.

[55] G. E. Du Plessis, L. Liebenberg, and E. H. Mathews, "The use of variable speed drives for cost-effective energy savings in South African mine cooling systems," *Applied Energy*, vol. 111, pp. 16–27, 2013.

[56] G. E. Du Plessis, D. C. Arndt, and E. H. Mathews, "The development and integrated simulation of a variable water flow energy saving strategy for deep-mine cooling systems," *Sustainable Energy Technologies and Assessments*, vol. 10, pp. 71–78, 2015.

[57] D. Apel, W. Liu, and V. Bindiganavile, "Simulation of the effects of thermo insulating shotcrete on the energy consumption of ventilation and cooling systems at deep

underground mines," in *Proceedings of the Mine Planning and Equipment Selection*, pp. 37–42, Dresden, Germany, October 2013.

[58] W. Chen, S. Liang, and J. Liu, "Proposed split-type vapor compression refrigerator for heat hazard control in deep mines," *Applied Thermal Engineering*, vol. 105, pp. 425–435, 2016.

[59] P. Guo, G. Zhu, and M. He, "HEMS technique for heat-harm control and geo-thermal utilization in deep mines," *International Journal of Coal Science and Technology*, vol. 1, no. 3, pp. 289–296, 2014.

[60] S. A. Ghoreishi-Madiseh, F. Hassani, and F. Abbasy, "Numerical and experimental study of geothermal heat extraction from backfilled mine stopes," *Applied Thermal Engineering*, vol. 90, pp. 1119–1130, 2015.

[61] E. Peralta Ramos, K. Breede, and G. Falcone, "Geothermal heat recovery from abandoned mines: a systematic review of projects implemented worldwide and a methodology for screening new projects," *Environmental Earth Sciences*, vol. 73, no. 11, pp. 6783–6795, 2015.

[62] P. Guo, M. He, L. Zheng, and N. Zhang, "A geothermal recycling system for cooling and heating in deep mines," *Applied Thermal Engineering*, vol. 116, pp. 833–839, 2017.

[63] T. Mimouni, F. Dupray, and L. Laloui, "Estimating the geothermal potential of heat-exchanger anchors on a cut-and-cover tunnel," *Geothermics*, vol. 51, pp. 380–387, 2014.

[64] M. Barla, A. Di Donna, and A. Perino, "Application of energy tunnels to an urban environment," *Geothermics*, vol. 61, pp. 104–113, 2016.

[65] C. Lee, S. Park, H.-J. Choi, I.-M. Lee, and H. Choi, "Development of energy textile to use geothermal energy in tunnels," *Tunnelling and Underground Space Technology*, vol. 59, pp. 105–113, 2016.

[66] P. Buhmann, C. Moormann, B. Westrich, N. Pralle, and W. Friedemann, "Tunnel geothermics-a German experience with renewable energy concepts in tunnel projects," *Geomechanics for Energy and the Environment*, vol. 8, pp. 1–7, 2016.

[67] J. C. López, A. L. Grindlay, and A. Peña-García, "A proposal for evaluation of energy consumption and sustainability of road tunnels: the sustainability vector," *Tunnelling and Underground Space Technology*, vol. 65, pp. 53–61, 2017.

[68] J. Jiang, *China's Energy Policy 2012*, Information Office of the State Council, Beijing, China, 2012.

[69] H. Long, Z. Qingjun, T. Puyuan, and H. Wenguang, *Technologies and Applications of Geophysical Exploration in Deep Geothermal Resources in China*, World Geothermal Congress, Melbourne, Australia, 2015.

[70] G. Wang, K. Li, D. Wen et al., *Assessment of Geothermal Resources in China*, Stanford University, Stanford, CA, USA, 2013.

[71] J. Zhu, K. Hu, X. Lu, X. Huang, K. Liu, and X. Wu, "A review of geothermal energy resources, development, and applications in China: current status and prospects," *Energy*, vol. 93, pp. 466–483, 2015.

[72] D. Chen and H. W. Chen, "Using the Köppen classification to quantify climate variation and change: an example for 1901–2010," *Environmental Development*, vol. 6, no. 1, pp. 69–79, 2013.

[73] A. Pmc, A. Cb, B. Aks, and R. Marchetti, "Worldwide dynamic predictive analysis of building performance under long-term climate change conditions," *Journal of Building Engineering*, vol. 42, no. 11, Article ID 103057, 2021.

[74] W. Ting, Z. Daowei, and S. Xiangjin, "Koppen's climate classification map for China," *Journal of the Meteorological Sciences*, vol. 40, pp. 752–760, 2020.

[75] Z. Wang, T. Zhang, M. Shao, T. Ai, and P. Zhao, "Investigation on snow-melting performance of asphalt mixtures incorporating with salt-storage aggregates," *Construction and Building Materials*, vol. 142, pp. 187–198, 2017.

[76] J. Wåhlin and A. Klein-Paste, "The effect of mass diffusion on the rate of chemical ice melting using aqueous solutions," *Cold Regions Science and Technology*, vol. 139, pp. 11–21, 2017.

[77] M. Chen, S. Wu, H. Wang, and J. Zhang, "Study of ice and snow melting process on conductive asphalt solar collector," *Solar Energy Materials and Solar Cells*, vol. 95, no. 12, pp. 3241–3250, 2011.

[78] Y. Lai, Y. Liu, and D. Ma, "Automatically melting snow on airport cement concrete pavement with carbon fiber grille," *Cold Regions Science and Technology*, vol. 103, pp. 57–62, 2014.

[79] J.-P. Won, C.-K. Kim, S.-J. Lee, J.-H. Lee, and R.-W. Kim, "Thermal characteristics of a conductive cement-based composite for a snow-melting heated pavement system," *Composite Structures*, vol. 118, pp. 106–111, 2014.

[80] A. D. W. Nuijten and K. V. Høyland, "Comparison of melting processes of dry uncompressed and compressed snow on heated pavements," *Cold Regions Science and Technology*, vol. 129, pp. 69–76, 2013.

[81] K. Liu, S. Huang, F. Wang, H. Xie, and X. Lu, "Energy consumption and utilization rate analysis of automatically snow-melting system in infrastructures by thermal simulation and melting experiments," *Cold Regions Science and Technology*, vol. 138, pp. 73–83, 2017.

[82] K. Liu, S. Huang, C. Jin, and H. Xie, "Prediction models of the thermal field on ice-snow melting pavement with electric heating pipes," *Applied Thermal Engineering*, vol. 120, 2017.

[83] P. Pan, "A review on hydronic asphalt pavement for energy harvesting and snowmelting," *Renewable and Sustainable Energy Reviews*, vol. 48, pp. 624–634, 2017.

[84] N. Yildirim and A. Hepbasli, "Exergetic aspects of snow melting using a geothermal heat pump system," in *Proceedings of the World Geothermal Congress 2015*, pp. 1–11, Melbourne, Australia, April 2015.

[85] H. Xu and Y. Tan, "Modeling and operation strategy of pavement snow melting systems utilizing low-temperature heating fluids," *Energy*, vol. 80, pp. 666–676, 2015.

[86] C. Han and X. Yu, "Feasibility of geothermal heat exchanger pile-based bridge deck snow melting system: a simulation based analysis," *Renewable Energy*, vol. 101, pp. 214–224, 2017.

[87] X. Wang, Y. Zhu, M. Zhu, Y. Zhu, H. Fan, and Y. Wang, "Thermal analysis and optimization of an ice and snow melting system using geothermy by super-long flexible heat pipes," *Applied Thermal Engineering*, vol. 112, pp. 1353–1363, 2014.

[88] T. R. Clyne, X. Li, M. Mo, and S. El, *Dynamic and Resilient Modulus of Mn/DOT Asphalt Mixtures*, University of Minnesota, Minneapolis, MN, USA, 2003.

[89] B. Barra, L. Momm, Y. Guerrero, H. A. Al-Qureshi, A. Mikowski, and R. Michels, "Temperature implications on rheological-mechanical behavior and design of high modulus dense asphalt mix," *Construction and Building Materials*, vol. 125, pp. 135–144, 2016.

[90] M. Kim, L. N. Mohammad, P. Phaltane, and M. A. Elseifi, "Density and SCB measured fracture resistance of temperature segregated asphalt mixtures," *International Journal of Pavement Research and Technology*, vol. 10, no. 2, pp. 112–121, 2017.

[91] M. S. Sakhaeifar, Y. Richard Kim, and B. E. Garcia Montano, "Individual temperature based models for nondestructive evaluation of complex moduli in asphalt concrete," *Construction and Building Materials*, vol. 137, pp. 117–127, 2017.
[92] M. Ryms, H. Denda, and P. Jaskuła, "Thermal stabilization and permanent deformation resistance of LWA/PCM-modified asphalt road surfaces," *Construction and Building Materials*, vol. 142, pp. 328–341, 2017.
[93] H. Jahanbakhsh, M. Karimi, F. Moghadas Nejad, and B. Jahangiri, "Viscoelastic-based approach to evaluate low temperature performance of asphalt binders," *Construction and Building Materials*, vol. 128, pp. 384–398, 2016.
[94] R. Zhang, H. Wang, J. Gao, Z. You, and X. Yang, "High temperature performance of SBS modified bio-asphalt," *Construction and Building Materials*, vol. 144, pp. 99–105, 2017.

Hindawi
Advances in Civil Engineering
Volume 2021, Article ID 9241867, 9 pages
https://doi.org/10.1155/2021/9241867

Research Article

Research on Photovoltaic Grid-Connected Control Strategy Based on Active Disturbance Rejection of Adaptive Extended State Observer

Dejun Liu,[1] **Jinfei Xu**,[2] **Ruonan Xue**,[2] **Chao Song**,[2] **and Zhenxiong Zhou**[2]

[1]*Engineering Training Center, Beihua University, Jilin, China*
[2]*College of Electrical and Information Engineering, Beihua University, Jilin, China*

Correspondence should be addressed to Zhenxiong Zhou; 742884852@qq.com

Received 29 June 2021; Revised 5 September 2021; Accepted 7 September 2021; Published 28 September 2021

Academic Editor: DONG LI

In the photovoltaic inverter grid-connected power generation system, the output power of photovoltaic panels is affected by illumination and temperature. The change of output power of photovoltaic panels will lead to the fluctuation of DC bus voltage. If the control is improper, it will directly affect the regular operation of the system. In order to improve the performance of the grid-connected inverter system, an active disturbance rejection control method based on adaptive extended state observer (ESO) is proposed. Firstly, a feedforward PI current inner loop controller is designed, which simplifies the structure of the control system and improves the tracking performance of the current. Then, the DC bus voltage outer loop ADRC is designed, and a conversion method that ignores the essential difference between nonlinear/time-varying and time-varying/linear is proposed. Through the conversion of time-invariant nonlinear system and time-varying linear system, the stability of the extended state observer is proved by the Routh criterion. Secondly, to solve the problem of mutual restriction between the stability and observation accuracy of the extended state observer, an adaptive function online automatic tuning ESO parameter method is proposed. Finally, the simulation results show that the proposed method has better dynamic and static performance, and the grid-connected voltage and current harmonics are small, which proves the correctness and effectiveness of the proposed method.

1. Introduction

Photovoltaic power generation has the characteristics of environmental protection and efficiency, which is widely used in the fields of electric power, agriculture, modern architecture, and so on [1]. It has become a research hotspot in the field of distributed generation of renewable energy. The grid-connected inverter is the essential equipment to connect photovoltaic array with power grid [2–4].

Since the output power of photovoltaic panels is affected by illumination and temperature [5], the DC-side bus voltage fluctuates, and improper control will directly affect the normal operation of the system. The existing technologies and methods to improve the stability of photovoltaic inverter grid-connected power generation system are mainly studied from three aspects: circuit structure, filter circuit, and control strategy. It is easy to induce resonance by using the filtering method, and it is easy to be affected by power grid impedance. The use of circuit structure leads to complex circuit structure; by improving the control strategy, the method becomes convenient, flexible, and low cost. The control strategy is usually the DC bus voltage control algorithm, controlled by the inverter. In the two-stage three-phase photovoltaic grid-connected system, the former stage is the maximum power point tracking control, and the latter stage is the grid-connected inverter control. The grid-connected inverter control is generally the bus voltage for the outer ring and the current loop for the inner ring structure. The inner current loop can be regulated by PI and PR [6, 7].

In order to improve the performance of bus voltage control, scholars put forward sliding mode control [8], model predictive control [9, 10], adaptive backstepping

control [2, 11], two-degree-of-freedom control [12], feedback linearization control [13, 14], feedforward decoupling control [15, 16], etc. These methods have achieved good results, but they do not consider the external disturbance problem and rely on the mathematical model of the system. Reference [17] adopts an adaptive fuzzy approximation strategy to control grid-connected inverter, but its learning algorithm relies on data information. Reference [18] introduces fuzzy control based on deadbeat grid-connected control, but the determination of fuzzy rules requires experience. In reference [19], particle swarm optimization (PSO) is used to optimize the grid connection design, but the local optimization performance is poor. In reference [20], the cascade control strategy of a fractional-order PID photovoltaic grid-connected system is adopted, but its parameter tuning is difficult.

The core of active disturbance rejection control (ADRC) is that the uncertain factors acting on the controlled object are regarded as "unknown disturbance," and it is observed and compensated with the input and output data of the object. It breaks through the limitations of "the absolute invariance principle" and "the internal model principle" [21–23].

In recent years, the theory and application of active disturbance rejection control (ADRC) have attracted the attention of scholars. They have been successfully applied to chemical, aerospace, electromechanical, power systems, and other systems. The nonlinear active disturbance rejection control of the photovoltaic energy storage bidirectional DC-DC converter is proposed [24]. In [25], the proportional differential link is introduced into the linear extended state observer to improve the disturbance rejection of the system. In reference [26], to improve the performance of a three-phase current controlled voltage source inverter, LADRC-based active damping control was proposed. In [27], a method to control the bus voltage of wind power inverter using improved second-order LADRC was put forward. Although these methods improve the disturbance rejection of the system, there are still some problems, such as chattering in steady state, complex stability analysis, and mutual restriction between stability and accuracy of extended state observer.

In this paper, a current inner loop feedforward PI controller is designed for the two-stage photovoltaic grid-connected inverter control system to improve the current tracking performance. An active disturbance rejection control strategy based on adaptive ESO is proposed to improve the disturbance rejection of the voltage outer loop. The design uses an adaptive function to automatically adjust the parameters of ESO online to achieve the effect of large error and small gain and small error and large gain. The method improves the stability and observation accuracy of ESO and solves the contradiction between the stability and observation accuracy of nonlinear ESO. On the other hand, aiming at the difficulty of nonlinear ESO stability analysis, a method of transforming the time-invariant nonlinear system into the time-varying linear system is proposed. It is more convenient for stability analysis. Finally, simulation experiment results show that the proposed method is effective and feasible.

2. Mathematical Model of Three-Phase Photovoltaic Grid-Connected Inverter

The two-stage three-phase photovoltaic grid-connected system is composed of solar photovoltaic cells, DC/DC converter circuit, and DC/AC inverter circuit. The front stage uses a boost circuit to track the maximum power point of the solar photovoltaic array, and the backstage uses a three-phase full-bridge inverter circuit to complete the grid-connected inverter from DC to AC. Each bridge arm consists of a power switch tube and a diode. The main circuit structure of the system is shown in Figure 1.

C is bus capacitance in the figure; S_{ij} $(i = a, b, c, j = 1, 2)$ are switching tubes; u_a, u_b, and u_c are output voltages of the inverter; i_a, i_b, and i_c are output currents of the inverter; e_a, e_b, and e_c are network voltages; and i_0 is the first-stage output current.

According to Kirchhoff voltage law (KVL), the dynamic voltage equation of PV grid-connected inverter is expressed as

$$\begin{bmatrix} \dfrac{di_a}{dt} \\ \dfrac{di_b}{dt} \\ \dfrac{di_c}{dt} \end{bmatrix} = \frac{1}{L}\begin{bmatrix} -R & 0 & 0 \\ 0 & -R & 0 \\ 0 & 0 & -R \end{bmatrix}\begin{bmatrix} i_a \\ i_b \\ i_c \end{bmatrix} + \begin{bmatrix} u_a - e_a \\ u_b - e_b \\ u_c - e_c \end{bmatrix}. \tag{1}$$

When the three-phase grid voltage is stable and symmetrical, the inverter side currents i_a, i_b, and i_c, grid voltages e_a, e_b, and e_c, and inverter output voltages u_a, u_b, and u_c are selected as state variables. Through 3/2 transformation, the mathematical model of grid-connected inverter in $\alpha\beta$ stationary coordinate system is obtained as follows:

$$L\frac{d}{\mathrm{d}t}\begin{bmatrix} i_\alpha \\ i_\beta \end{bmatrix} + \begin{bmatrix} R & 0 \\ 0 & R \end{bmatrix}\begin{bmatrix} i_\alpha \\ i_\beta \end{bmatrix} = \begin{bmatrix} e_\alpha \\ e_\beta \end{bmatrix} - \begin{bmatrix} u_\alpha \\ u_\beta \end{bmatrix}, \tag{2}$$

where u_α, u_β and i_α, i_β are the components of inverter output voltage and current on the $\alpha\beta$ axis and e_α and e_β are the components of grid voltage on the $\alpha\beta$ axis.

Through the $2s/2r$ rotation transformation, the mathematical model of the AC side of the grid-connected inverter in the dq synchronous rotating coordinate system is

$$\begin{cases} u_d = Ri_d + L\dfrac{\mathrm{d}i_d}{\mathrm{d}t} - \omega L i_q + e_d, \\ \\ u_q = Ri_q + L\dfrac{\mathrm{d}i_q}{\mathrm{d}t} + \omega L i_d + e_q, \end{cases} \tag{3}$$

where R and L represent the equivalent resistance and inductance of the grid and ω is the angular frequency of the AC network.

According to equation (3), let the state equation of the AC side of the grid-connected inverter be

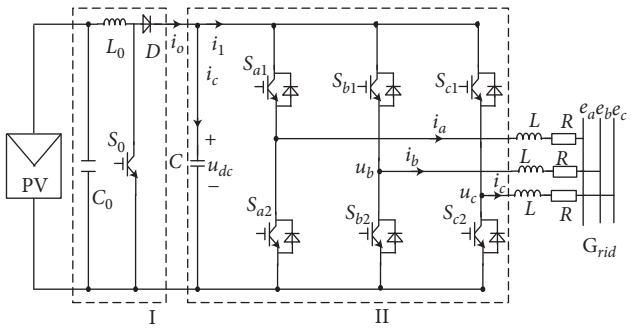

Figure 1: Two-stage PV grid-connected inverter topology.

$$\begin{cases} \dot{x}_1 = \dfrac{1}{L}\left(u_d - Rx_1 + \omega L x_2 - e_d\right), \\ \dot{x}_2 = \dfrac{1}{L}\left(u_q - Rx_2 - \omega L x_1 - e_q\right). \end{cases} \tag{4}$$

3. Design of Controller

The control system adopts double closed-loop control, which is primarily composed of internal and external loop controllers, phase-locked loop (PLL), voltage (current) transform (abc/dq), static/rotary transform (dq/$\alpha\beta$), and pulse generator. The outer loop adopts the active disturbance rejection controller (ADRC), and the inner loop adopts the PI controller with feedforward compensation. The control structure diagram is shown in Figure 2.

3.1. Design of Inner Loop Controller. From equation (3),

$$\begin{cases} L\dfrac{\mathrm{d}i_d}{\mathrm{d}t} = u_d - Ri_d + \omega L i_q - e_d, \\ L\dfrac{\mathrm{d}i_q}{\mathrm{d}t} = u_q - Ri_q - \omega L i_d - e_q. \end{cases} \tag{5}$$

For the controlled object shown in equation (5), if the grid current is used as the feedback of the current loop and the feedforward PI controller is adopted, the control equation is obtained:

$$\begin{cases} u_d^* = k_p\left(i_d^* - i_d\right) + k_i\dfrac{i_d^* - i_d}{s} + e_d - \omega L i_d + Ri_d, \\ u_q^* = k_p\left(i_q^* - i_q\right) + k_i\dfrac{i_q^* - i_q}{s} + e_q + \omega L i_q + Ri_q, \end{cases} \tag{6}$$

where k_p and k_i are proportional and integral gains of current inner loop PI regulator, respectively, and u_d^* and u_q^* are the components of the modulation voltage of the inverter on the dq axis.

It is generally considered that u_d^* and u_q^* are approximately equal to u_d and u_q; therefore, by combining equations (5) and (6),

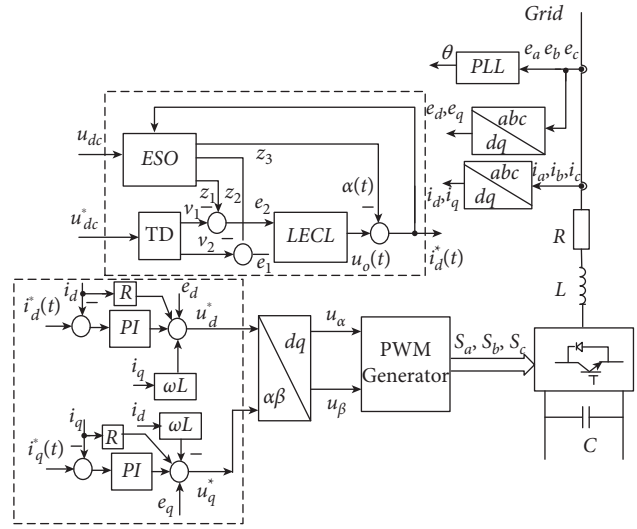

Figure 2: Block diagram of control system structure.

$$\left(Ls + \frac{k_i}{s} + k_p\right) i_d(s) = \left(k_p + \frac{k_i}{s}\right) i_d^*(s). \tag{7}$$

The closed-loop transfer function is presented as

$$G_i(s) = \frac{i_d(s)}{i_d^*(s)} = \frac{k_p + k_i/s}{Ls + k_p + k_i/s} = \frac{k_p s + k_i}{Ls^2 + k_p s + k_i}. \tag{8}$$

3.2. Design of Outer Loop Controller. The outer loop adopts the active disturbance rejection controller (ADRC), and the control block diagram is shown in Figure 3. TD is the differential tracker, LECL is the linear error control law, and ESO is the extended state observer.

From Figure 3, $G_t(s)$ is the transfer function of the power electronic converter, and its expression is

$$G_t(s) = \frac{u_{\mathrm{dc}}(s)}{i_d(s)} = \frac{k_s}{T_s s + 1}. \tag{9}$$

The generalized object transfer function of ADRC is

$$G_p(s) = \frac{k_p s + k_i}{Ls^2 + k_p s + k_i}\,\frac{k_s}{T_s s + 1}. \tag{10}$$

Because T_s is small, according to the engineering design criterion [28], equation (10) is approximated as a second-order system with uncertainties, which can be constructed as shown in the following equation:

$$G_p(s) \approx \frac{k}{s^2 + a_1 s + a_2} + \Delta(s). \tag{11}$$

The differential equation of the system in the form of equation (11) can be expressed as

$$\ddot{y} = f(y, \dot{y}, \xi) + \mathrm{bu} = -a_1\dot{y} - a_2 y + \xi + \mathrm{bu}, \tag{12}$$

where y is the system output; ξ is the external disturbance; u is the system input; a_1 and a_2 are the controlled system parameters; b is the control gain; and $f(y, \dot{y}, \xi)$ is the

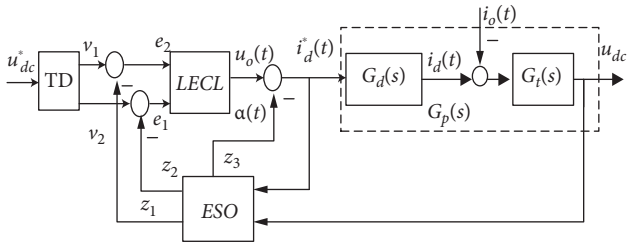

Figure 3: Block diagram of double closed-loop control system.

synthesis of the internal and external disturbance. Most systems (a_1, a_2, and b) are difficult to obtain accurately; let the second-order system be expressed as

$$\ddot{y} = d + b_0 u, \tag{13}$$

where $d = f(y, \dot{y}, \xi) + (b - b_0)u$ is the total disturbance to be observed and b_0 is known.

Let $x_1 = y$, $x_2 = \dot{y}$, $x_3 = f(y, \dot{y}, \xi, t) = -a_1\dot{y} - a_2 y + \xi + (b - b_0)u$, and the equation of state can be obtained as follows:

$$\begin{cases} \dot{x}_1 = x_2, \\ \dot{x}_2 = x_3 + b_0 u, \\ \dot{x}_3 = \dot{f}(y, \dot{y}, \xi, t) = w(t). \end{cases} \tag{14}$$

The following nonlinear tension state observer is designed for system (14), and its differential equation is

$$\begin{cases} e = z_1 - y, \\ \dot{z}_1 = z_2 - \beta_{01} e, \\ \dot{z}_2 = z_3 - \beta_{02}\mathrm{fal}(e, \alpha_1) + b_0 u, \\ \dot{z}_3 = -\beta_{03}\mathrm{fal}(e, \alpha_2), \end{cases} \tag{15}$$

where β_{01}, β_{02}, and β_{03} are the gains of nonlinear tensor state observer and $\mathrm{fal}(e, \alpha) = |e|^{\alpha}\mathrm{sign}(e)$.

The nonlinear tensor state observer is asymptotically stable by adequately selecting β_{01}, β_{02}, and β_{03}. That is to realize the real-time tracking of x_1, x_2 and x_3, namely, $z_1 \longrightarrow x_1$, $z_2 \longrightarrow x_2$, and $z_3 \longrightarrow x_3$. Let

$$u = \frac{-z_3 + u_0}{b_0}. \tag{16}$$

Then, the second-order system can be transformed into an integral series type in the following form:

$$\ddot{y} = d + b_0 u = f(y, \dot{y}, \xi) + (b - b_0)u + b_0 u \approx z_3 + b_0 u = u_0. \tag{17}$$

The following control law is adopted:

$$u_0 = k_p(r - z_1) + k_d(\dot{r} - z_2) + \frac{k_i}{s}(r - z_1), \tag{18}$$

where r is the reference signal. Let $\dot{r} = 0$, and because $z_1 \longrightarrow y$ and $z_2 \longrightarrow \dot{y}$, the closed-loop transfer function of the system is

$$\begin{aligned} \ddot{y} &= k_p(r - z_1) + k_d(\dot{r} - z_2) + \int k_i(r - z_1)\mathrm{d}t \\ &= k_1(r - y) - k_2\dot{y} + \int k_i(r - y)\mathrm{d}t, \end{aligned} \tag{19}$$

$$\frac{y(s)}{r(s)} = \frac{k_d s^2 + k_p s + k_i}{s^3 + k_d s^2 + k_p s + k_i}, \tag{20}$$

$$\varphi_{\mathrm{pid}}(s) = s^3 + k_d s^2 + k_p s + k_i. \tag{21}$$

It can be concluded from equation (21) that if the output variables of nonlinear tension state observer are asymptotically stable, the stability of the system depends on k_p, k_i, and k_d.

3.3. Estimation Error Analysis of ESO. Let $e_1 = z_1 - x_1$, $e_2 = z_2 - x_2$, $e_3 = z_3 - x_3$, and equation (14) can be written as

$$\begin{cases} \dot{z}_1 - \dot{x}_1| = z_2 - \beta_{01}(z_1 - x_1) - x_2 = \dot{e}_1 = e_2 - \beta_{01} e_1, \\ \dot{z}_2 - \dot{x}_2| = z_3 - \beta_{02}\mathrm{fal}(e_1) + b_0 u - x_3 - b_0 u = \dot{e}_2 = e_3 - \beta_{02}\mathrm{fal}(e_1), \\ \dot{z}_3 - \dot{x}_3| = -w(t) - \beta_{03}\mathrm{fal}(e_1) = \dot{e}_3 = -w(t) - \beta_{03}\mathrm{fal}(e_1), \end{cases} \tag{22}$$

where $\mathrm{fal}(\cdot)$ is a smooth and continuous function, which can be regarded as a linear function in any small neighborhood of its independent variable. It is considered that $\mathrm{fal}(\cdot)$ is composed of countless linear functions. When the observer order is the same as the object order, the principle of ignoring the essential difference between the nonlinear/time-varying and time-varying/linear proposed in this paper is used. The parameter time-invariant differential equation in equation (22) is equivalent to the parameter time-varying differential equation. That is, the constant coefficients β_{01}, β_{02}, and β_{03} in equation (22) are converted into time-varying coefficients $\beta_{01}(t)$, $\beta_{02}(t)$, and $\beta_{03}(t)$, and $\mathrm{fal}(e_1)$ is replaced by e_1; then, equation (23) can be obtained.

$$\begin{cases} \dot{e}_1 = e_2 - \beta_{01}(t)e_1, \\ \dot{e}_2 = e_3 - \beta_{02}(t)e_1, \\ \dot{e}_3 = -w(t) - \beta_{03}(t)e_1. \end{cases} \tag{23}$$

Let $\beta_{01}(t) = \beta_{01}$, $\beta_{02}(t) = \beta'_{02}$, and $\beta_{03}(t) = \beta'_{03}$; it can be obtained from equation (23) that

$$\begin{cases} \varepsilon_1 = e_1 = z_1 - x_1, \\ \varepsilon_2 = e_2 - \beta_{01} e_1 = z_2 - x_2 - \beta_{01} e_1, \\ \varepsilon_3 = e_3 - \beta'_{02} e_1 - \beta_{01}\dot{e}_1. \end{cases} \tag{24}$$

The derivation of equation (24) can be obtained as

$$\begin{cases} \dot{\varepsilon}_1| = \dot{e}_1 = z_2 - \beta_{01}(z_1 - x_1) - x_2 = \dot{e}_1 = e_2 - \beta_{01}e_1 = \varepsilon_2, \\ \dot{\varepsilon}_2 = \dot{e}_2 - \beta_{01}\dot{e}_1 = \dot{z}_2 - \dot{x}_2 - \beta_{01}\dot{e}_1 = e_3 - \beta'_{02}e_1 - \beta_{01}\dot{e}_1 = \varepsilon_3, \\ \dot{\varepsilon}_3| = \dot{e}_3 - \beta'_{02}\dot{e}_1 - \beta_{01}\ddot{e}_1 = \dot{e}_3 - \beta'_{02}\dot{e}_1 - \beta_{01}(\dot{e}_2 - \beta_{01}\dot{e}_1), \\ | = -\beta_{01}\varepsilon_3 - \beta'_{02}\varepsilon_2 - \beta'_{03}\varepsilon_1 - w(t). \end{cases} \tag{25}$$

When $w(t) = 0$, the Laplace transform of the third line of the above equation is

$$s^3 + \beta_{01}s^2 + \beta'_{02}s + \beta'_{03} = 0. \tag{26}$$

From the Routh stability criterion, it can be concluded that the sufficient and necessary conditions for the stability of the system are that β_{01}, β'_{02}, and β'_{03} are all greater than zero. Furthermore, under the condition $\beta_{01} \bullet \beta'_{02} > \beta'_{03}$, the zero solutions of the system $e_1(t) = 0, e_2(t) = 0$, and $e_3(t) = 0$ are globally asymptotically stable.

When the disturbance $w(t)$ is considered, it is bounded, i.e., $|w(t)| \geq w_0$, and the system has a steady-state error. From the final value theorem, the following equation can be obtained:

$$\begin{aligned} |e_1(t)| &\leq \frac{w_0}{\beta'_{03}}, \\ |e_2(t)| &\leq \frac{\beta_{01}w_0}{\beta'_{03}}, \\ |e_3(t)| &\leq \frac{\beta_{02}w_0}{\beta'_{03}}. \end{aligned} \tag{27}$$

It can be seen that when β_{01}, β'_{02} are smaller and β'_{03} is larger, the observation errors of state x_1, x_2 and x_3 are smaller. However, the stability should meet the requirements of $\beta_{01} \bullet \beta'_{02} > \beta'_{03}$, so the parameter tuning of the observer needs to be comprehensively considered.

3.4. ESO Adaptive Extended State Observer. From the above analysis, it can be obtained that the stability of the extended state observer is directly related to the stability of the system. The larger β'_{03} is, the shorter the estimation time is and the smaller the steady-state error is. However, if β'_{03} is too large, the estimated value will not converge. Besides, β_{01} and β'_{02} affect the transition process and stability of state estimation, and too large values can also cause estimation instability. Therefore, this paper adopts the adaptive function tuning method, and the designed parameter tuning function is

$$\beta_i = A + B \cdot e^{(-\lambda|z_1 - y|)}, \tag{28}$$

where A is the minimum base value, B is the dynamic extremum, and λ is the attenuation coefficient.

The function has the characteristics of a small function value when the error is significant and an enormous function value when the error is small so that the extended state observer converges quickly and the steady-state error is small. The problem of mutual restriction between observer stability and observation accuracy with constant parameters is avoided.

4. Simulation Research

To verify the effectiveness of the grid-connected inverter control algorithm proposed in this paper, the simulation model of the photovoltaic grid-connected inverter is built by using MATLAB/Simulink simulation software. The model is connected to a 35 kV power grid through a DC-DC boost converter, three-phase inverter, and three-phase coupling transformer. The system's main circuit is shown in Figure 1, and the system control structure is shown in Figure 2. For the front stage boost circuit, the "incremental conductance + integral regulator" technology is used to realize the maximum power tracking of the PV cells. The primary parameters of the main circuit are summarized in Table 1.

The parameters of the extended state observer and the linear error control law are shown in Table 2.

Figure 4 shows the setting curves of light intensity and temperature.

To verify the superiority of the control algorithm proposed in this article, the simulation experiments of the voltage loop controller are PID, ADRC with constant parameter ESO, and ADRC with adaptive ESO, respectively. The inner current loop controller parameters under the three outer loop control modes are as follows: $k_p = 0.3$, $k_i = 30$. Figure 5 shows the DC bus voltage curves under the action of different controllers. Figure 6 shows the response curves of adaptive ESO and ordinary ESO.

From Figure 5, it can be obviously seen that the overshoot of adaptive ESO active disturbance rejection control is small and the response time is short before the disturbance is added. When the disturbance is added, the DC bus voltage fluctuation of adaptive ESO active disturbance rejection control is small and restored quickly to the expected value.

It can be seen from Figure 6 that the adaptive ESO observation has the advantages of smooth observation state, small fluctuation, and fast convergence compared with the constant parameter ESO. The reason why the initial ADRC has small overshoot and fast response is that the differential tracker (TD) effectively arranges the transition process. At the same time, since the adaptive ESO active disturbance rejection control adopts online parameter self-tuning, which effectively realizes the effect of large error and small gain and small error and large gain. Therefore, the state observation is smooth and has fast convergence and good disturbance rejection.

Figure 7 shows the A-phase voltage and current curves of ADRC with adaptive ESO, ADRC with constant parameter ESO, and PID control, respectively.

Table 1: Primary parameters of the main circuit.

Parameters	Value	Unit
Rated output power	100	kW
Bus capacitance	100	μF
Open-circuit voltage	500	V
Inductance	0.25	mH
Resistance	0.002	Ω
Grid frequency	50	Hz

Table 2: Parameters of the controller.

Parameters	Value
β_{01}	1
β_{02}	$20 + 15 \cdot e^{(-30\lvert z_1 - y\rvert)}$
β_{03}	$10 + 10 \cdot e^{(-30\lvert z_1 - y\rvert)}$
k_{pu}	20
k_{iu}	800
k_{du}	0.1

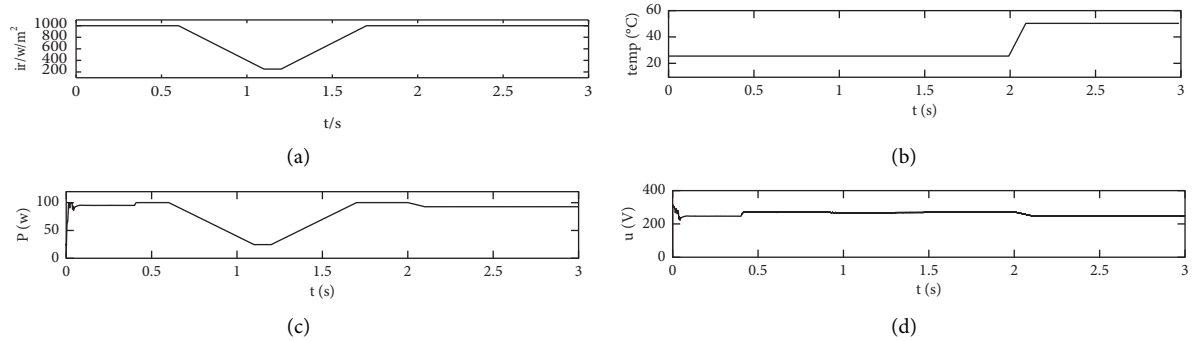

Figure 4: Setting curve of light intensity and temperature change.

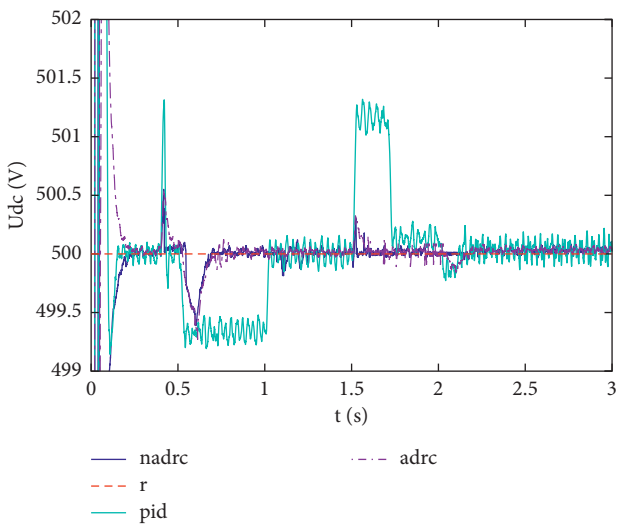

Figure 5: Response curves of the DC bus voltage.

It can be seen from Figure 7 that compared with ordinary ADRC, the improved ADRC has a smaller initial response current fluctuation frequency and faster current regulation speed. It only needs about 1.5 cycles to quickly realize that the output current and voltage of the grid-connected inverter are in phase, indicating that the grid-connected inverter can operate with high power factor. However, the PID control takes a long time to adjust and requires two cycles. The output current of the grid-connected inverter cannot be in phase with the grid voltage quickly, and the output current has burrs and is not smooth.

In order to further compare the control performance, harmonic analysis is carried out on the output A-phase voltage and current of the inverter. Tables 3 and 4 show the harmonic analysis of A-phase voltage and current controlled by ADRC with adaptive ESO, ADRC with constant parameters ESO, and PID.

From Tables 3 and 4, it can be seen that the basic wave amplitude of the output voltage of the grid-connected inverter is $2.792 * 10^4$, and the total harmonic content of the voltage is 0.02%. The basic wave amplitude of current is 2.237, and the overall harmonic content of current is 1.68%. The basic wave amplitude of the output voltage of the conventional active disturbance rejection control grid-connected inverter is $2.789 * 10^4$, and the total harmonic content of the voltage is 0.02%. The basic wave amplitude of current is 2.236, and the overall harmonic content of current is 1.74%. Besides, PI control

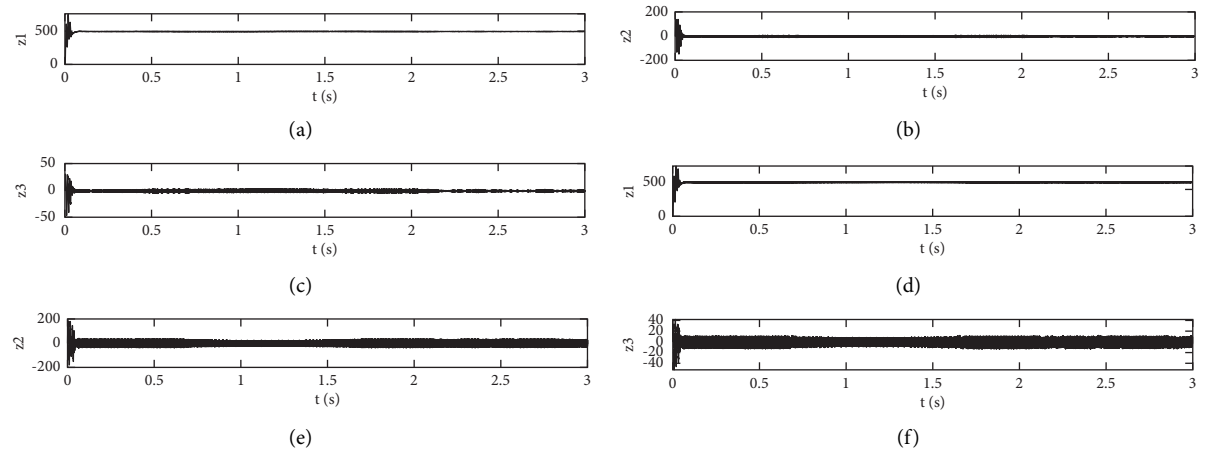

Figure 6: Response curves of adaptive ESO and ordinary ESO.

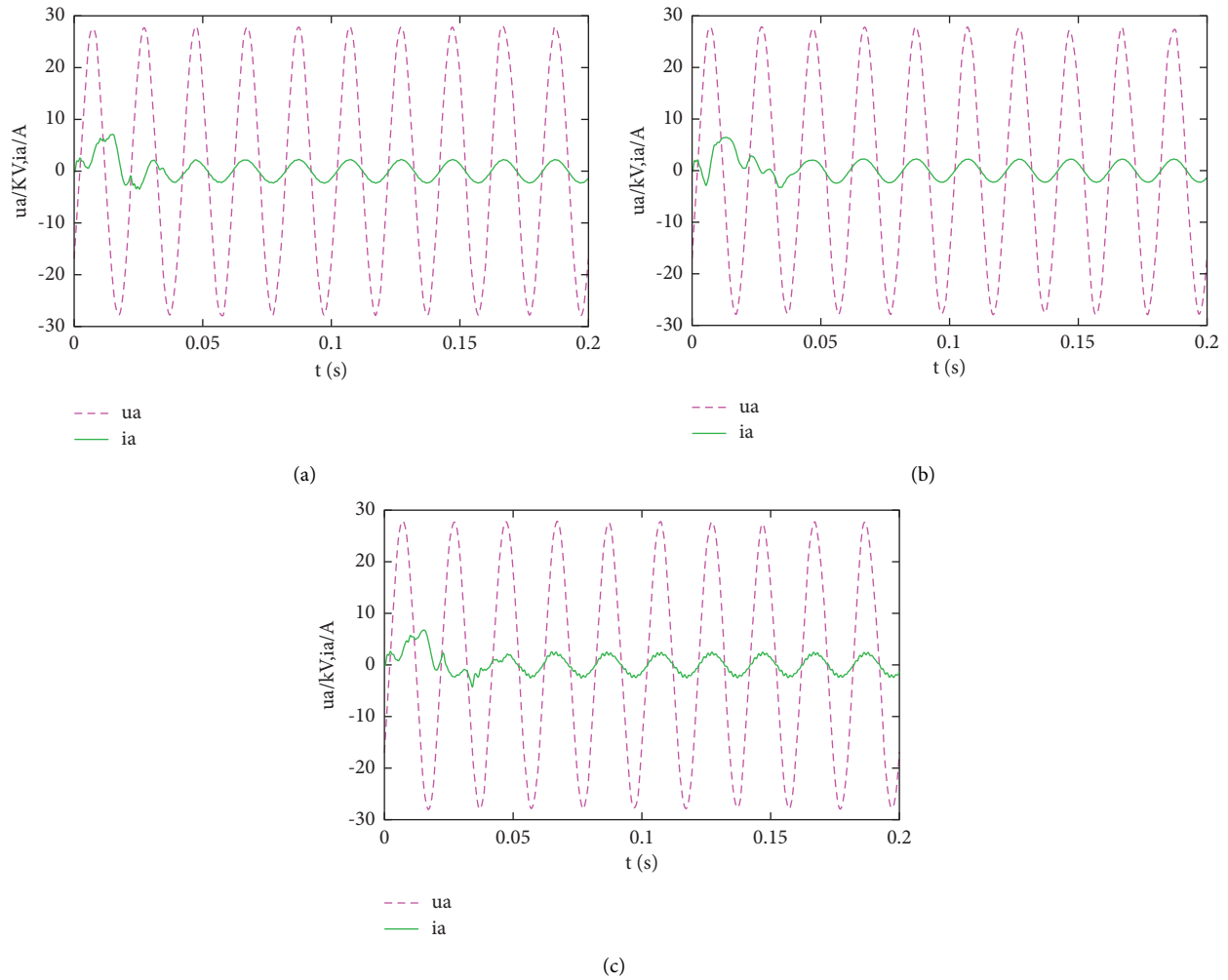

Figure 7: u_a and i_a response curves. (a) u_a and i_a response curves of the improved ADRC. (b) u_a and i_a response curves of the ADRC. (c) u_a and i_a response curves of the PID control.

grid-connected inverter output voltage fundamental wave amplitude is $2.789 * 10^4$, and the overall voltage harmonic content is 0.08%. The basic wave amplitude of current is 2.358, and the overall harmonic content of current is 9.33%. Therefore, a conclusion can be drawn that the proposed control strategy of grid-connected inverter output current and voltage of the total harmonic content is small, better than the traditional ADRC and PID control.

Table 3: Harmonic analysis comparison of phase A voltage.

Controllers	Fundamental (50 Hz)	THD (total harmonic distortion) (%)
Improved ADRC	$2.792 * 10^4$	0.02
LADRC	$2.789 * 10^4$	0.02
PI	$2.789 * 10^4$	0.08

Table 4: Harmonic analysis comparison of phase A current.

Controllers	Fundamental (50 Hz)	THD (total harmonic distortion) (%)
Improved ADRC	2.237	1.68
LADRC	2.236	1.74
PI	2.358	9.33

5. Conclusions

This paper considers the influence of uncertain factors such as light intensity and temperature changes and combined with the strong anti-interference ability of active disturbance rejection control. Aimed at the above characteristics, a control method of active disturbance-rejection grid-connected inverter based on adaptive ESO is proposed. In this method, adaptive function online automatic ESO tuning parameters can achieve fast and accurate state observation estimation. The following conclusions are obtained through experiments:

(1) This method equates the time-invariant differential equation to the parameter time-varying differential equation, so that it is convenient to use the Routh stability criterion to analyze the stability of the nonlinear extended states.

(2) The ESO parameter tuning function is designed to realize the online self-tuning of ESO parameters, eliminate the contradiction between the stability of ESO with constant parameters and the observation accuracy, improve the observation performance, and increase the stability of ESO.

(3) Compared with the traditional active disturbance rejection and PID control, this method has better dynamic and static performance and strong robustness under external interference.

Data Availability

The data used to support the findings of this study are available from the corresponding author upon request.

Conflicts of Interest

The authors declare that there are no conflicts of interest regarding the publication of this paper.

Acknowledgments

This study was supported by the Jilin Science and Technology Research Project of Education Department (2015148), Jilin Education Department Project (JJKH20200042KJ), and Jilin Provincial Development and Reform Commission Project (2019C058-1).

References

[1] A. Mesloub, A. Ghosh, G. A. Albaqawy, E. Noaime, and B. Alsolami, "Energy and daylighting evaluation of integrated semitransparent photovoltaic windows with internal light shelves in open-office buildings," *Advances in Civil Engineering*, vol. 2020, Article ID 8867558, 21 pages, 2020.

[2] T. Yang, Z. Cai, and Q. Xun, "Adaptive backstepping-based H${_{\infty}}$ robust controller for photovoltaic grid- connected inverter," *IEEE Access*, vol. 8, pp. 17263–17272, 2020.

[3] Y. Yang, K. Zhou, and F. Blaabjerg, "Current harmonics from single-phase grid-connected inverters-examination and suppression," *IEEE Journal of Emerging and Selected Topics in Power Electronics*, vol. 4, no. 1, pp. 221–233, 2016.

[4] Y. Guan, Y. Wang, Y. Xie, Y. Liang, A. Lin, and X. Wang, "The dual-current control strategy of grid-connected inverter with LCL filter," *IEEE Transactions on Power Electronics*, vol. 34, no. 6, pp. 5940–5952, 2019.

[5] R. Madurai Elavarasan, A. Ghosh, T. K. Mallick, A. Krishnamurthy, and M. Saravanan, "Investigations on performance enhancement measures of the bidirectional converter in PV-wind interconnected microgrid system," *Energies*, vol. 12, no. 14, p. 2672, 2019.

[6] C. Wang, X. Li, L. Guo, and Y. W. Li, "A nonlinear-disturbance-observer-based DC-bus voltage control for a hybrid AC/DC microgrid," *IEEE Transactions on Power Electronics*, vol. 29, no. 11, pp. 6162–6177, 2014.

[7] X. R. Liu, C. Gao, and Z. L. Wang, "DC-bus voltage control for PV grid-connected inverter based on nonlinear disturbance observer," *Power System Technology*, vol. 44, no. 3, pp. 897–906, 2020.

[8] N. Marcel and N. ClaudiuIonel, "Fractional-order control of grid-connected photovoltaic system based on synergetic and sliding mode controllers," *Energies*, vol. 14, no. 2, p. 510, 2021.

[9] Y. Shan, J. Hu, and J. M. Guerrero, "A model predictive power control method for PV and energy storage systems with voltage support capability," *IEEE Transactions on Smart Grid*, vol. 11, no. 2, pp. 1018–1029, 2020.

[10] H. T. Nguyen and J.-W. Jung, "Disturbance-rejection-based model predictive control: flexible-mode design with a modulator for three-phase inverters," *IEEE Transactions on Industrial Electronics*, vol. 65, no. 4, pp. 2893–2903, 2018.

[11] A. Ahmad, N. Ullah, N. Ahmed et al., "Robust control of grid-tied parallel inverters using nonlinear backstepping approach," *IEEE Access*, vol. 7, pp. 111982–111992, 2019.

[12] M. Hanif, V. Khadkikar, W. Xiao, and J. L. Kirtley, "Two degrees of freedom active damping technique for LCL filter-based grid connected PV systems," *IEEE Transactions on Industrial Electronics*, vol. 61, no. 6, pp. 2795–2803, 2014.

[13] N.-B. Lai and K.-H. Kim, "Robust control scheme for three-phase grid-connected inverters with LCL-filter under unbalanced and distorted grid conditions," *IEEE Transactions on Energy Conversion*, vol. 33, no. 2, pp. 506–515, 2018.

[14] D. Chen, Y. Qiu, Y. Chen, and Y. He, "Nonlinear PWM-controlled single-phase boost mode grid-connected photovoltaic inverter with limited storage inductance current," *IEEE Transactions on Power Electronics*, vol. 32, no. 4, pp. 2717–2727, 2017.

[15] H. Zhang, J. Xian, J. Shi, S. Wu, and Z. Ma, "High performance decoupling current control by linear extended state observer for three-phase grid-connected inverter with an LCL filter," *IEEE Access*, vol. 8, pp. 13119–13127, 2020.

[16] C.-Y. Liao, W.-S. Lin, Y.-M. Chen, and C.-Y. Chou, "A PV micro-inverter with PV current decoupling strategy," *IEEE Transactions on Power Electronics*, vol. 32, no. 8, pp. 6544–6557, 2017.

[17] M. Shadoul, H. Yousef, R. Al Abri, and A. Al-Hinai, "Adaptive fuzzy approximation control of PV grid-connected inverters," *Energies*, vol. 14, no. 4, p. 942, 2021.

[18] Z. H. Zheng, T. X. Zhang, and J. X. Zhang, "Application of fuzzy control in a photovoltaic grid-connected inverter," *Journal of Electrical and Computer Engineering*, vol. 2018, Article ID 3806372, 10 pages, 2018.

[19] H. A. Kefale, E. M. Getie, and K. G. Eshetie, "Optimal design of grid-connected solar photovoltaic system using selective particle swarm optimization," *International Journal of Photoenergy*, vol. 2021, Article ID 6632859, 9 pages, 2021.

[20] A. Badis, M. N. Mansouri, and M. H. Boujmil, "Cascade control of grid-connected PV systems using TLBO-based fractional-order PID," *International Journal of Photoenergy*, vol. 2019, Article ID 4325648, 17 pages, 2019.

[21] W. Tan and C. Fu, "Linear active disturbance-rejection control: analysis and tuning via IMC," *IEEE Transactions on Industrial Electronics*, vol. 63, no. 4, pp. 2350–2359, 2016.

[22] J. Han, "From PID to active disturbance rejection control," *IEEE Transactions on Industrial Electronics*, vol. 56, no. 3, pp. 900–906, 2009.

[23] J. Li, X. H. Qi, H. Wan, and Y. Xia, "Active disturbance rejection control: theoretical results summary and future researches," *Control Theory & Applications*, vol. 34, no. 3, pp. 281–295, 2017.

[24] H. Yang, S. Luo, and X. D. Sun, "Research on active disturbance rejection control method of bidirectional DC-DC converter for photovoltaic energy storage," *Acta Energiae Solaris Sinica*, vol. 39, no. 5, pp. 1342–1350, 2018.

[25] Y. F. Cao, Y. H. Wu, Y. Q. Ye, and Y. Xiong, "Active disturbance rejection control strategy of differential feedforward for inverter," *Proceedings of the CSU-EPSA*, vol. 43, no. 5, pp. 136–142, 2019.

[26] A. Benrabah, D. Xu, and Z. Gao, "Active disturbance rejection control of LCL-filtered grid-connected inverter using padé approximation," *IEEE Transactions on Industry Applications*, vol. 54, no. 6, pp. 6179–6189, 2018.

[27] X. S. Zhou, M. Liu, and Y. J. Ma, "Improved bus voltage control of second-order LADRC wind power inverter," *Proceedings of the CSU-EPSA*, vol. 32, no. 6, pp. 43–50, 2020.

[28] Y. Ruan, *Automatic Control System for Electric Drive*, China Machine Press, Beijing, China, 2010.

Hindawi
Advances in Civil Engineering
Volume 2021, Article ID 8851685, 19 pages
https://doi.org/10.1155/2021/8851685

Review Article

A Systematic Review on Indoor Environmental Quality in Naturally Ventilated School Classrooms: A Way Forward

Nishant Raj Kapoor,[1,2] **Ashok Kumar**,[1,2] **Chandan Swaroop Meena**,[1,2] **Anuj Kumar**,[1,2] **Tabish Alam**,[1,2] **Nagesh Babu Balam**,[1,2] **and Aritra Ghosh**[3]

[1]*CSIR-Central Building Research Institute, Roorkee 247667, India*
[2]*Academy of Scientific and Innovative Research (AcSIR), Ghaziabad 201002, India*
[3]*University of Exeter, Penryn, TR10 9FE, Cornwall, UK*

Correspondence should be addressed to Nishant Raj Kapoor; nishant@cbri.res.in, Chandan Swaroop Meena; chandanswaroop2008@gmail.com, and Aritra Ghosh; a.ghosh@exeter.ac.uk

Received 28 August 2020; Revised 19 January 2021; Accepted 27 January 2021; Published 18 February 2021

Academic Editor: Andreas Lampropoulos

This review presents the existing state-of-the-art practices of indoor environmental quality (IEQ) in naturally ventilated school buildings and is mainly focused on the components of IEQ like thermal comfort, indoor air quality with ventilation, and visual and acoustic comfort. This article also discusses the impacts of COVID-19 on naturally ventilated school buildings, highlighting the obviousness of dynamic applications that concentrate on reducing COVID-19 effects in naturally ventilated school buildings. The importance of the concerned issues and factors are discussed in detail for future research direction. This review is a step toward the development of the IEQ standard for naturally ventilated school buildings.

1. Introduction

1.1. Overview. In developing countries, people are likely to spend more of their time indoors. People spent approx 90% of their total time indoors [1]. People spend about 65% or more of their time at their homes, depending on various factors such as age, gender, job type, indoor comfort, and indoor environmental quality [2]. Based on these findings, the indoor environmental conditions are important for learning, health, wellbeing, general working patterns, and economic growth. As per the National Building Code of India Part IV–2016 [3], buildings are classified into nine types, namely, residential, educational, institutional, assembly, business, mercantile, industrial, store, and hazardous. Educational buildings like schools, universities, and colleges are some of the most important buildings where one-fifth of the world population spends more than 30% of their time [4, 5]. The quality of learning and performing various tasks are directly related to the indoor environmental quality (IEQ) of any building. Good IEQ in educational buildings enhances the health and the learning capabilities of students and increases productivity and efficiency [6]. However, most of the IEQ studies done in India and around the globe focus on residential and commebuildings [7], whereas research studies on school buildings are scarce in India. The overall indoor environmental quality of a regularly occupied space in the long term is determined by ergonomics, indoor thermal comfort, electromagnetic radiation level, quality of indoor air, acoustic comfort, hygiene, visual comfort, furniture-space layout, micro/macroorganisms, and aesthetics [8, 9]. According to the National Institute for Occupational Safety and Health (NIOSH) 2013 [10], IEQ is defined as "the quality of a building's environment concerning the health and wellbeing of its occupants and includes aspects of design, analysis, and operation that lead to energy-efficient, healthy, and comfortable buildings."

There is a direct relationship between the building's indoor conditions and an occupant's health. Factors such as poor maintenance, bad IEQ, and building age will lead to

worsening of the building's condition and have a negative impact on the occupant's health. Educational buildings with poor IEQ can reduce the concentration and performance of occupants. Fromme et al. [11] discussed the positive effects of good IEQ on the teaching and learning process in students and teachers. IEQ affects occupant's confidence, performance, absenteeism, learning outcome, and job satisfaction [12–16]. Carlopio and de Dear et al. [17, 18] explained how poor job satisfaction can lead occupants to leave a job. Building IEQ interacts dynamically with its user and affects them physiologically and psychologically [19–21]. The unhealthy buildings, in the long run, are very harmful to their users and can cause illness and various types of disease. Clinically, it is defined as building-related illness (BRI) and sick building syndrome (SBS) [22]. BRI symptoms can be clinically defined and have identifiable causes, whereas symptoms of SBS can be seen in occupants for a short duration, but the cause of symptoms is not known. Symptoms associated with BRI are chest tightness, fever, chills, cough, and muscle ache, and symptoms of SBS are eye, throat, or nose irritation; headaches; dry or itchy skin; dry cough; nausea and dizziness; fatigue; odors' sensitivity; and difficulty in concentration. Most of the SBS complaints report relief after leaving the building, while BRI complaints require a long duration for recovery. The causes of SBS are inadequate ventilation, outdoor-indoor chemical and biological contaminants, etc. All the causes of BRI and SBS are directly related to the IEQ of a building; thus, it becomes more important to study the IEQ in school buildings [22–25]. Catalina and Ioardache [26] focused on enhancing the demand for IEQ studies in school buildings. School buildings include preschool (kindergarten), primary school (elementary school), upper primary (middle) school, secondary school, and senior secondary school. Different schools have different age groups of students, which is presented in Figure 1. The National Education Policy 2020 [27] has modified the Indian educational structure recently, which is also presented in Figure 1. In India, approximately 1.4 million schools are owned and run by the government [28]. The majority of Indian school buildings are naturally ventilated (NV) and mixed-mode ventilated schools are minimum.

1.2. Objectives of the Study. Indoor environmental quality (IEQ) inside a building is the key element to make a building suitable for human habitation, learning, and working. The IEQ in naturally ventilated school buildings is an important component because students in the age group of 3–18 years spend an ample amount of time (4–7 hours) in schools. Based on the prior state of the art, the research area of NV school buildings is in the premature stage and needs further research on IEQ. And more so, IEQ is a major challenge in the COVID-19 scenario for sustainable indoor environments in naturally ventilated school buildings. It is affecting the performance and health of the inhabitants. The IEQ study is a necessary component in the area of school building research for the wellbeing and better performance of the students.

Therefore, the main aim of this article is to identify the necessity of IEQ in NV school buildings during the COVID-19 scenario for maintaining the IEQ and also to suggest the future research direction. The objectives are as follows: (i) to understand the existing knowledge of IEQ and comfort in NV school buildings and (ii) to identify research and data gaps in the developed knowledge and propose future research related to IEQ in NV school classrooms.

The paper contains a general introduction of IEQ and school buildings in the first section. The second section explains the review methodology adopted. The IEQ in NV school buildings is discussed in detail with all its components in the third and fourth sections. The fifth section describes COVID-19 impacts on NV schools. The sixth section contains a combined discussion and conclusion with some key ideas for future work focusing on providing better IEQ in NV school buildings.

2. Methodology

A four-stage procedure is adopted for the creation of this review. The four stages are presented in Figure 2.

For identification, a preliminary survey for an up-to-date published review article is performed. According to the preliminary survey, an outcome research criterion is fixed and important keywords for the NV school buildings are identified. These are: IEQ, thermal comfort, indoor air quality, teacher performance and productivity, lighting and illumination, acoustics in schools, sick building syndrome, building-related illness, ventilation, and integration of daylight. For the literature review, Web of Science, IEEE Access, Research Gate, Academia, and Google Scholar are used. Standards and reports are collected from official websites. In the classification stage, preclassification is done based on abstracts. Irrelevant articles are discarded from the review. All the included articles are read full and articles falling out of criteria are removed. After detailed analyses of the articles reviewed, as shown in Figure 3, all the ideas generated through the understanding of existing knowledge are organized and linked together to form a systematic review, which is then followed by a conclusion and future directions.

2.1. Indoor Environmental Quality. Healthy and comfortable life is the topmost priority of every building user. Corresponding to health and wellbeing, the quality of a built environment for its occupant inside a building is referred to as indoor environmental quality. IEQ involves a series of complex trends that merge Indoor Air Quality (IAQ), noise disturbance, occupant density, indoor lighting, daylighting, ventilation, room temperature, cleanliness, indoor humidity, and ergonomics. All these factors add up and we call it IEQ as a whole; it simply defines the importance of building engineering in molding the health of building occupants living or working inside. The main IEQ components are thermal comfort (TC), visual comfort (VC), indoor air quality (IAQ) (including ventilation), and acoustic comfort

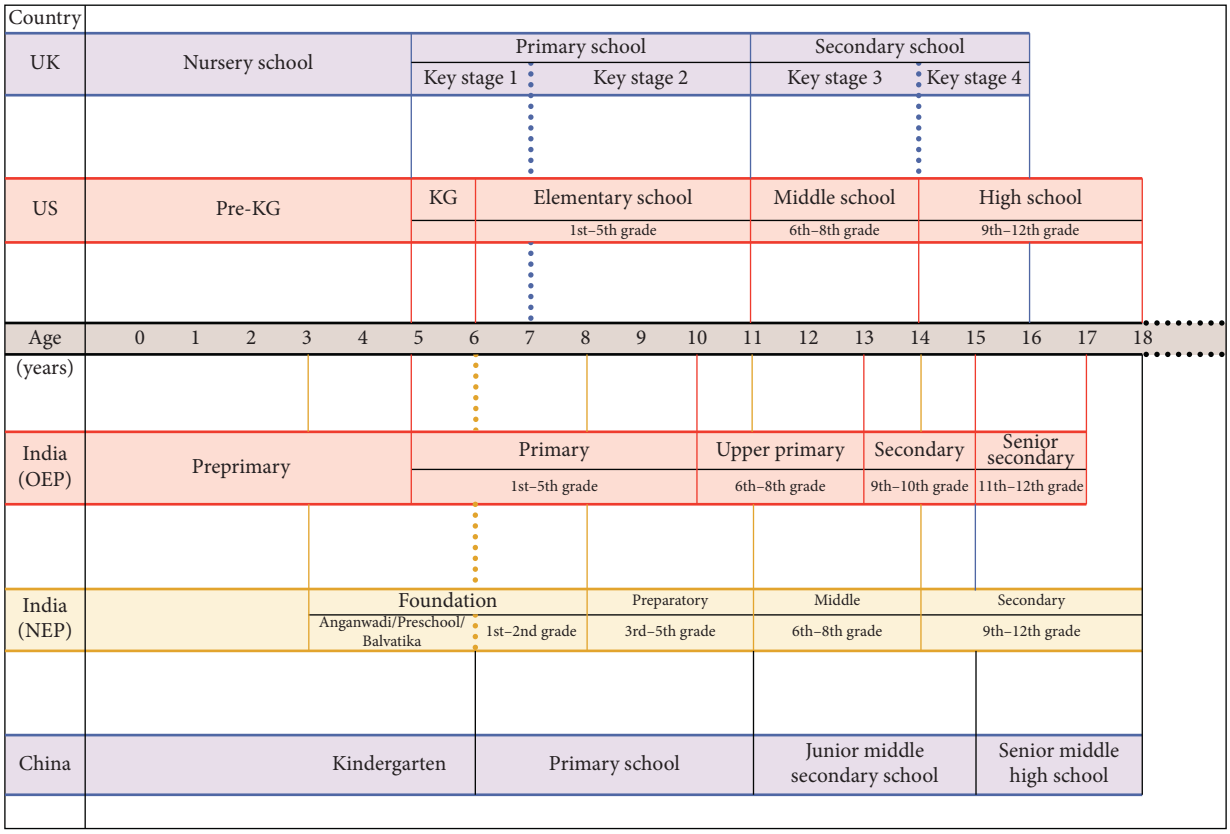

∗OEP - Old education policy

∗NEP - National education policy

Figure 1: Structure of the educational system of different countries.

Figure 2: Four stages for review.

(AcC). There are no IEQ codes specifically for schools but some related codes are included in Table 1.

In NV schools, productivity, concentration, and efficiency are increased due to good IEQ conditions, and health impacts are the least on students and teachers. Students and teachers spend approximately half of their total indoor time in school buildings majorly in classrooms. In the majority of cases, there is a shortage of funds for providing a better indoor environment in schools globally. NV schools of urban areas are more prone to poor IAQ and excessive noise conditions. Most of the schools are situated near markets or surrounded by busy surroundings in urban areas. The balance between low noise and good air circulation in the classroom through an open window is difficult to achieve in a noisy and polluted urban environment. Schneider [39] studied the relationship between relative humidity in school buildings and student absenteeism patterns. The study indicated that when the humidity is more, more students feel sick and fungal growth is also increased.

Hanushek and Rivkin [40] explained that teachers work for less salary and even perform better if the IEQ is good inside classrooms. Becker et al. [41] and Fisk et al. [42] explained that good IEQ can lead toward large economic benefits, reduced health issues, and annual productivity gains. Studies show that poor IEQ has various long- and short-term health impacts on building occupants [43]. Poor IAQ can lead to severe health issues such as allergies, headaches, nausea, dizziness, asthma, and other respiratory and cardiovascular diseases [44, 45]. In addition, conditions such as bad thermal comfort (<16°C and >33.7°C) [46], poor acoustics (background noise > 35 db and reverberation time > 0.7 seconds) [38], and improper lighting (inadequate, i.e., <200 lux or excessively bright, i.e., >500 lux) [30] could increase the stress level in an occupant's body and increase health risks like sleep disorder, concentration loss, amnesia, digestive problems, anger, etc. Studies considered in this review are depicted in Table 2.

An indoor environment with good IEQ improves the occupant's mood, which affects the comfort perception of the occupant. Productivity increases with good health and improves the mood of the worker inside the building, which is well supported by research [47]. Kielb et al. [48] researched New York public school teachers' satisfaction with indoor environmental features of the classroom. They found that inadequate ventilation and poor building conditions are directly associated with various ill-health

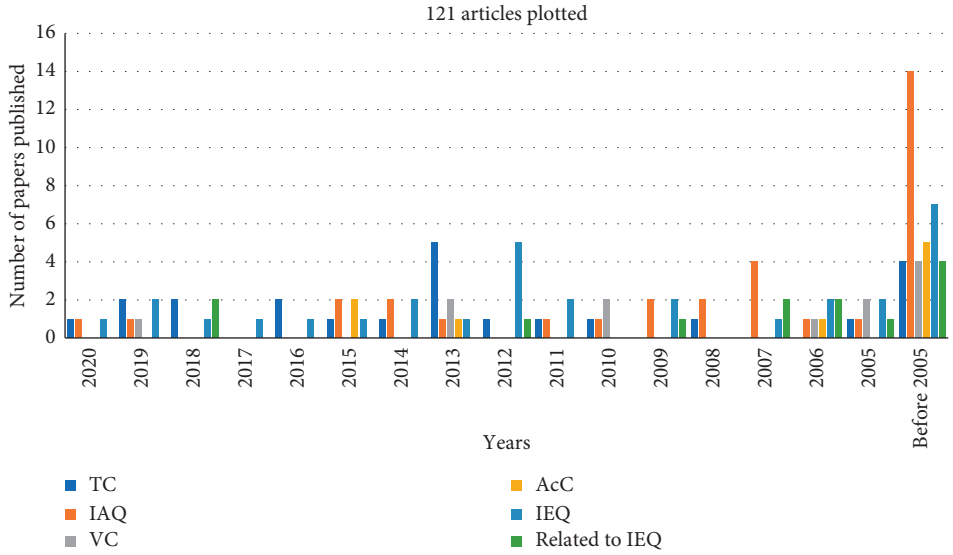

Figure 3: Number of papers published over the years on classroom IEQ parameters.

Table 1: Indian and international codes on IEQ parameters.

Codes	Parameters			
	Thermal comfort	Visual comfort	Indoor air quality and ventilation	Acoustic comfort
Indian national codes	SP-41 [29]NBC, 2016 [30], ISHRAE 10001 : 2019 [31]	SP-41 [29]NBC, 2016 [30], ISHRAE 10001 : 2019 [31]	ISHRAE 10001 : 2019 [31]	NBC, 2016 [30] ISHRAE 10001 : 2019 [31]
International codes	ASHRAE 55 [32], ISO 7730 [33], EN 16798 [34]	EN 12665 [35], ISO 8995 [36]	ASHRAE 62.1 [37]	ANSI S12.60 [38]

Table 2: IEQ parameters study spread over the publication years.

Publication year	TC	IAQ	VC	AcC	IEQ	Related to IEQ	Cited papers
2020	1	1	—	—	1	—	3
2019	2	1	1	—	2	—	6
2018	2	—	—	—	1	2	5
2017	—	—	—	—	1	—	1
2016	2	—	—	—	1	—	3
2015	1	2	—	2	1	—	6
2014	1	2	—	—	2	—	5
2013	5	1	2	1	1	—	10
2012	1	—	—	—	5	1	6
2011	1	1	—	—	2	—	4
2010	1	1	2	—	—	—	4
2009	—	2	—	—	2	1	5
2008	1	2	—	—	—	—	3
2007	—	4	—	—	1	2	7
2006	—	1	1	1	2	2	7
2005	1	1	2	—	2	1	7
Before 2005	4	14	4	5	7	4	39
Total	23	33	12	9	31	13	121

symptoms. Poor IEQ enhanced the probability of taking sick leaves due to regular ill-health [49–51]. Significant absenteeism affects student's results, which, in turn, affects them psychologically. Kumar et al. [52] discussed various sensing technologies to enhance the IEQ in buildings. By using intelligent systems, school buildings can easily increase the IEQ. In the joint India-UK project, "Learn-BPE" [53], researchers have performed an occupants' survey to assess the indoor quality in ten buildings including one educational building. The researchers pointed out that IEQ must be given prime importance while designing buildings or retrofitting old ones. There are global opportunities for conducting IEQ

research in school buildings, especially in naturally ventilated (NV) school buildings, as students show significant adaptive behavior according to the indoor environmental changes.

2.2. Components of Indoor Environment. In this study, ventilation is considered as part of IAQ and daylighting as part of visual comfort (VC). The main four IEQ components are depicted in Figure 4 and discussed in this section concerning NV classrooms in school buildings.

2.2.1. Thermal Comfort in Naturally Ventilated Classrooms. Building user satisfaction with an indoor thermal environment is known as thermal comfort. According to the American Society of Heating, Refrigerating and Air-Conditioning Engineers (ASHRAE) Standard 55 [32], thermal comfort is the state of mind that expresses the satisfaction level of the building user with thermal surroundings inside the building. Langevien et al. [54] described that the three ways to assess human responses to comfort are thermal sensation, thermal acceptability, and thermal preferences. The perception of a building user regarding thermal surroundings is the user's thermal sensation. The degree up to which a building user accepts thermal surroundings is thermal acceptability. The ideal thermal environment according to the building user is the thermal preference of the user.

In India, National Building Code, 2016 [30] climate classification is used for the research while at a global scale most of the researchers use Koppen climate classification system. NBC climate classification is based on temperature and humidity levels. Koppen system is based on the coolest and the warmest month temperatures and precipitation criteria [55]. The general classification criteria of both the systems are jotted down briefly in Table 3.

Thermal comfort depends on six parameters, out of which four are environmental parameters such as relative humidity, air speed, mean radiant temperature, and dry bulb temperature. Two personal parameters that majorly affect thermal comfort are metabolic rate and clothing [56]. In addition, four localized factors are also considered nowadays while assessing thermal comfort; these are vertical air temperature difference, radiant temperature asymmetry, floor temperature, and drafts [57]. Age, gender, race, individual condition, geographic location, cultural impact, type of work, and climate are various other factors that affect the occupant perception about thermal sensation [58, 59].

Pinto et al. [60] explain the relationship between ventilation and thermal comfort in a naturally ventilated school building. However, according to the authors, most of the teachers prefer a closed window to control outside noise and extra heat coming inside from the open window in NV schools. Wargocki and Wyon [61] discussed the impacts of the thermal environment over teaching and distraction in a naturally ventilated classroom. Performance and wellbeing are reduced due to poor thermal surroundings. Bargh and Shalev [62] presented that experiencing "physical warmth" can increase the positive feelings of occupants and, thus, potentially increase the performance.

Thermal comfort is also influenced by the behavioral adjustment and the physiological and psychological dimensions of the occupant. There are various models, indices, and charts to assess thermal comfort, such as Predicted Mean Vote (PMV), Resultant Temperature (RT), Effective Temperature (ET), Adaptive Model, Tropical Summer Index (TSI), Heat Stress Index (HSI), Wet-Bulb Globe Temperature (WBGT), Equatorial Comfort Index (ECI), Index of Thermal Stress (ITS), Wind Chill Equivalent Temperature (WCET), Predicted 4 Hour Sweat Rate (P_4SR), India Model for Adaptive Comfort (IMAC), Percentage People Dissatisfied (PPD), Humidex, Standard Effective Temperature (SET), Predicted Thermal Sensation (PTS), and the Givoni model, the Mahoney model, and the Olgyay model.

Two models are used widely to assess thermal comfort. For conditioned buildings, PMV/PPD model given by P. Ole Fanger in 1970 is generally used. For nonair-conditioned buildings, the Adaptive model given by Richard J. de Dear [57] is used. The Adaptive model is based on real-time field studies, i.e., hundreds of studies showing the dynamic relation between the occupant adjusting the thermal environment by means of clothing, fans, operable windows, sunshades, etc.

Comfort estimation is more precise in adaptive approach, as it considers adaptations during the change in the thermal environment as the human body tries to maintain its temperature [63]. In NV schools, the adaptive model is the most suitable model to assess thermal environmental conditions.

International Organization for Standardization code ISO 7730 [33] is based on the PMV model. The limitation of the PMV model is that it is a chamber-method-based study and is not suitable for natural human interaction with the surroundings. It predicts a high level of dissatisfaction due to a lack of personal, social, cultural, and climate context.

Tropical Summer Index (TSI) is the index proposed by Sharma and Ali [64] to find the thermal comfort level along with the optimum conditions and range of thermally acceptable surroundings in warm-humid and hot-dry Indian climate. The Standard Effective Temperature (SET) model or Pierce 2-node model is another model developed by A.P. Gagge [65]. This model represents the human response to the thermal surroundings. This model's calculation is the same as the PMV model; the main difference is that it considers human physiology in measuring skin wettedness and temperature. ASHRAE accepted this model in 1996. However, later research tested this model with experimental data and explored that it underestimates skin wettedness and overestimates skin temperature.

Occupants living in NV buildings have a wider range of comfort temperature than the occupants living in air-conditioned buildings. Occupants overestimate and underestimate the thermal comfort, respectively, in warm places and cold places when using the PMV model. The adaptive model chart is based on extensive field studies throughout the globe which relates inside comfort temperature to prevailing outside temperature and defines 80% and 90% satisfaction zones.

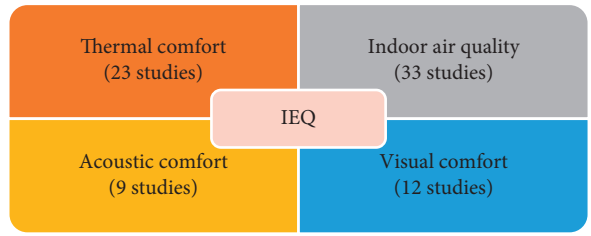

Figure 4: IEQ components and studies considered for review.

Table 3: Global and Indian climate classification.

Region	Major climate group	Temperature (warmest month)	Temperature (coolest month)
Global, according to Koppen–Geiger Theory [55]	Tropical	>18°C	>18°C
	Dry	≥18°C	≤0°C
	Temperate	≥10°C	≥ −3°C and <18°C
	Continental	≥10°C	≤ −3°C
	Polar and alpine	≤10°C	≤0°C
	Highland	Temperature is highly dependent on adjacent zone traits and overall elevation	
Region	Major climate zone	Mean of monthly temperature	Mean of monthly relative humidity
Asia (India), according to NBC 2016, India [30]	Hot and dry	>30°C	<55%
	Warm and humid	>30°C > 25°C	>55% > 75%
	Temperate	25–30°C	<75%
	Cold	<25°C	All values
	Composite	When 6 months or more do not fall in any of the categories	

Fanger [66] gives an equation that is related to PMV to assess the percentage of the dissatisfied, known as the PPD (Predicted Percentage of Dissatisfied) model. More than 80% of people satisfied included population resulted as a satisfactory outcome for the PPD model. Draught sensation is due to the increased air velocity, and it can have both positive and negative effects on thermal comfort depending on the conditions. In normal conditions, draught sensation due to increased air flow rate can cause localized thermal dissatisfaction, but in warm conditions, it improves comfort. The draught model was included in ISO 7730 [33] and ASHRAE 55 [32]. Draught rating is the percentage of people dissatisfied with the air flow. India Model for Adaptive Comfort (IMAC) is prepared based on data collected from office buildings and does not consider other types of buildings. Manu et al. [67] stated that Indian subjects are less sensitive to temperature changes because of their adaptive behavior.

ISO 7730 [33] considers Fanger's model while ASHRAE 55 [32] is majorly focused on the adaptive model. EN15251 [68] modified as European Committee for Standardization (CEN) EN 16798 : 2019 [34] considers Nicol and Humphreys work as their basis. However, there is no globally accepted code as yet for naturally ventilated school buildings. Hence, there is the need to develop a code on IEQ in naturally ventilated school buildings.

Bronsema [69] recommended a separate comfort temperature for summer and winter. For school buildings, Bronsema recommends 22.1°C in winter and 24.5°C in summer. The author explains the interaction between the thermal environment and the surrounding air quality. CEN/TC 156 technical report CR 1752–1998 suggested 23.5°C temperature in summer and 20°C temperature in winter for European schools as a comfortable temperature.

Seppanen and Fisk [70] did a meta-analysis of studies, which shows that SBS symptoms increase by 12% for every 1°C rise in temperature over 28°C. At 21.5°C, the occupant performance is optimal. However, temperatures less than 20°C and more than 23°C can affect the performance of the occupant by 10%.

Thermal comfort can impact the performance and wellbeing of occupants thus influencing their morale, and this simultaneously increases complaints regarding indoor conditions [71]. Nakano et al. [72] explained that high temperature impacts mathematical ability. By measuring brain-blood flow, it is found that due to mental load, the performance of teachers is reduced in high temperature. Some studies say that due to a lack of control over the thermal environment, absenteeism is increased, thus resulting in lower performance and achievement. Increased controls can increase thermal comfort. However, Melikov et al. [73] and Newsham et al. [14] found that access to such

controls did not increase or decrease thermal and visual comfort. Andersen [74] researched personal control of thermal comfort using ventilation and its impact on occupant comfort by using an online survey. Occupants feel more comfortable in any environment when they have the self-ability to control the environment. Occupants in NV buildings are more satisfied than occupants of mechanically ventilated buildings.

Singh et al. [75] tested 900 subjects in naturally ventilated classrooms for their behavioral adaptations. They found that in NV buildings, students are more adaptive in behavior and can easily modify their comfort by opening windows, switching-on fans, and changing clothing levels. Noda et al. [76] tested 6 classrooms in 3 schools for thermal comfort by both subjective and objective assessment. 97 students of age 9–11 years who participated in the study were having a wide range of comfort perception in the classroom. Singh et al. [77] reviewed previous literature on thermal comfort in classrooms. In India, most of the schools are naturally ventilated, and the students are quite adaptive in behavior. The authors have suggested preparing standards for different age groups and proposed thermal comfort equations based on the adaptive approach for classrooms.

2.2.2. IAQ in Naturally Ventilated Classrooms. Quality of indoor air is one of the most important components inside the built environment. The combined behavior of various factors and dynamic interaction with other components make it difficult for users to identify IAQ problems [78]. In the different indoor environments, there are different sources of pollution depending upon the building type (residential, school, office, market). Kamaruzzaman [79] studied workplace conditions and explained that most studies discuss reactive measures regarding IAQ and that very few studies describe the building construction and design to enhance IAQ. Except for indoor sources, outdoor pollution also affects the quality of indoor air. Bad IAQ can cause sick building syndrome (SBS) effects in the occupant, which in long term can be converted into building-related illness (BRI) and become harmful to one's health. Poor IAQ potentially influences the performance of students and teachers. A negative effect like sickness absence in school is common due to poor IAQ and inadequate ventilation.

Stetzenbach et al. [80] reported that air freshness can be measured by measuring suspended Particulate Matter (PM) and volatile organic compound (VOC) concentration indoors. Mendell and Heath [20] studied air quality, thermal comfort, and their impact on students' performance. More indoor humidity and increased organic pollutants are the reason behind increased respiratory illness and asthma. Heinsohn and Cimbala [81] explored the relationship between newer design solutions like underfloor air diffuser, displacement ventilation, and their impacts on indoor air pollution. However, maximum schools did not adopt these solutions. To improve IAQ, identification of the source of contamination, i.e., the flooring material type, paint on walls and desk, and equipment used in class, is important. These sources can affect children's health severely and increase the chances of respiratory illness and asthma.

Many schools use carpets to enhance the indoor air quality in classrooms. However, Fisk [19] found that removal of carpet from indoor can improve performance and potentially reduce the level of physical contaminants. Removing carpet resulted in better air quality and fewer headaches, dizziness, and SBS symptoms. Removal of carpet enhanced performance, i.e., 6.5% of text-typing amount, 3.1% on a timed test, and 3.8% score in logical reasoning. After self-assessment, it is found that reduced incidents of headaches are the reason for enhanced performance after removing the carpet. Tortolero et al. [82] examined carpets of 80 classrooms to test surface loading due to organic pollutants. 30% of the examined classrooms had an unacceptable level of insect and fungal allergens. Foarde and Berry [83] compared tiled floor classroom with carpet floor classroom. The tiled floor classroom had a higher concentration of aerosol particulate. The carpet floor classroom had a highly contaminant sink and high surface loading. Between teacher-student performance and the type of flooring, there are various acoustics and psychological differences. Bullock [84] found that in hard tiled floor classrooms students score higher in mathematics than in carpeted floor classrooms. However, out of 111 classrooms, only 5% of the classrooms had carpet; this limits the validity of the study.

Schneider [51] conducted a study using Chicago and Washington DC school teachers to find out the condition of the school environment, the relation between IEQ, and the impact on teachers' health. Referring to school facilities, most of the health complaints were related to air quality. More than 50% of teachers report a problem and one-third of the teachers have poor health conditions due to poor school environment. Kielb et al. [48] surveyed teachers of primary and secondary schools in New York State. Of 501 teachers, most of them say that classroom air quality is not good. Approximately, 40% of teachers reported at least one health symptom. Headaches, allergies, and throat irritation are the most common symptoms among them. Classrooms have at least two related symptoms, and the strong reasons are dust, mold, paint odors, and other indoor pollutants.

Wyon [21, 85] reported that poor air quality can influence worker comfort and potentially reduce performance by 6%. Lorsch and Abdou [86] reported that people feel more concentrated and comfortable when air conditioning is used. Performance of conditioned space user is increased between 5 and 15%. Without humidity control, teachers experience discomfort in the summer months. For an ideal learning environment, humidity control plays a crucial role in achieving better IAQ. Cross ventilation is generally responsible for maintaining the classroom environment in NV classrooms. Air enters through doors, windows, and cracks, and fresh air occupies the room volume, meanwhile stale air exits through the opposite side openings, if any. An illustration is presented in Figure 5 for a better understanding. A primary school classroom design for 40 students was drafted according to IS 8827–1978 [87]. According to the recommendation of the standard, the classroom of size (6100 mm × 7300 mm) has three ceiling fans. Each fan is of

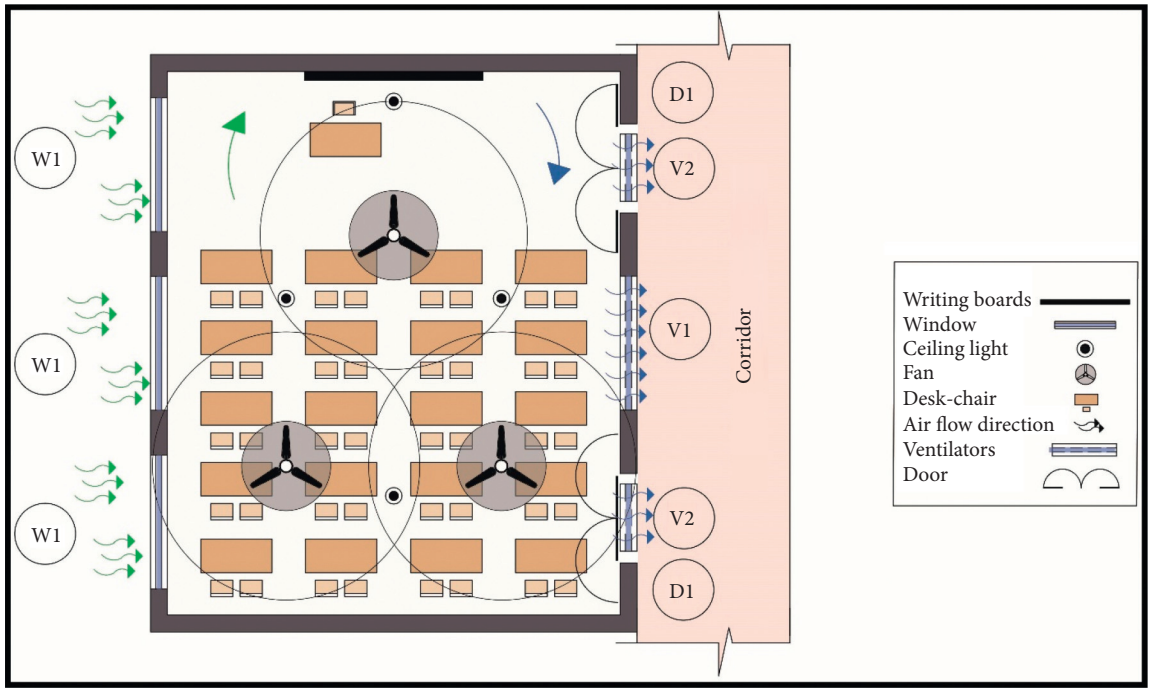

Figure 5: Air flow in the naturally ventilated classroom.

ø 1200 mm and effectively circulates air in the circle of ø 3600 mm, thus covering the whole occupied area of the classroom showing better air circulation inside. Windows (W1) of size 1800 mm × 1200 mm, ventilators of sizes {1800 mm × 600 mm (V1) and 1200 mm × 600 mm (V2) }, and door {1200 mm × 2100 mm (D1)} help in regulating fresh air from outside by replacing indoor stale air.

For controlling pollutants through the reduction approach, ASHRAE 62.1–2013 [76] specifies minimum outdoor air supply rates in buildings. Three liters per second per person outdoor air is the minimum requirement for classroom ventilation. Ventilation flow rate <0.152 m^3/s is termed as "Still Air"; this is harmful, as pollutants remain suspended in the air and occupants breathe them in, which can harm their health and result in discomfort. Technical report CR-1752 (1998) [88] developed by European committee CEN/TC 156 classifies ventilation change rate for classrooms, ranging from 0.47 to 1.18 cubic foot per minute/square foot into three categories, i.e., 15%, 20%, and 30% discomfort [89]. The values of the various gases for good indoor air quality for humans are mentioned in Table 4. The values can serve as a reference for NV classrooms as they are determined for residential buildings.

Bronsema et al. [69] developed a design guide to assess the performance of buildings for comfort and health. Based on the US EPA standard and World Health Organization (WHO) recommendation, upper limits of major and minor influential contaminants are decided. EPA recommended that PM_{10}must be lower than 150 $\mu g/m^3$ in 24 hours, while inhalable $PM_{2.5}$ must be restricted up to 35 $\mu g/m^3$ in 24 hours. However, the WHO recommends lower levels for PM_{10} ranging less than 20 $\mu g/m^3$. Occupational Safety and Health Administration (OSHA) and NIOSH determined a safe exposure range for different contaminants. NIOSH uses 10 hours' and OSHA uses 8 hours' exposure period for concentration limits [69].

According to the Indian Society of Heating, Refrigerating and Air Conditioning Engineers (ISHRAE) standard 10001 : 2019 [31], there are two ways to measure and monitor IAQ; in the first way, major IAQ parameters are tested two times in each season and three times a day (i.e., 9 : 00–11 : 00 AM, 12 : 00–2 : 00 PM, and 3 : 00–5 : 00 PM), a total of 18 results per year. All minor IAQ parameters are tested 2 times a year and 3 times a day, up to a total of 6 results per year. Microbial counts are tested 2 times a year. The second way suggests continuous monitoring of major IAQ parameters, i.e., a minimum of one reading per hour round the year and one reading for cross verification of the system—8760 results per year can be recorded. All the minor IAQ parameters are tested 2 times a year and 3 times a day—a total of 6 results per year are accumulated. Formaldehyde and microbial count can be tested in the first way. But this is not applicable to school buildings; therefore, there is a need to research and update the standards for school buildings.

Schweiker et al. [90] found that during a controlled study in a test chamber, subjects had higher skin temperature when windows are not operable. Subjects drank more water during that period possibly due to high air pollution inside. Barrett et al. [91] suggested that, for avoiding poor IAQ, glare, and overheating later, one must consider building orientation, shading design, devices, and the position and size of windows at the design stage. Heschong et al. [92] found that operable windows can enhance student performance and can achieve 7% better results in mathematics and reading than those in fixed window classrooms. Daisey et al. [93] reviewed many

Table 4: Air quality parameters and their suitable range.

Parameters		Suitable concentration			
		EPA	WHO	OSHA	Canadian
Major influential	CO_2	—	—	5000 ppm	3500 (L)
	CO	9 ppm	90 ppm [15 min]	50 ppm	11 ppm [8 h]
	$PM_{2.5}$	15 $\mu g/m^3$ [1 yr]	—	5 mg/m^3	0.1 mg/m^3 [1 h]
	PM_{10}	$\mu g/m^3$	—	—	—
	CH_2O (formaldehyde)	—	0.081 ppm[30 min]	0.75 ppm	0.1 ppm (L)
Minor influential	SO_2	0.03 [1 yr]	0.048 ppm [24 h]	5	0.019 ppm
	NO_2	0.05 [1 yr]	0.1 ppm [1 h]	5 ppm (C)	0.05 ppm
	O_3	0.12 [1 h]0.08	0.064 ppm [8 h]	0.1 ppm	0.12 ppm [1 h]

studies and found that by increasing natural ventilation, there is an increment of about 14% in speed and performance of the schoolwork. The review revealed that air quality in schools is very poor when compared to offices, as schools are neglected severely.

Haghihat and Donnini [94] reported that if temperature and ventilation conditions are under the direct control of building space users, less health symptoms, increased performance, and reduced absenteeism are some major outcomes. When air quality is enhanced due to controlled ventilation and temperature, the worker's performance increases up to 6.5%. However, sometimes energy consumption is also increased due to improved ventilation. However, if schools are properly designed initially, NV schools can save a lot of money along with providing much better comfort inside the classrooms. Yu et al. [95] established a fresh air system filter selection method and proposed a method to find out outdoor $PM_{2.5}$ concentrations.

2.2.3. Ventilation. Ventilation is the flow of outdoor air indoors for diluting the indoor air and increasing air quality primarily and for removing stale air inside. Ventilation is generally considered a part of Indoor Air Quality. Studies done in the past reported that carbon dioxide concentration is an IAQ indicator that depends on ventilation [96]. Ventilation also affects the thermal comfort inside a building by dehumidification of the space. According to ASHRAE 62.1 [37], ventilation supplies or removes air from indoors to maintain humidity, air contaminant levels, and temperature inside the occupied space.

Ventilation is divided into four types: (i) natural ventilation, (ii) mechanical ventilation, (iii) mixed-mode ventilation, and (iv) infiltration. However, the present review focuses on natural ventilation only, which is achieved by passive design and approaches like stack effect, wind pressure, and diffusion.

Kajtar et al. [97] experimented and found the effect of carbon dioxide on human health indoors and the effect of fresh air supply rate indoors. Poor ventilation increases carbon dioxide concentration in the classroom. Based on ventilation requirement in schools, UK Building Bulletin 101 [98] recommend that the average concentration of carbon dioxide during operational hours in school should not exceed 1500 ppm. It also sets out the minimum supply rate of 3 liters/second per person fresh air in the classroom. Shaughnessy et al. [99] examined one classroom among 87 schools for their carbon dioxide levels. The study shows that test scores improved with more ventilation. Croome et al. [100] explained that occupants frequently complain about odors and carbon dioxide but complain less about higher organic pollution and poor ventilation rates indoors. Building users change their behavior, feel uncomfortable, and sometimes show ill-health symptoms without realizing that these are due to ventilation rate and air quality [81].

Shendell et al. [101] nudge the idea of IAQ relation with ventilation through the concentration of carbon dioxide present indoors. Poor ventilation and bad IAQ is the reason behind absenteeism in schools. They found that absenteeism is increased by 10–20% when carbon dioxide is above 1000 ppm due to poor ventilation rates. Poor ventilation is the major cause of absenteeism and influences the outcomes of the education system negatively by affecting teachers and students. Wargocki and Wyon [61] found that adequate ventilation rates can reduce stress. Fresh air reduces stress; students feel less hunger in properly ventilated classrooms. Performance is severely affected by air flow rates in classrooms. Liang et al. [56] studied on indoor carbon dioxide level as an indicator for ventilation requirement. Ventilation rates could not be predicted accurately on the basis of the carbon dioxide concentration they added. Araya [102] found that natural ventilation is not a good ventilation technique for schools situated at polluted locations.

Haghighat and Donnini [94] studied air distribution techniques and ventilation control display. The relationship between IAQ and ventilation is complex; however, greater comfort with IAQ is perceived by building occupants for a higher ventilation rate. Demand Control Ventilation (DCV) products are available readily in the market for CO_2-based ventilation purposes, but updates are required. ASHRAE [37] codes are used for designing ventilation systems globally. Peng et al. [103] proposed an integrated low-energy ventilation (ILEV) system for primary schools in cold regions. ILEV can increase indoor air quality by using plants in sunspaces for absorbing CO_2. ILEV also increases thermal comfort inside classrooms with saving of approximately 88% energy and providing economic benefits up to 42 years with 8 years payback period. However, this study majorly focused on plant's ability in classrooms, which depends upon various assumptions. Sunlight is low in cold climates, which can

potentially reduce the photosynthesis speed in plants. Most of the educational buildings in India work on natural ventilation and some are using mixed-mode ventilation techniques. Therefore, there is a need to develop code/guidelines for NV school buildings.

2.2.4. Visual Comfort in Naturally Ventilated Classrooms. Good visual environment provides comfort due to the adequate level of task visibility and lack of strain on the occupant's eyes. Visual comfort is essential for productivity and health [104–106]. According to EN 12665, 2002 [35], visual comfort is "a subjective condition of visual wellbeing induced by the visual environment."

Research shows that daylighting enhances occupant productivity, reduces stress, and is advantageous for an occupant's wellness [107]. Daylight is also associated with the positive attitude of an occupant, negligible eye strain, reduced fatigue, and lower error and defects in work. Alrubaih et al. [108] described two types of natural daylighting systems in buildings. Window opening is an example of a side lighting and skylight or any other opening in the building roof is used for providing top lighting.

Lighting design standards in India are National Building Code (NBC) 2005 (Part 8, Section 1) [109], SP-41 [29], IS: 2440 [110], and IS: 7942 [111]. Illuminating Engineering Society of North America (IESNA), International Organization for Standardization (ISO), Commission Internationale de l'Eclairage (CIE), Association Argentina de Luminotécnia (AADL), and many others are some bodies that provide international standards. UK Building Bulletin 90 [112] guides to create a good lighting design for schools. In six sections, the Bulletin covers most aspects from lighting design to integration of artificial lighting and natural daylight. It sets out the standard maintained Illuminance of 300 lux in the classrooms. Similarly, Jain et al. [113] have developed an android app for integrating natural daylight with artificial lighting for Improving Building Energy Efficiency of Residential and Commercial Buildings during the daytime in all Sky Conditions of the United Kingdom.

Abdou [114] discussed the effect on wellbeing, comfort, and performance due to the physical environment of lighting. Rice [115] explored that there is a difference in views; some people say that there is no effect of illuminance, color, and lighting on them, but others claim that their mood is directly impacted by these factors. Therefore, the performance of such people is affected severely due to variation in mood. Inadequate lighting can cause various mental and physical effects, thereby rendering the building as one of poor quality. Hanford and Figueiro [116] also supported the fact that illumination level, lighting spectral distribution, and design can potentially affect mood and thus the performance of building users. Ocvirk et al. [117] explained that bright colors and strong lighting can enhance the comfort and happiness of building users. Aries et al. [118] experimentally found that good control over lighting and bright lights can potentially improve occupant mood and thus performance. Therefore, classrooms must be designed to cater to all possible functions at all different levels to increase psychological benefits. Overall, classroom illumination is important for enhancing positive attitude in teachers and students rather than focused light on some areas in the classroom [119].

Nicol et al. [120]worked on daylight effects and effects of blinds on lighting. The outcome showed that those users who can control natural daylight easily are more comfortable in comparison to other users who are unable to control it. However, the illuminance level is not in adequate control according to the outside lighting level. The orientation of windows is important along with window control strategies for natural daylight [121]. Bessoudo et al. [122] found that the southern part of the building received more direct sunlight than the northern part. Therefore, to reduce glare problems associated with direct sunlight, southern facade windows need shading devices and more blinds than the northern sides in a building. More use of glass in building facade and poor design increases glare problems and thus increased blinds and shadings. This reduces natural daylight indoors and slowly artificial light usage is increased. This will lead to excessive energy consumption and increased carbon dioxide emission [123].

Most people prefer natural daylight over artificial light as it reduces stress levels and enhances health conditions. Good integration of both natural and artificial light can enhance the performance and productivity up to 15% and 20–26%. Ashok Kumar et al. [124] have developed an android app for integrating daylight with artificial lighting for improving building energy efficiency during daytime in all climates for India.

Ghisi and Tinker [125] proposed a method to find out the energy-saving potential when daylight was used; their results showed 11%–86% of reduction in electricity consumption for lighting due to daylight.

Solar heat gain and daylight glare produce ill effects; on the other hand, dynamic lighting spectrum and outside view influence building users positively [126]. Hathaway [127] connected natural daylight with the performance of building users in the school. The visual environment of the classroom affects the learning, attendance, and thus performance of students and teachers. Rice [115] found that when teachers and students can easily control their lighting environment, they feel that a more positive and adjusted, appropriate level of lighting helps them in increasing their performance. However, Lewy et al. [128] found that during summers, surplus sunlight illuminance can create uncomfortable conditions for students and teachers in classrooms. Aries et al. [118] pointed out that there are fewer scientific studies around the globe that are well documented and have statistically proven the relation between daylight and associated health effects, especially depression. In a building occupant survey in Bhopal, people consider daylight and lighting a more important component of IEQ [129]. The human eye can adapt to changes quickly, but effects like disturbance while working, stress, and eye damage can occur due to frequent change in natural light intensities. Simultaneously, artificial light is also dangerous for human health, as it contains ultraviolet rays. Eyestrain, fatigue, and frequent headaches are general symptoms caused by poor artificial lighting [92].

For better learning outcomes, there must be controlled daylight and adequate artificial lighting in the whole classroom equally. Eyestrain, headaches, fever, and muscular pain are common symptoms due to a lack of lighting design and control [119]. Reinhart focused on luminance ratio as an important factor while designing light. Luminance ratio is the ratio between the darkest and the brightest points in an area. For safety when performing various tasks, a minimum level of illuminance, defined by various building and lighting codes, is required. NBC, 2016 [30] prescribes the minimum illuminance levels (200 lux) in classrooms. A general illustration of natural daylight and artificial lighting in a naturally ventilated classroom is shown in Figure 6. The classroom shown in Figure 6 will have sunlight during morning and afternoon times through windows and doors. Thus, one can easily save energy by reducing artificial lighting in the classroom. Morning daylight will provide excellent light and generate low heat, which is healthy for occupants.

Daylight harvesting is one of the best solutions to save 10% of energy, which is utilized in artificial lighting. Li et al. [130] designed and analyzed an active daylight harvesting system for utilizing daylight. Occupancy sensors, time scheduling, daylight dimming, bi-level switching, and demand lighting are the various types of lighting control.

Common lighting strategies are scheduling, tuning, daylighting, lumen maintenance, demand limiting, and adaptation compensation. By choosing the proper strategy and control system, one can reduce the lighting load of a building. There are very limited studies around the globe that show the relationship between artificial light, daylight, and associated comfort along with long- and short-term health impacts in school buildings.

2.2.5. Acoustic Comfort in Naturally Ventilated Classrooms. Acoustic comfort is the quality of the building to safeguard its inhabitants from surrounding noises and offer them a better acoustic environment in which they can easily communicate without any extra effort. Generally, occupants have minimum control over indoor acoustic conditions and their sources. People living in noisy indoors may feel stress, hypertension, rage, sleep disturbances, ear-aches, etc., and generally be more irritable and talk loudly as being habitual to shouting [131–133]. Hearing sensitivity is impacted by sound pressure waves. Physical characteristics of sound, source distance, and space conditions are the major factors that affect sound quality. Major space conditions are sound absorption, reverberation time, and insulation. Receiver conditions and age also play a vital role in hearing and thus mutate their perceptions regarding the surrounding environment [134, 135].

Studies in Germany show that occupants with low income are prone to acoustic discomfort more than high-income group occupants [136]. Occupants can have concentration impairment issues and other mental problems when they are continuously exposed to noises. Acoustic comfort directly affects occupant's productivity, comfort, and health [137, 138]. UK building bulletin 93 [139] is focused on the acoustic design of schools. It describes the minimum acoustic performance standards in school buildings for a better teaching and learning experience. It sets out the upper limit of 35 dB for the indoor ambient noise level of new build classrooms.

The current education system is using the digital mode of teaching in which different audio affects listeners in different ways as the perception and physiological mechanism of every listener is different. Bad acoustics can result in reduced teacher and student performance, less student focus, tiredness in listeners, and low quality of communication. According to Tiesler et al. [140], it is very difficult for students and teachers to ignore the unwanted sound and background noise. In the sitting position, it is difficult for teachers to gain the attention of the class as voice is depressed by the various indoor and outdoor noises. The depression of the teacher's voice increased for students sitting at distant positions as distance influences sound pressure level [141]. To cater to the needs of the classroom, teachers generally teach in a standing position to effectively convey their lessons and gain proper attention from the students sitting in the classroom. Indoor-outdoor noises decay the quality of teacher's voice up to some extent; Figure 7 is illustrating the noise scenario. Noise is coming from outer sources by infiltration from windows, vents and doors, and indoor sources such as students talking to each other during the lecture.

Serra and Biassoni [142] revealed that higher cost impacts the acoustic quality in US schools. Acoustic problems must be considered during the design stage of a building and for that, it is essential to access and define as to what is going to happen outdoors and indoors [143, 144]. For human hearing, 20–20,000 Hz is the comfortable sound range. For clear communication and normal speech, the background noise level must be less than 45 dB in educational buildings. Reverberation time must be between 0.6 and 0.8 for better listening in theoretical classrooms. For the acoustic design of schools, the American National Standards Institute ANSI/ASA S12.60–2010/Part-1 standard [38] recommends that background noise must be limited to 35 dB in school buildings and a reverberation time of 0.60 seconds.

Acoustic comfort is the least researched component among the major components of IEQ in India. Proper testing and evaluation of noise need to be performed at the building site before construction, and the results after the construction need to be verified to create some index or model to predict the noise, particularly along highways and noisy places. Thus, there is a need to carry out further research in this domain.

2.3. Impact of COVID-19 on School Buildings. Due to the COVID-19 pandemic, most of the governments temporarily closed schools in an attempt to reduce the spread of COVID-19. Currently, more than 60% of students enrolled globally in level 0 to level 3 (International Standard Classification of Education) are affected [145]. At the global peak of COVID-19, from 30 March 2020 to 05 April 2020, 91.3% (more than

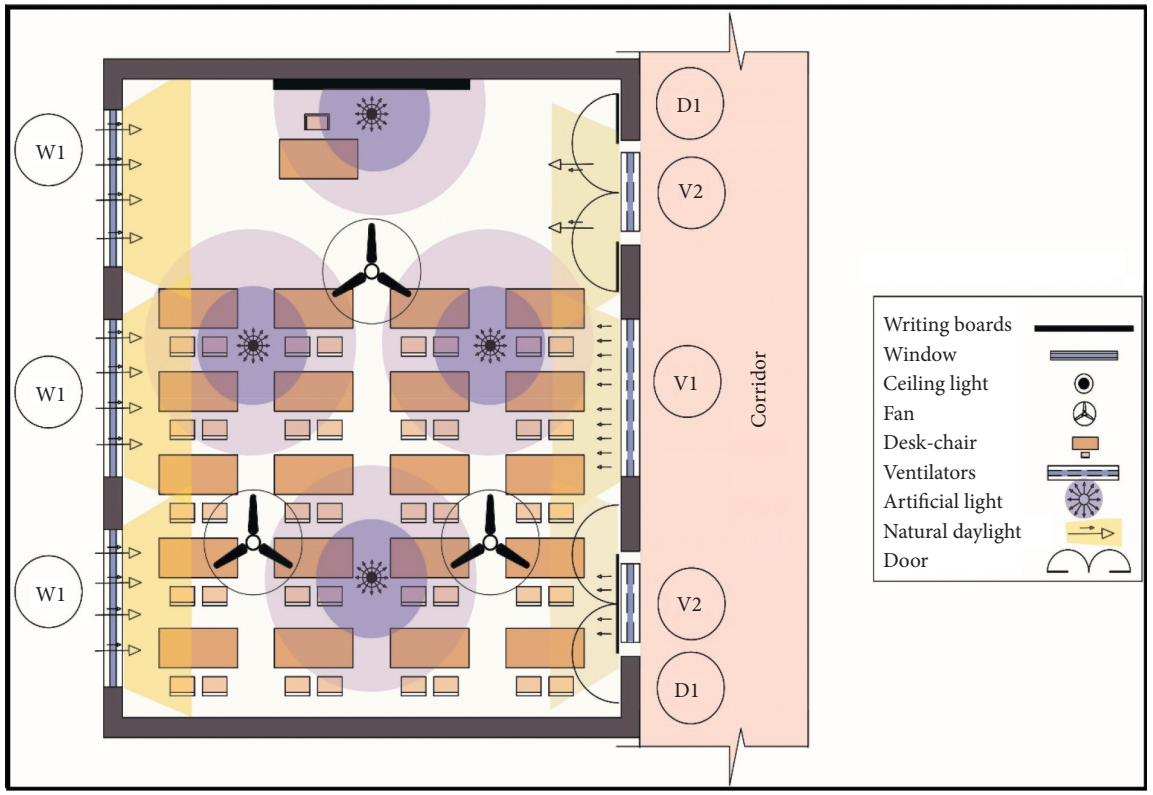

Figure 6: Lighting in a naturally ventilated classroom.

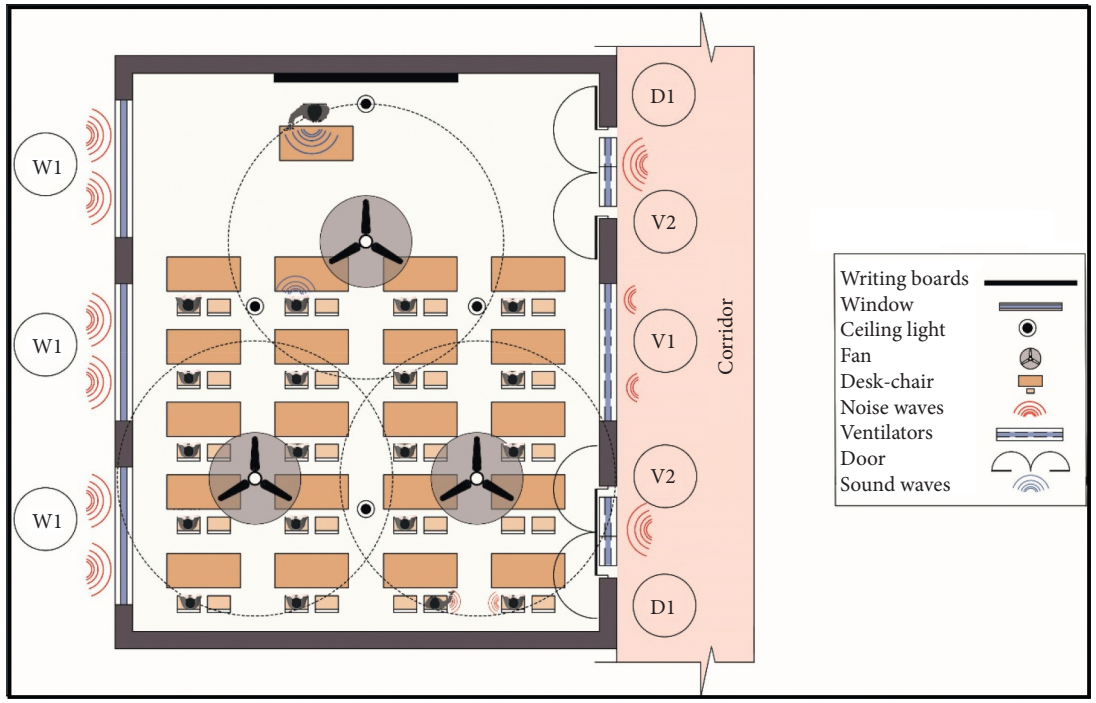

Figure 7: Sound interrupted by indoor-outdoor noise in the naturally ventilated classroom.

1.5 billion students) of the total enrolled learners are affected across 194 countries due to the lockdown situation. The primary health concern is to prevent the spread of COVID-19; however, due to the disrupted education system, every government wants to reopen schools as soon as possible. For considering the stakeholder's consent, it is essential to quickly gather information and perform rapid response surveys. An UNESCO report [145] points toward "How to

Reopen Schools," considers 6 key dimensions, out of which 2 dimensions are wellbeing/protection and learning, and these depend upon IEQ. As COVID-19 is spreading through contaminated air, natural ventilation is not good for classrooms. Currently, there is no study related to COVID-19 impact on the school classroom. Some regulatory bodies [146, 147] emphasize on maintaining good IEQ to reduce the spread of COVID-19 in the current situation, but they are not specifically for school buildings. Thus, it is important to carry out research, particularly for school classrooms, as students are the most vulnerable group in the current situation.

3. Discussion and Conclusion

This paper presented a systematic review of the studies around the globe related to indoor environmental quality components, namely, thermal comfort, indoor air quality, ventilation, visual comfort, daylight, and acoustic comfort in naturally ventilated school classrooms. SBS and BRI are also discussed in brief for a better understanding of the need for IEQ in naturally ventilated school buildings. It is found that there are no globally accepted codes and Indian standards till date that can serve as the basis for maintaining/providing good IEQ in NV school classrooms. Present conditions indicate that there is a dire need for more scientific efforts to achieve more accurate comfort limits. A more precise and accurate methodology is needed to standardize the process conforming to all types of climates.

Although some codes separately deal with individual components or with multiple components, comfort limits vary widely in different standards. Therefore, more studies are needed to explore the IEQ in NV school classrooms worldwide for developing country-specific guidelines. In India, the studies on IEQ are scarce and scattered.

Therefore, country-specific IEQ codes and guidelines in relation to naturally ventilated school buildings need to be developed. To accomplish this, a real-time assessment of IEQ and comfort in NV classrooms is essential.

Similarly, poorly ventilated buildings and systems enhance the risk of indoor virus transmission. Airborne transmitted diseases in the form of aerosols (nuclei droplets), such as MERS (Middle East Respiratory Syndrome), SARS (Severe Acute Respiratory Syndrome), and COVID-19, have confirmed that in the future these kinds of viruses will be a great danger. In general, there are two routes of infection spread in closed spaces. First, aerosol generated by the infected person is directly inhaled by the exposed person. This occurs when the distance between the infected person and the exposed person is less than 1.5 m. Second, aerosol generated by the infected person's activities (like sneezing, coughing, etc.) is mixed in the room air and with air flow; the droplet nuclei travel and enter into the system of the exposed person. This occurs for large distances, generally greater than 1.5–2.0 m [148, 149]. Moharir et al. [150] found that if the distance is more than 2.5 m and the contact time between any COVID-19 patient and an exposed healthy person is less than 20 minutes inside a room, the chances of virus transmission through the air is low. Figure 8 shows the reduction of infection with an increase in the distance between the infected and the healthy person.

The transmission of Corona virus in the school buildings is a challenging issue and there is no proper evidence to prevent the transmission of this type of pandemic inside naturally ventilated school buildings. The researchers are trying to find solutions for controlling the transmission of Corona virus among humans and to find escape routes/technologies to save the students' lives if the virus has entered the buildings. Some researchers are working on finding ways to prevent the transmission of Corona virus from infected humans due to inhalation of airborne particles indoors. Therefore, the best way to escape from the Corona virus inside the buildings is to bring in fresh air after proper filtration and remove the infected inside air through an exhaust (ventilation) into open space via ducts, etc. Many air filters are available to prevent the polluted air to filter out the $PM_{2.5}$ particles, etc. The existing air filtration techniques are not suitable to filter out the Corona virus because the virus size is less than 0.1 nm and most of the available air filters' porosity is approximately 0.3 nm. Therefore, the prevention strategy during COVID-19 in naturally ventilated school buildings is also to be developed.

Students are the future of any country; it is, therefore, essential to provide them a healthy and comfortable learning environment. This article is a primary step in this direction. A schematic diagram of the proposed filtration system for a naturally ventilated classroom is depicted in Figure 9.

The following conclusions can be drawn from the review:

(i) There are many international studies on IEQ; however, there are very few studies for naturally ventilated Indian school buildings.

(ii) Comfort temperature among the subjects varies largely; so, for better prediction, it is necessary to develop a country-specific comfort model for school buildings.

(iii) None of the studies tried to find out the interrelation between different components of comfort in school buildings. Most of the studies consider different seasons but a few studies consider the whole year; as temperature varies throughout the year, it is necessary to consider daily, weekly, monthly, and seasonal changes.

(iv) There are fewer IEQ studies reported in developed countries. Achieving SDG's 4th goal is not enough; IEQ must be considered as an important component in developing the education system, and stakeholders must be trained and informed regarding this.

(v) Hawthorne effect is neglected in most of the studies. Few multi-factor studies are available relating to IEQ parameters. So it is very difficult to comment on the combined effect of parameters on students in school classrooms. Therefore, there is a need to develop a methodology for the combined impact of the parameters on IEQ.

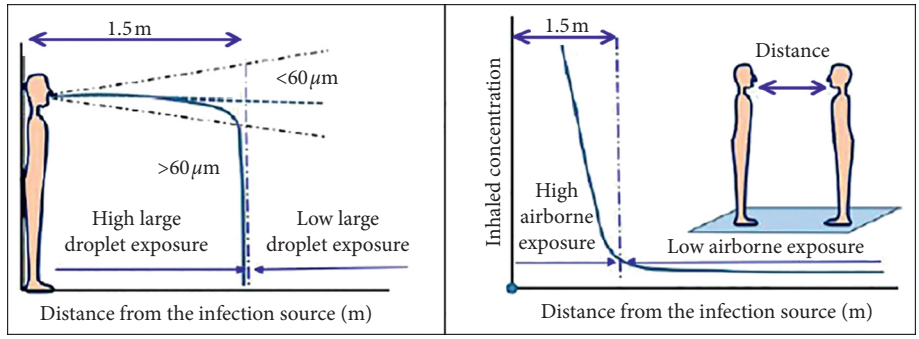

Figure 8: Short-range, close contact, and long-range exposure of droplets and droplet nuclei (source: [151]).

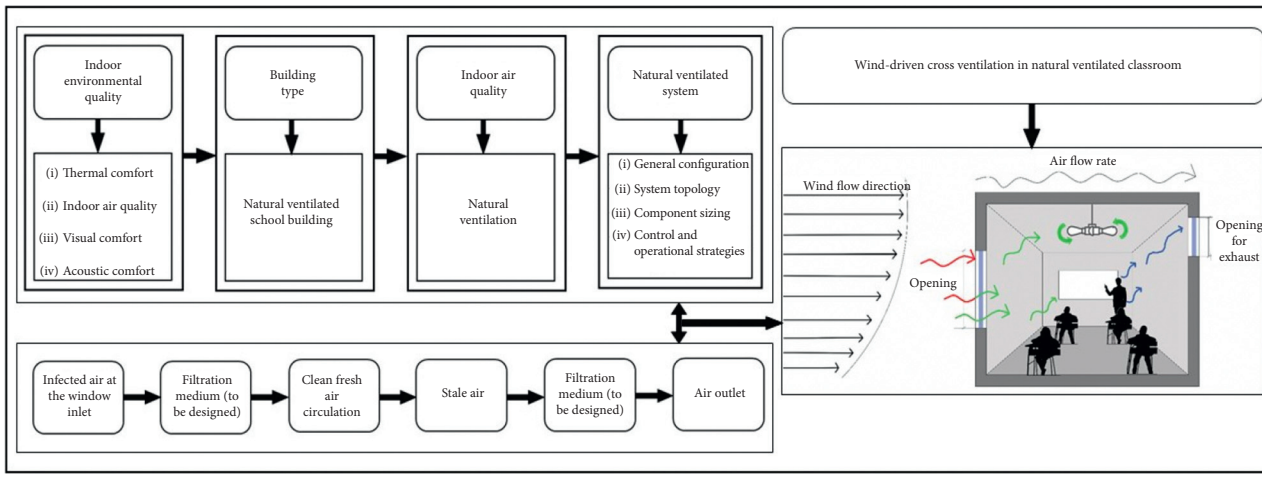

Figure 9: Schematic diagram of the proposed filtration system for an NV classroom.

(vi) Different authors adopt different methods for assessing the performance of students; therefore, it is hard to compare as our results and the results of different studies vary significantly. Therefore, there is a need to develop a generic universal methodology on this.

(vii) Less attention is given to acoustic and visual comfort in school buildings; however, a few studies consider the comfort components and found that they are equally important when the focus of the study is on performance and productivity. The standard procedures and well-accepted models of different comfort components are much-needed aspects of school IEQ. Therefore, there is a need to develop a generic methodology/guidelines for acoustic and visual comfort in school buildings.

(viii) No well-accepted code or standard comfort criteria exist for naturally ventilated school buildings. A few studies combine energy efficiency with the IEQ in educational buildings but not particularly in naturally ventilated school buildings. Therefore, there is a need to develop adaptive comfort models/algorithms for NV school buildings.

3.1. Future Direction

(i) All the existing schools and other types of buildings need to be retrofitted for improving IEQ and comfort. This requires the development of guidelines and the authors are researching on this.

(ii) For the design and construction of new buildings, a special publication as an Annexure to the National Building Code or a separate document is required. The authors are working on the preparation of the guidelines.

(iii) Similarly, for air-conditioned schools and other buildings, the strategies for air-decontamination are immediately required. Therefore, the authors are researching in this direction to prevent the spread of coronavirus or similar types of viruses that can prevail in the future, in different types of buildings including malls, auditoriums, and offices.

Disclosure

The work reported in this article forms a part of the AcSIR Ph.D. work of the first author being carried out at CSIR-CBRI, Roorkee. The article is published with the permission

of the Director, CSIR-Central Building Research Institute, Roorkee.

Conflicts of Interest

The authors declare that there are no conflicts of interest regarding the publication of this paper.

Acknowledgments

The authors thank Garima Bhanot and Simran Taneja for preparing the figures and drawings in this study. This research was funded by the Department of Science and Technology (DST), New Delhi, India.

References

[1] N. E. Klepeis, W. C. Nelson, W. R. Ott et al., "The National Human Activity Pattern Survey (NHAPS)," *Journal of Exposure Analysis and Environmental Epidemiology*, vol. 11, no. 3, pp. 231–252, 2001.

[2] S. Brasche and W. Bischof, "Daily time spent indoors in German homes - baseline data for the assessment of indoor exposure of German occupants," *International Journal of Hygiene and Environmental Health*, vol. 208, no. 4, pp. 247–253, 2005.

[3] National Building Code of India, *Part-4 Fire and Life Safety*, Bureau of Indian Standards, Delhi, India, 2016.

[4] V. D. Giuli, O. D. Pos, and M. D. Carli, "Indoor environmental quality and pupil perception in Italian primary schools," *Building and Environment*, vol. 56, pp. 335–345, 2012.

[5] A. Lizzio, K. Wilson, and R. Simons, "University students' perceptions of the learning environment and academic outcomes: implications for theory and practice," *Studies in Higher Education*, vol. 27, no. 1, pp. 27–52, 2002.

[6] A. Karapetsis and E. Alexandri, "Indoor environmental quality and its impacts on health – case study: school building," in *Proceedings of the EinB2016 – 5th International Conference "Energy in Buildings*, Botanique, Greece, November 2016.

[7] M. C. Lee, K. W. Mui, L. T. Wong, W. Y. Chan, E. W. M. Lee, and C. T. Cheung, "Student learning performance and indoor environmental quality (IEQ) in air-conditioned university teaching rooms," *Building and Environment*, vol. 49, pp. 238–244, 2012.

[8] C. J. Beemer, K. A. S. Yoder, S. J. Schuldt et al., "A brief review on the mental health for select elements of the built environment," *Indoor and Built Environment*, pp. 1–14, 2019.

[9] S. Choi, D. A. Guerin, H.-Y. Kim et al., "Indoor environmental quality of classrooms and student outcomes: a path analysis approach," *Journal of Learning Spaces*, vol. 2, no. 2, 2013.

[10] National Institute for Occupational Safety and Health, *NIOSH 2013 CDC-Indoor Environmental Quality-NIOSH Workplace Safety and Health*, Center for Disease Control and Prevention, Atlanta, GA, USA, 2013.

[11] H. Fromme, D. Twardella, S. Dietrich et al., "Particulate matter in the indoor air of classrooms-exploratory results from Munich and surrounding area," *Atmospheric Environment*, vol. 41, no. 4, pp. 854–866, 2007.

[12] S. E. Higgins, E. Hall, K. Wall et al., *The Impact of School Environments: A Literature Review*, The Centre for Learning and Teaching-School Education, University of Newcastle, Callaghan, Australia, 2005.

[13] S. M. Kennedy, M. Hodgson, and L. D. Edgettet, "Subjective assessment of listening environments in university classrooms: perceptions of students," *Journal of the Acoustical Society of America*, vol. 119, no. 1, pp. 299–309, 2005.

[14] G. Newsham, J. Brand, C. Donnelly, J. Veitch, M. Aries, and K. Charles, "Linking indoor environment conditions to job satisfaction: a field study," *Building Research and Information*, vol. 37, no. 2, pp. 129–147, 2009.

[15] P. Temple and O. Filippakou, *Learning Spaces for the 21st Century: A Review of the Literature*, Thesis, University of London, London, UK, 2007.

[16] J. C. Vischer, "The effects of the physical environment on job performance: towards a theoretical model of workspace stress," *Stress and Health*, vol. 23, no. 3, pp. 175–184, 2007.

[17] J. R. Carlopio, "Construct validitb by of a physical work environment satisfaction questionnaire," *Journal of Occupational Health Psychology*, vol. 1, no. 3, pp. 330–344, 1996.

[18] R. de Dear, J. Kim, C. Candido, and M. Deuble, "Adaptive thermal comfort in Australian school classrooms," *Building Research & Information*, vol. 43, no. 3, pp. 383–398, 2015.

[19] W. J. Fisk, "Health and productivity gains from better indoor environments and their relationship with building energy efficiency," *Annual Review of Energy and the Environment*, vol. 25, no. 1, pp. 537–566, 2000.

[20] M. J. Mendell and G. A. Heath, "Do indoor pollutants and thermal conditions in schools influence student performance? A critical review of the literature," *Indoor Air*, vol. 15, no. 1, pp. 27–52, 2005.

[21] D. P. Wyon and Wargocki, "How indoor environment affects performance," *Ashrae Journal*, vol. 55, no. 3, pp. 46–52, 2013.

[22] J. M. Seltzer, "Building-related illnesses," *Journal of Allergy and Clinical Immunology*, vol. 94, no. 2, pp. 351–361, 1994.

[23] P. S. Burge, "Sick building syndrome," *Occupational and Environmental Medicine*, vol. 61, no. 2, pp. 185–190, 2004.

[24] S. Joshi, "The sick building syndrome," *Indian Journal of Occupational and Environmental Medicine*, vol. 12, no. 2, pp. 61–64, 2008.

[25] P. Wargocki, D. P. Wyon, Y. K. Baik, G. Clausen, and P. O. Fanger, "Perceived air quality, sick building syndrome (SBS) symptoms and productivity in an office with two different pollution loads," *Indoor Air*, vol. 9, no. 3, pp. 165–179, 1999.

[26] T. Catalina and V. Iordache, "IEQ assessment on schools in the design stage," *Building and Environment*, vol. 49, pp. 129–140, 2012.

[27] Government of India, *National Education Policy-2020*, Ministry of Human Resource Development, New Delhi, India, 2020.

[28] A. Jindal, "Thermal comfort study in naturally ventilated school classrooms in composite climate of India," *Building and Environment*, vol. 142, pp. 34–46, 2018.

[29] Bureau of Indian Standards, *Handbook on Functional Requirements of Buildings (SP-41)*, Bureau of Indian Standards, New Delhi, India, 1987.

[30] National Building Code of India, *Bureau of Indian Standards*, National Building Code of India, New Delhi, India, 2016.

[31] Indian Society of Heating, *Refrigerating and Air Conditioning Engineers, Indoor Environmental Quality Standard (ISHRAE-10001)*, Indian Society of Heating, New Delhi, India, 2019.

[32] ASHRAE Standard 55-2010, *Thermal Environmental Conditions for Human Occupancy*, ASHRAE Standard 55-2010, Atlanta, GA, USA, 2010.

[33] ISO, *ISO7730:2005*, ISO, Geneva, Switzerland, 2005.

[34] European Standards, *Energy Performance of Buildings—Ventilation for Buildings—Part 1: Indoor Environmental Input Parameters for Design and Assessment of Energy Performance of Buildings Addressing Indoor Air Quality (EN16798-1)*, Comité Euroéen de Normalisa, Brussels, Belgium, 2019.

[35] European Standard, *Light and Lighting-Basic Terms and Criteria for Specifying Lighting Requirements (EN12665)*, Comité Européen de Normalisation, Brussels, Belgium, 2002.

[36] ISO, CIE, *Lighting of Indoor Work Places*, ISO, Geneva, Switzerland, 2002.

[37] American Society of Heating, *Refrigerating and Air-Conditioning Engineers, Ventilation for Acceptable Indoor Air Quality (ASHRAE62.1)*, American Society of Heating, Atlanta, GA, USA, 2013.

[38] American National Standards Institute, *American National Standard Acoustical Performance Criteria, Design Requirements, and Guidelines for Schools, Part 1: Permanent Schools (ANSI-ASAS12.60, Part 1)*, Acoustical Society of America, Melville, NY, USA, 2010.

[39] M. Schneider, *Do School Facilities Affect Academic Outcomes*, 2002.

[40] E. A. Hanushek and S. G. Rivkin, "Harming the best: how schools affect the black-white achievement gap," *Journal of Policy Analysis and Management*, vol. 28, no. 3, pp. 366–393, 2009.

[41] R. Becker, I. Goldberger, and M. Paciuk, "Improving energy performance of school buildings while ensuring indoor air quality ventilation," *Building and Environment*, vol. 42, no. 9, pp. 3261–3276, 2007.

[42] W. J. Fisk, Q. Lei-Gomez, and M. J. Mendell, "Meta-analyses of the associations of respiratory health effects with dampness and mold in homes," *Indoor Air*, vol. 17, no. 4, pp. 284–296, 2007.

[43] M. S. Jaakkola, R. Quansah, T. T. Hugg, S. A. M. Heikkinen, and J. J. K. Jaakkola, "Association of indoor dampness and molds with rhinitis risk: a systematic review and meta-analysis," *Journal of Allergy and Clinical Immunology*, vol. 132, no. 5, pp. 1099–1110, 2013.

[44] G. R. Passarelli, "Sick building syndrome: an overview to raise awareness," *Journal of Building Appraisal*, vol. 5, no. 1, pp. 55–66, 2009.

[45] D. Thivel, A. Tremblay, P. M. Genin et al., "Physical activity, inactivity, and sedentary behaviors: definitions and implications in occupational health," *Front Public Health*, vol. 6, no. 288, 2018.

[46] A. Jindal, "Investigation and analysis of thermal comfort in naturally ventilated secondary school classrooms in the composite climate of India," *Architectural Science Review*, vol. 62, no. 6, pp. 466–484, 2019.

[47] M. A. Mujeebu, *Introductory Chapter: Indoor Environmental Quality*, pp. 1–13, IntechOpen, London, UK, 2019.

[48] C. Kielb, S. Lin, N. Muscatiello, W. Hord, J. Rogers-Harrington, and J. Healy, "Building-related health symptoms and classroom indoor air quality: a survey of school teachers in New York State," *Indoor Air*, vol. 25, no. 4, pp. 371–380, 2015.

[49] N. E. Ebbehoj, H. W. Meyer, H. Wurtz et al., "Molds in floor dust, building-related symptoms, and lung function among male and female schoolteachers," *Indoor Air*, vol. 15, no. 10, pp. 7–16, 2005.

[50] J. Ervasti, M. Kivimaki, I. Kawachi et al., "School environment as predictor of teacher sick leave: data-linked prospective cohort study," *BMC Public Health*, vol. 12, no. 770, pp. 1–8, 2012.

[51] M. Schneider, "Linking school facility conditions to teacher satisfaction and success," ERIC publication reports-research, pp. 1–5, ERIC, Washington, DC, USA, 2003.

[52] A. Kumar, A. Singh, M. K. Singh, P. Mahanta, and S. C. Mukhopadhyay, "Sensing technologies for monitoring intelligent buildings: a review," *IEEE Sensors Journal*, vol. 18, no. 12, pp. 4847–4860, 2018.

[53] R. Gupta, M. Gregg, S. Manu et al., "Customized performance evaluation approach for Indian green buildings," *Building Research & Information*, vol. 47, no. 1, pp. 56–74, 2019.

[54] J. Langevin, J. Wen, and P. L. Gurian, "Modeling thermal comfort holistically: bayesian estimation of thermal sensation, acceptability, and preference distributions for office building occupants," *Building and Environment*, vol. 69, pp. 206–226, 2013.

[55] M. C. Peel, B. L. Finlayson, and T. A. McMahon, "Updated world map of the Köppen-Geiger climate classification," *Hydrology and Earth System Sciences Discussions, European Geosciences Union*, vol. 11, no. 5, pp. 1633–1644, 2007.

[56] H.-H. Liang, C.-P. Chen, W.-M. Shih, S.-C. Lo, and H.-Y. Liao, "Satisfaction of occupants toward indoor environment quality of certified green office buildings in Taiwan," *Building and Environment*, vol. 72, pp. 232–242, 2014.

[57] R. J. de Dear, T. Akimoto, E. A. Arens et al., "Progress in thermal comfort research over the last twenty years," *Indoor Air*, vol. 23, no. 6, pp. 442–461, 2013.

[58] G. A. Heath and M. J. Mendell, "Do indoor environments in schools influence student performance? A critical review of the literature," *Indoor Air Journal*, vol. 15, pp. 27–32, 2005.

[59] Z. S. Zomorodian, M. Tahsildoost, and M. Hafezi, "Thermal comfort in educational buildings: a review article," *Renewable and Sustainable Energy Reviews*, vol. 59, pp. 895–906, 2016.

[60] M. Pinto, R. Almeida, P. Pinho et al., "Experimental assessment of IAQ improvement in naturally ventilated educational buildings," in *Proceedings of the 40th IAHS World Congress on Housing Sustainable Housing Construction*, pp. 1–10, Funchal, Portugal, December 2014.

[61] P. Wargocki and D. P. Wyon, "Effects of HVAC on student performance," *ASHRAE Journal*, 2006.

[62] J. A. Bargh and I. Shalev, "The substitutability of physical and social warmth in daily life," *American Psychological Association Journal EMOTION*, vol. 12, pp. 154–162, 2012.

[63] L. Schellen, M. Loomans, M. de Wit, and W. van Marken Lichtenbelt, "The influence of different cooling techniques and gender on thermal perception," *Building Research and Information*, vol. 41, no. 3, pp. 330–341, 2013.

[64] M. R. Sharma and S. Ali, "Tropical summer index-a study of thermal comfort of Indian subjects," *Building and Environment*, vol. 21, no. 1, pp. 11–24, 1986.

[65] A. P. Gagge, A. P. Fobelets, and L. G. Berglund, "A standard predictive Index of human response to thermal environment," *Transactions/American Society of Heating, Refrigerating and Air-Conditioning Engineers*, vol. 92, no. 2B, pp. 709–731, 1986.

[66] J. V. Hoof, "Forty years of Fanger's model of thermal comfort: comfort for all?" *Indoor Air*, vol. 18, no. 3, pp. 182–201, 2008.

[67] S. Manu, Y. Shukla, R. Rawal, L. E. Thomas, and R. de Dear, "Field studies of thermal comfort across multiple climate zones for the subcontinent: India Model for Adaptive Comfort (IMAC)," *Building and Environment*, vol. 98, pp. 55–70, 2016.

[68] European Standards, *Indoor Environmental Input Parameters for Design and Assessment of Energy Performance of Buildings Addressing Indoor Air Quality, Thermal Environment, Lighting and Acoustics (EN 15251)*, Comité Européen de Normalisation, Brussels, Belgium, 2006.

[69] B. Bronsema et al., *Performance Criteria of Buildings for Health and comfort (Report of International Society of Indoor Air Quality and Climate*, International Council for Research and Innovation in Building and Construction (CIB) Task Group TG 42, CIB Number 192), The Netherlands, 2004.

[70] O. Seppanen and W. Fisk, "Some quantitative relations between indoor environmental quality and work performance or health," *HVAC&R Research*, vol. 12, no. 4, pp. 957–973, 2006.

[71] S. Barbhuiya and S. Barbhuiya, "Thermal comfort and energy consumption in a UK educational building," *Building and Environment*, vol. 68, pp. 1–11, 2013.

[72] J. Nakano, S.-i. Tanabe, and K.-i. Kimura, "Differences in perception of indoor environment between Japanese and non-Japanese workers," *Energy and Buildings*, vol. 34, no. 6, pp. 615–621, 2002.

[73] A. Melikov, G. Pitchurov, K. Naydenov, and G. Langkilde, "Field study on occupant comfort and the office thermal environment in rooms with displacement ventilation," *Indoor Air*, vol. 15, no. 3, pp. 205–214, 2005.

[74] R. V. Andersen, J. Toftum, K. K. Andersen, and B. W. Olesen, "Survey of occupant behaviour and control of indoor environment in Danish dwellings," *Energy and Buildings*, vol. 41, no. 1, pp. 11–16, 2009.

[75] M. K. Singh, S. Kumar, R. Ooka, H. B. Rijal, G. Gupta, and A. Kumar, "Status of thermal comfort in naturally ventilated classrooms during the summer season in the composite climate of India," *Building and Environment*, vol. 128, pp. 287–304, 2018.

[76] L. Noda, A. V. P. Lima, J. F. Souza et al., "Thermal and visual comfort of schoolchildren in air-conditioned classrooms in hot and humid climates," vol. 182, pp. 1–12, 2020.

[77] M. K. Singh, R. Ooka, H. B. Rijal, S. Kumar, A. Kumar, and S. Mahapatra, "Progress in thermal comfort studies in classrooms over last 50 years and way forward," *Energy and Buildings*, vol. 188-189, pp. 149–174, 2019.

[78] A. Szczurek, M. Maciejewska, and M. Wyłomańska, "Method to characterize collective impact of factors on indoor air," *Physica A: Statistical Mechanics and Its Applications*, vol. 420, pp. 190–199, 2015.

[79] S. N. Kamaruzzaman, C. O. Egbu, E. M. A. Zawawi et al., "The effect of indoor environmental quality on occupants' perception of performance: a case study of refurbished historic buildings in Malaysia," *Energy and Buildings*, vol. 43, no. 2-3, pp. 407–413, 2011.

[80] L. D. Stetzenbach, M. P. Buttner, and P. Cruz, "Detection and enumeration of airborne biocontaminants," *Current Opinion in Biotechnology*, vol. 15, no. 3, pp. 170–174, 2004.

[81] R. J. Heinsohn and J. M. Cimbala, *Indoor Air Quality Engineering: Environmental Health and Control of Indoor Pollutants*, Marcel Dekker, New York; Basel, NY, USA, 2003.

[82] S. R. Tortolero, L. K. Bartholomew, S. Tyrrell et al., "Environmental allergens and irritants in schools: a focus on asthma," *Journal of School Health*, vol. 72, no. 1, pp. 33–38, 2002.

[83] K. Foarde and M. Berry, "Comparison of biocontaminant levels associated with hard vs. carpet floors in nonproblem schools: results of a year long study," *Journal of Exposure Science and Environmental Epidemiology*, vol. 14, no. S1, pp. S41–S48, 2004.

[84] C. C. Bullock, "The relationship school building conditions and student achievement at the middle school level in the commonwealth of Virginia," Dissertation report, Virginia Tech, Blacksburg, VA, USA, 2007.

[85] D. P. Wyon, "The effects of indoor air quality on performance and productivity," *Indoor Air*, vol. 14, pp. 92–101, 2004.

[86] H. Lorsch and O. Abdou, "The impact of the building indoor environment on occupant productivity-Part 1-Recent studies, measures and costs. Part 2-Effects of temperature. Part 3-Effects of indoor air quality," *InFuel and Energy Abstracts*, 1995.

[87] Bureau of Indian Standards, *Recommendations for Basic Requirements of School Buildings (IS-8827)*, Bureau of Indian Standards, New Delhi, India, 1978.

[88] European Standard, Technical report (CR-1752-1998), Comité Européen de Normalisation, Brussels, Belgium, 1998.

[89] B. W. Olesen, "International standards for the indoor environment," *Indoor Air*, vol. 14, no. s7, pp. 18–26, 2004.

[90] M. Schweiker, S. Brasche, W. Bischof, M. Hawighorst, and A. Wagner, "Explaining the individual processes leading to adaptive comfort: exploring physiological, behavioural and psychological reactions to thermal stimuli," *Journal of Building Physics*, vol. 36, no. 4, pp. 438–463, 2013.

[91] P. Barrett, F. Davies, Y. Zhang, and L. Barrett, "The impact of classroom design on pupils' learning: final results of a holistic, multi-level analysis," *Building and Environment*, vol. 89, pp. 118–133, 2015.

[92] L. Heschong, R. L. Wright, and S. Okura, "Daylighting impacts on human performance in school," *Journal of the Illuminating Engineering Society*, vol. 31, no. 2, pp. 101–114, 2002.

[93] J. M. Daisey, W. J. Angell, and M. G. Apte, "Indoor air quality, ventilation and health symptoms in schools: an analysis of existing information," *Indoor Air*, vol. 13, no. 1, pp. 53–64, 2003.

[94] F. Haghighat and G. Donnini, "Impact of psycho-social factors on perception of the indoor air environment studies in 12 office buildings," *Building and Environment*, vol. 34, no. 4, pp. 479–503, 1999.

[95] W. Yu, L. Wang, Q. Wang et al., "Design selection and evaluation method of PM2.5 filters for fresh air systems," *Journal of Building Engineering*, vol. 27, 2020.

[96] O. A. Seppänen, W. J. Fisk, and M. J. Mendell, "Association of ventilation rates and CO2 concentrations with health andOther responses in commercial and institutional buildings," *Indoor Air*, vol. 9, no. 4, pp. 226–252, 1999.

[97] L. Kajtár, L. Herczeg, E. Láng et al., "Influence of carbon-dioxide pollutant on human well-being and work intensity," in *Proceedings of Healthy Buildings Conference HB 2006-Healthy Buildings: Creating a Healthy Indoor Environment for People*, pp. 85–90, Lisboa, Portugal, August 2006.

[98] UK Building Bulletin 101, Ventilation of School Buildings (BB 101), UK, 2005.

[99] H. Shaughnessy, U. D. J. Moschandreas, and R. J. Shaughnessy, "Association between substandard classroom ventilation rates and students' academic achievement," *Indoor Air*, vol. 21, no. 2, pp. 121–131, 2010.

[100] C. Croome, D. J. Clements, N. Kocchar et al., "Ventilation rates in schools," *Building and Environment*, vol. 43, no. 3, pp. 362–367, 2008.

[101] D. G. Shendell, A. M. Winer, R. Weker, and S. D. Colome, "Evidence of inadequate ventilation in portable classrooms: results of a pilot study in Los Angeles County," *Indoor Air*, vol. 14, no. 3, pp. 154–158, 2004.

[102] C. C. Araya, C. Shrubsole, H. Altamirano et al., "Should schools located in polluted areas be naturally ventilated? A case study from Chile," in *Proceeding of 4th Masters Conference: People and Buildings*, London, UK, September 2014.

[103] Z. Peng, W. Deng, and R. Tenorio, "An integrated low-energy ventilation system to improve indoor environment performance of school buildings in the cold climate zone of China," *Building and Environment*, vol. 182, 2020.

[104] J. A. Leech, W. C. Nelson, R. T. Burnett, S. Aaron, and M. E. Raizenne, "It's about time: a comparison of Canadian and American time-activity patterns," *Journal of Exposure Science and Environmental Epidemiology*, vol. 12, no. 6, pp. 427–432, 2002.

[105] D. K. Serghides, C. K. Chatzinikola, and M. C. Katafygiotou, "Comparative studies of the occupants' behaviour in a university building during winter and summer time," *International Journal of Sustainable Energy*, vol. 34, no. 8, pp. 528–551, 2014.

[106] J. A. Veitch, "Psychological processes influencing lighting quality," *Journal of the Illuminating Engineering Society*, vol. 30, no. 1, pp. 124–140, 2013.

[107] L. Edwards and P. Torcellini, *Literature Review of the Effects of Natural Light on Building Occupants*, National Renewable Energy Lab., Golden, CO. USA, 2002.

[108] M. S. Alrubaih, M. F. M. Zain, M. A. Alghoul, N. L. N. Ibrahim, M. A. Shameri, and O. Elayeb, "Research and development on aspects of daylighting fundamentals," *Renewable and Sustainable Energy Reviews*, vol. 21, pp. 494–505, 2013.

[109] National Building Codes of India, *NBC Part-4 Building Types inIndia*, Bureau of Indian Standards, New Delhi, India, 2005.

[110] Indian Standards, *Guide for Daylighting of Buildings (IS-2440)*, Bureau of Indian Standards, New Delhi, India, 1975.

[111] Indian Standards, *Code of Practice for Daylighting of Educational Buildings (IS-7942)*, Bureau of Indian Standards, New Delhi, India, 1976.

[112] UK Building Bulletin 90, Lighting Design for Schools (BB 90), UK, 1999.

[113] K. Jain, A. Kumar, and A. Kumar, App for Integrating Daylight with Artificial Lighting for Improving Building Energy Efficiency of Residential and Commercial Building during Daytime in All Sky Conditions of United Kingdom (ROC-SW-12453/2019), Extracts from The Register of Copyrights, Copyright Office GOI, 2019.

[114] O. A. Abdou, "Effects of luminous environment on worker productivity in building spaces," *Journal of Architectural Engineering*, vol. 3, no. 3, pp. 124–132, 1997.

[115] J. K. Rice, *Teacher Quality: Understanding the Effectiveness of Teacher Attributes*, 2003.

[116] N. Hanford and M. Figueiro, "Light therapy and Alzheimer's disease and related dementia: past, present, and future," *Journal of Alzheimer's Disease*, vol. 33, no. 4, pp. 913–922, 2013.

[117] G. O. Ocvirk, *Art Fundamental: Theory and Practice*, McGraw-Hill, New York, NY, USA, 2009.

[118] M. B. C. Aries, J. A. Veitch, and G. R. Newsham, "Windows, view, and office characteristics predict physical and psychological discomfort," *Journal of Environmental Psychology*, vol. 30, no. 4, pp. 533–541, 2010.

[119] M. John and E. H. Timothy, "Illuminating the classroom environment," *School Planning and Management*, vol. 44, no. 2, pp. 34–45, 2005.

[120] F. Nicol, M. Wilson, and C. Chiancarella, "Using field measurements of desktop illuminance in European offices to investigate its dependence on outdoor conditions and its effect on occupant satisfaction, and the use of lights and blinds," *Energy and Buildings*, vol. 38, no. 7, pp. 802–813, 2006.

[121] H. Zhang, E. Arens, D. Kim, E. Buchberger, F. Bauman, and C. Huizenga, "Comfort, perceived air quality, and work performance in a low-power task-ambient conditioning system," *Building and Environment*, vol. 45, no. 1, pp. 29–39, 2010.

[122] M. Bessoudo, A. Tzempelikos, A. K. Athienitis, and R. Zmeureanu, "Indoor thermal environmental conditions near glazed facades with shading devices - Part I: experiments and building thermal model," *Building and Environment*, vol. 45, no. 11, pp. 2506–2516, 2010.

[123] P. Barrett and Y. Zhang, "Teachers' views on the designs of their primary schools," *Intelligent Buildings International*, vol. 4, no. 2, pp. 89–110, 2012.

[124] A. Kumar, A. Kumar, and K. Jain, *"Apps for Integrating Daylight with Artificial Lighting for Improving Building Energy Efficiency during Daytime in All Climatesof India," Extracts from the Register of Copyrights, Copyright Office GOI, ROC-SW-12111/2019*, 2019.

[125] E. Ghisi and J. A. Tinker, "An ideal window area concept for energy efficient integration of daylight and artificial light in buildings," *Building and Environment*, vol. 40, no. 1, pp. 51–61, 2005.

[126] G. W. Evans, "Child development and the physical environment," *Annual Review of Psychology*, vol. 57, no. 1, pp. 423–451, 2006.

[127] W. E. Hathaway, "Effects of school lighting on physical development and school performance," *The Journal of Educational Research*, vol. 88, no. 4, pp. 228–242, 2010.

[128] A. Lewy, T. Wehr, F. Goodwin, D. Newsome, and S. Markey, "Light suppresses melatonin secretion in humans," *Science*, vol. 210, no. 4475, pp. 1267–1269, 1980.

[129] N. R. Kapoor and J. P. Tegar, "Human comfort indicators pertaining to indoor environmental quality parameters of residential buildings in Bhopal," *International Research Journal of Engineering and Technology*, vol. 5, pp. 2395–0056, 2018.

[130] X. Li, Y. Wei, J. Zhang, and P. Jin, "Design and analysis of an active daylight harvesting system for building," *Renewable Energy*, vol. 139, pp. 670–678, 2019.

[131] K. D. Kryter, "Non-auditory effects of environmental noise," *Environmental Noise*, pp. 389–398, 1986.

[132] K. D. Kryter, *The Effects of Noise on Man*, Elsevier, Amsterdam, The Netherlands, 2013.

[133] Y. Osada, "An overview of health effects on noise," *Journal of Sound and Vibration*, vol. 127, no. 3, pp. 407–410, 1988.

[134] T. Z. Chang, R. Mehta, S. J. Chen, P. Polsa, and J. Mazur, "The effects of market orientation on effectiveness and efficiency: the case of automotive distribution channels in Finland and Poland," *Journal of Services Marketing*, vol. 13, no. 4/5, pp. 407–418, 1999.

[135] M. A. Wallenius, "The interaction of noise stress and personal project stress on subjective health," *Journal of Environmental Psychology*, vol. 24, no. 2, pp. 167–177, 2004.

[136] M. Kohlhuber, A. Mielck, S. K. Weiland, and G. Bolte, "Social inequality in perceived environmental exposures in relation to housing conditions in Germany," *Environmental Research*, vol. 101, no. 2, pp. 246–255, 2006.

[137] U. Landstrom, E. Akerlund, A. Kjellberg, and M. Tesarz, "Exposure levels, tonal components, and noise annoyance in working environments," *Environment International*, vol. 21, no. 3, pp. 265–275, 1995.

[138] I. Rabiyanti, I. Rahmaniar, and J. C. P. Putra, "Effect of acoustic and thermal comfort to support learning process in a university," *Procedia Engineering*, vol. 170, pp. 280–285, 2017.

[139] UK Building Bulletin 93, *Acoustic Design of Schools: Performance Standard*, 2015.

[140] G. Tiesler, R. Machner, and H. Brokmann, "Classroom acoustics and impact on health and social behaviour," *Energy Procedia*, vol. 78, pp. 3108–3113, 2015.

[141] L. M. Rantala, S. Hakala, S. Holmqvist, and E. Sala, "Classroom noise and teachers' voice production," *Journal of Speech, Language, and Hearing Research*, vol. 58, no. 5, pp. 1397–1406, 2015.

[142] M. R. Serra and E. C. Biassoni, "Urban noise and classroom acoustical conditions in the teaching-learning process," *International Journal of Environmental Studies*, vol. 56, no. 1, pp. 41–59, 1998.

[143] P. M. Bluyssen, M. Aries, and P. V. Dommelen, "Comfort of workers in office buildings: the European HOPE project," *Building and Environment*, vol. 46, no. 1, pp. 280–288, 2011.

[144] P. M. Bluyssen, S. Janssen, L. H. van den Brink et al., "Assessment of wellbeing in an indoor office environment," *Building and Environment*, vol. 46, no. 12, pp. 2632–2640, 2011.

[145] UNESCO, *Framework for Reopening Schools*, UNESCO, Paris, France, 2020.

[146] GOI, *Guidelines on Disinfection of Common Public Places Including Offices*, GOI, New Delhi, 2020.

[147] ISHRAE, *COVID-19 Guidance Document for Air Conditioning and Ventilation*, ISHRAE, Chennai, India, 2020.

[148] Z. T. Ai and A. K. Melikov, "Airborne spread of expiratory droplet nuclei between the occupants of indoor environments: a review," *Indoor Air*, vol. 28, no. 4, pp. 500–524, 2018.

[149] V. Mathai, A. Das, J. A. Bailey et al., "Airflows inside passenger cars and implications for airborne disease transmission," *Science Advances*, vol. 7, no. 1, Article ID eabe0166, 2020.

[150] S. C. Moharir, T. S. Chandra, A. Goel et al., *Detection of SARS-CoV-2 in the Air from Hospitals and Closed Rooms Occupied by COVID-19 Patients*, Medrxiv Preprint, 2021.

[151] L. Liu, Y. Li, P. V. Nielsen, J. Wei, and R. L. Jensen, "Short-range airborne transmission of expiratory droplets between two people," *Indoor Air*, vol. 27, no. 2, pp. 452–462, 2017.

Hindawi
Advances in Civil Engineering
Volume 2021, Article ID 6670930, 15 pages
https://doi.org/10.1155/2021/6670930

Research Article

Thermal Behaviour Analysis and Cost-Saving Opportunities of PCM-Integrated Terracotta Brick Buildings

A. Chelliah,[1] **Shaik Saboor**,[1] **Aritra Ghosh**,[2,3,4] **and Karolos J. Kontoleon**[5]

[1]*School of Mechanical Engineering, Vellore Institute of Technology, Vellore - 632014, Tamil Nadu, India*
[2]*Environment and Sustainability Institute, University of Exeter, Penryn, Cornwall TR10 9FE, UK*
[3]*College of Engineering, Mathematics and Physical Sciences, Renewable Energy, University of Exeter, Penryn, Cornwall TR10 9FE, UK*
[4]*Renewable Energy, Stella Turk Building, University of Exeter, Penryn, Cornwall TR10 9FE, UK*
[5]*Department of Civil Engineering, Aristotle University of Thessaloniki, University Campus, Gr 54124 Thessaloniki, Greece*

Correspondence should be addressed to Shaik Saboor; saboor.nitk@gmail.com

Received 17 October 2020; Revised 3 January 2021; Accepted 23 January 2021; Published 8 February 2021

Academic Editor: Loke Foong

Buildings contribute greatly to global energy use and consumption. The energy consumption of buildings is significant due to the integration of heating, ventilation, and cooling systems. Evidently, the utilization of phase change materials (PCMs) in building design can adequately reduce air-conditioning costs of buildings by diminishing external heat gains and losses. Moreover, the adoption of natural, eco-friendly, and cost-effective materials, such as terracotta bricks, can be valuable from an environmental point of view. This paper intends to assess the air-conditioning cost-saving potential of several PCM stuffed terracotta brick configurations. In that respect, the encapsulated PCMs were filled in the hollows of terracotta bricks. For the aims of this study, five different types of PCMs were considered, in relation to the thermophysical properties of their solid and liquid state (OM18: organic mixture, HS22: hydrated salt, OM29, OM32, and OM37). In addition, three PCM-stuffed terracotta brick configurations were examined with reference to the number of the PCM layers (PCMTB-A with one PCM layer, PCMTB-B with two PCM layers, and PCMTB-C with three PCM layers). Therefore, fifteen PCM-stuffed terracotta brick configurations were analysed numerically, related to environmental conditions that refer to two different scenarios in India (hot dry and composite climates). Results have unveiled that the OM32 PCM assemblies have shown better thermoeconomic performance compared to the other types of PCM. With respect to the most advantageous number of PCM layers, the evidence of this analysis has exposed that the PCMTB-C case has shown the highest annual air-conditioning cost-savings and the highest yearly carbon emission mitigations in both climates (Ahmedabad and Lucknow). In hot-dry climates, the PCMTB-C with OM32 PCM exhibited the highest annual air-conditioning cost-saving ($ 74.7), the highest annual carbon emission mitigation (1.43 ton/kWh), and the moderate payback period (22.5 years) compared to the other cases. To conclude, the findings of this study suggest a suitable way to improve the decision-making process of building design, while bridging the performance gap in terms of energy efficiency and sustainability.

1. Introduction

Climate change and environmental degradation pose a fundamental threat to mankind. Commercial and residential buildings require a large amount of energy for heating, ventilation, and cooling systems, while they are also responsible for global warming and depletion of nonrenewable fossil fuels. In developing countries like India, the construction sector is growing rapidly due to economic progress and the growth of urban communities. Buildings constitute about 40% of global consumption of electricity, with residential buildings accounting for three-quarters of the overall energy consumption and one-third of world GHG emissions [1]. Many countries have implemented policies in place to improve energy efficiency in buildings by ameliorating the effects of climate change. People spend over 90% of their time in buildings by paying special attention to a safe, clean, and comfortable indoor environment [2].

The traditional means of building thermal conveniences are mechanical air-conditioning systems that are energy-intensive and detrimental to the environment. In this regard, energy-efficient and environmentally friendly techniques applied to boost thermal comfort at a zero or low power consumption are passive heating and cooling systems [3, 4]. Towards this goal, terracotta bricks that are made of fired clay and have a good density which can provide a fair thermal resistance to building envelopes can be considered.

Thermal energy storage by using PCMs is a tolerable passive cooling approach to moderate heat flows through building envelopes. PCMs can absorb a significant amount of heat during the melting stage (from solid to liquid), as well as they can release the absorbed heat during the solidification stage (from liquid to solid) [5]. The ability of PCMs to provide high energy storage and their characteristics to retain thermal storage at a constant temperature make their utilization attractive for several building applications [6]. As it is widely known, PCMs are commonly categorized as organic, inorganic, and eutectic, while they should have certain characteristics such as a nontoxic and noncorrosive behaviour, a suitable thermal conductivity, a desirable latent heat, and a low cost, to attain the fundamental goal of energy efficiency sustainably [7]. Organic PCMs mostly show noncorrosive properties and congruent melting points. In addition to that, the melting point and heat of the fusion of certain organic PCMs are suitable for the cooling/heating of buildings [7]. The method to embed PCMs in the encapsulation material with a scale exceeding 5 mm is called macroencapsulation of PCMs, while the shape of the shell can vary (cylinders, tubes, cubes, sticks, etc.). Macroencapsulated PCMs can be used in any type, size, and dimension of the building envelope [8]. An active system with PCMs has a separate storage unit within the building to be settled, which is considered to be a demerit for the end-users. The main benefit of incorporating PCMs into building materials is that less space is required, while they can be formulated with a certain behavioural pattern at the very early stages of building construction [9]. In the literature, various shell materials having the potential for thermal energy storage at high temperatures are examined [10]. Moreover, several studies reviewed and addressed the thermal efficiency of PCM-integrated buildings as wallboard configurations assisted by the operation of the HVAC unit [11–18]. PCM wallboards in buildings have recorded an advantageous reduction of the decrement factor and increase of the time lag, as regards the propagation of a periodic heatwave [19–22]. Zhou et al. analytically investigated a ventilated Trombe wall integrated with double PCM wallboard (Inside and outside) and reported the energy storage and release efficiency of 20.2% (exterior) and 20.25% (interior) at the optimum PCM thicknesses (8 mm for exterior and 28 mm for interior) [23].

Yoon et al. [24] experimentally studied a scaled model of a PCM integrated cool roof system and reported a better performance for the RT44 PCM assembly for a white roof in comparison with the Bio 26PCM assembly for a brown roof. Jin et al. [25] conducted the experiments and reported that the placement of the PCM pouch at a distance of (1/5) L from the interior wall surface improves the overall thermal comfort conditions. Tunçbilek et al. [26] conducted numerical simulation on PCM-integrated office building and reported energy savings of up to 12.8% with PCM of 23 mm thickness located at the inner side of the wall. A review of the use of macroencapsulated PCMs for various building enclosures was presented in detail [27]. The thermal efficiency of a concrete wall integrated with PCMs was analysed numerically by Lie et al. As seen, the incorporation of a 10 mm thick PCM layer in a vertical wall leads to approximately 20–30% reduction of heat gains through buildings located in hot tropical climates [28]. The thermal performance of the PCM integrated brick was numerically investigated by Tunçbilek et al. [29], and they reported the optimum PCM's melting temperatures as 18°C and 26°C, respectively, for winter and summer seasons.

The PCM thermal shield position of a building model was experimentally investigated and optimized by Lee et al. The results exposed the optimal location of PCM layers from the inner surface for various wall orientations [30]. The PCM impact on building energy consumption was simulated for one whole year in five different cities in China by using Energy Plus. Results have underlined a significant energy saving in buildings integrated with PCMs [31]. PCM integration in buildings was also modelled and simulated in terms of energy demands, by Yun et al. [32]. Results have indicated a reduction in cooling cost by 7.48%, while a six years' payback period was estimated. A building model integrated with PCMs for economic analysis was carried out with Energy Plus software by Solgi et al.; as seen, the consideration of PCMs in buildings lowered the energy requirements for certain thermal comfort requirements, although it is not rational from an economical point of view in Iran due to the high cost of PCMs and the low costs of electricity [33].

The literature revealed that there is no significant information on the air-conditioning cost-saving potential, carbon emission mitigation, and payback period by adopting PCM stuffed terracotta bricks in buildings. In this respect, the current study aims to analyze numerically three different configurations of PCM stuffed terracotta bricks; in addition, five different types of PCMs, such as OM18, HS22, OM29, OM32, and OM37, were assessed for two different scenarios in India (hot dry and composite climates). The thermophysical properties of the assumed PCMs were measured experimentally for both solid and liquid phases. This paper explores the unsteady thermal characteristics of PCM stuffed terracotta bricks and utilizes an unsteady thermal transmittance methodology to determine the air-conditioning cost-saving within buildings. This paper also presents the mitigation of carbon emissions and the resulted payback periods for all analysed PCM stuffed terracotta brick buildings. The findings of this study help in the design of energy-efficient buildings with PCM integrated terracotta bricks.

2. Materials and Methods

2.1. Materials. The terracotta bricks are natural materials made of clay that shows eco-friendly behaviour. The terracotta bricks are moulded with hollows to accommodate

PCMs, while they are fired at 1000–1200°C for four hours to obtain certain strength; after firing, they may obtain a compressive strength of more than 3.5 N/mm^2. Moreover, the terracotta bricks are lighter than the conventional bricks, showing an absorption capacity that ranges within 15–20%. In this work, solid and hollow terracotta bricks were considered, and the hollows of the terracotta bricks were stuffed with various commercially available PCM materials. The analysed PCMs refer to HS22 (hydrated salt), OM18, OM29, OM32, and OM37 (organic mixtures) to accomplish the thermoeconomic analysis. The number of the above-mentioned abbreviations illustrates the melting temperature value of each PCM.

2.2. Experimental Methodology. Thermophysical properties of terracotta bricks (in solid-state) and PCMs (in solid and liquid state) were measured by using an experimental setup as illustrated in Figure 1. The viscometer consists of cooling and heating elements to cool and heat PCMs when measuring thermal conductivity for both solid and liquid states. With stability ranging up to ±0.04°C, the system has a temperature range within −20°C to 170°C. In that respect, the appropriate temperature has been set by using the digital reading display. It consists of a bath tank that heats or cools water to an appropriate temperature. PCMs were surrounded externally, around the cup, by hot or cold water. The hot or cold water was transferred externally from the bath tank to the measuring system by a close -loop. PCMs such as OM18, HS22, and OM29 are cooled in the viscometer when calculating their thermal conductivity with a low freezing point below the atmospheric temperature at the solid-state. On the other hand, PCMs such as OM32 and OM37 are easily melted above the air temperature; due to this, PCMs were heated in the viscometer to test their liquid thermal conductivity.

The KD2 thermal property analyser (hot wire probe method) was used to measure the thermal conductivity of PCMs according to the ASTM standard [34, 35]. It consists of a cable, a probe, and a monitor to display the related data. There are two pins on the probe; the first one is used as a heating source by electric pulse, while the second one acts as a receiver. Pins have a diameter of 1.3 mm and a length of 3 cm with a distance of 6 mm to each other. The thermal conductivity of the solid and liquid states of the PCMs is determined by the resulted temperatures through the time domain. The thermal conductivity in the range of 0.02 W/(m·K) to 2.00 W/(m·K) can be determined with an accuracy of ±10%. The volumetric specific heat can also be determined in the range of 0.50 to 4.00 MJ/(m^3·K) with an accuracy of ±10%.

The densities of PCMs were measured with a ± 1% accuracy by applying a specific gravity bottle process. The volume of the PCM in the liquid state was measured in the container, and its weight was measured in the weighing machine. The differences between the weight of the bottle and the weight of the bottle with the PCM provide the PCM's weight in the liquid state. The density, the weight, and the volume of the liquid PCM were measured by the specific gravity. Nevertheless, uncertainties were noted for each

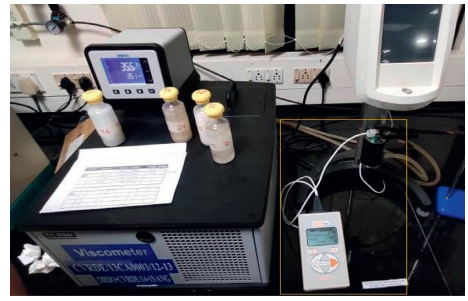

Figure 1: Experimental setup with viscometer and KD2 pro-thermal property analyser.

PCM, with reference to the evaluation of their thermal conductivity and specific heat [36]. Table 1 shows the thermal conductivity and specific heat values of the plaster, the terracotta brick, and the studied PCMs on both solid and liquid states (with uncertainties). The phase transition temperatures of PCMs were measured using differential scanning calorimetry [37, 38] and are presented in Table 1.

2.3. Design Methodology. The outline of analysed terracotta bricks and their corresponding dimensions is depicted in Figure 2:

(i) Figures 2(a) and 2(b) illustrate the design of a solid terracotta brick size of 0.29 m long × 0.14 m wide × 0.09 m high.

(ii) Figures 2(c) and 2(d) show the design of a terracotta brick integrated with one PCM layer (PCMTB-A).

(iii) Figures 2(e) and 2(f) show the design of a terracotta brick integrated with two PCM layers (PCMTB-B).

(iv) Figures 2(g) and 2(h) show the design of a terracotta brick integrated with three PCM layers (PCMTB-C).

Each PCM layer within the terracotta brick is of the size 0.29 m × 0.06 m × 0.01 m. Figure 3(a) shows the cube-shaped building model (3.00 m × 3.00 m × 3.00 m) considered for the objectives of this work. The terracotta bricks are laid in and bound together with plaster; accordingly, the bond between bricks and plaster is equal to 0.0125 m. Furthermore, the thickness of the conventional reinforced cement concrete (RCC) roof is 0.15 m, while as seen in Figure 3(b), both sides of its structure are covered with a plaster of 0.0125 m.

2.4. Analytical Methodology. As it is well known, the cooling loads through building envelopes can be diminished by adjusting their thermal mass, as well as by increasing their thermal resistance. PCM stuffed terracotta bricks can significantly improve the thermal mass and thermal resistance of building structure.

The steady-state transmittance (U_s) relies exclusively on the thermal conductivity of the involved materials. Therefore, a steady-state transmittance signifies only the thermal resistance. On the contrary, an unsteady-state transmittance

Table 1: Thermophysical properties of studied building materials.

	Phase transition range	Solid PCM temp.	k (W/(m·K))		Liquid PCM temp.	Cp (kJ/(kg·K))		ρ (kg/m^3)	
PCM	(°C)	(°C)	Solid	Liquid	(°C)	Solid	Liquid	Solid	Liquid
OM18	14–20	14	0.182 ± 0.002	0.176 ± 0.003	28	2.93 ± 0.02	2.70 ± 0.02	907 ± 6	871 ± 5
HS22	18–28	15	1.14 ± 0.001	0.57 ± 0.005	28	2.28 ± 0.06	2.53 ± 0.03	1651 ± 3	1556 ± 4
OM29	24–33	20	0.293 ± 0.004	0.173 ± 0.007	33	2.33 ± 0.02	2.72 ± 0.01	976 ± 5	880 ± 3
OM32	28–38	28	0.219 ± 0.002	0.145 ± 0.002	40	3.13 ± 0.01	2.82 ± 0.02	926 ± 4	875 ± 2
OM37	33–40	33	0.17 ± 0.003	0.14 ± 0.002	45	2.56 ± 0.04	2.63 ± 0.02	974 ± 2	865 ± 3
Plaster		—	0.721 ± 0.005	—	—	1.76 ± 0.04	—	840 ± 3	—
Terracotta brick		—	0.62 ± 0.004	—	—	0.816 ± 0.04	—	1950 ± 5	—

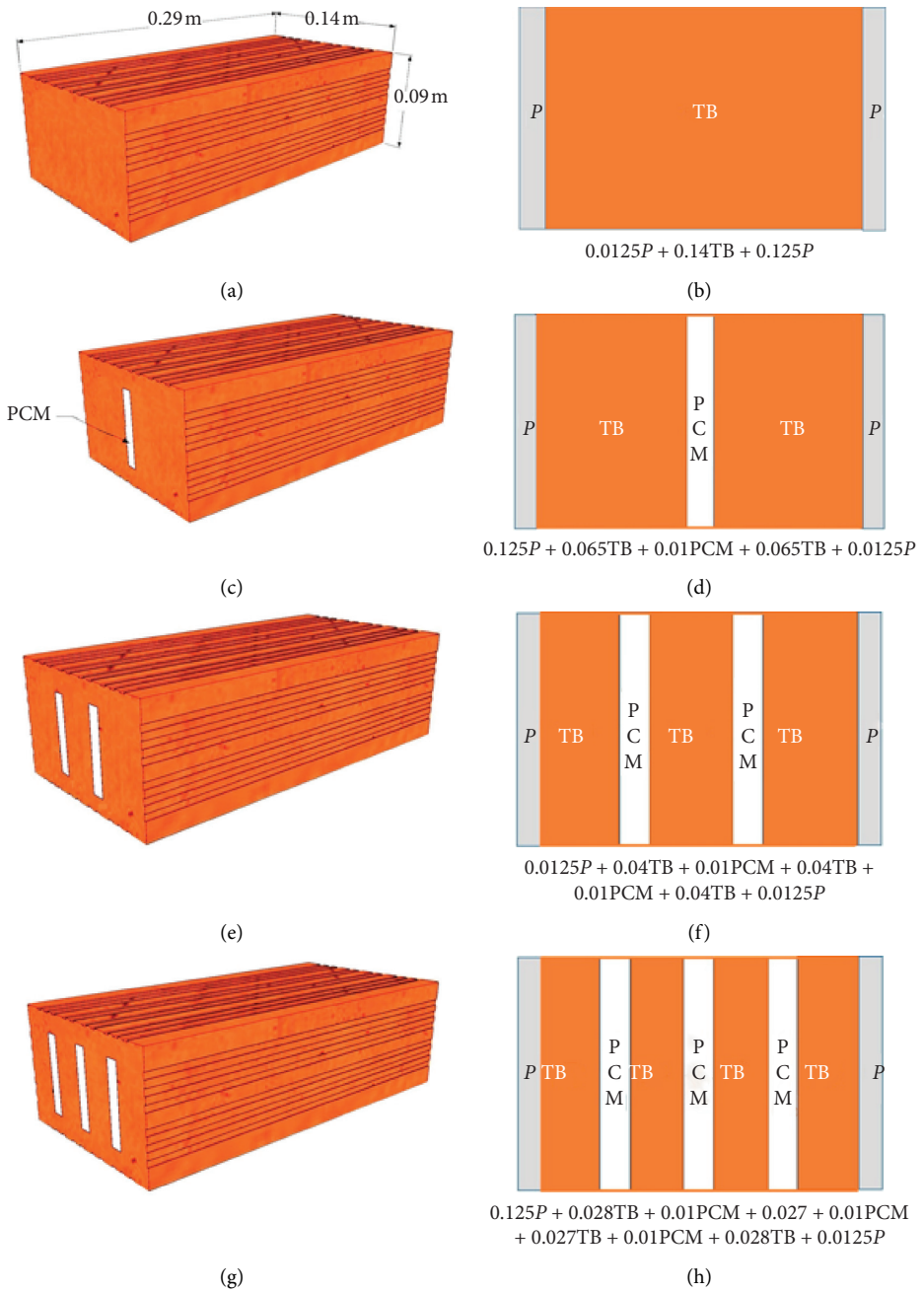

Figure 2: Outline of assumed terracotta brick geometries: (a)-(b) solid terracotta brick; (c)-(d) terracotta brick with one PCM layer; (e)-(f) terracotta brick with two PCM layers; (g)-(h) terracotta brick with three PCM layers.

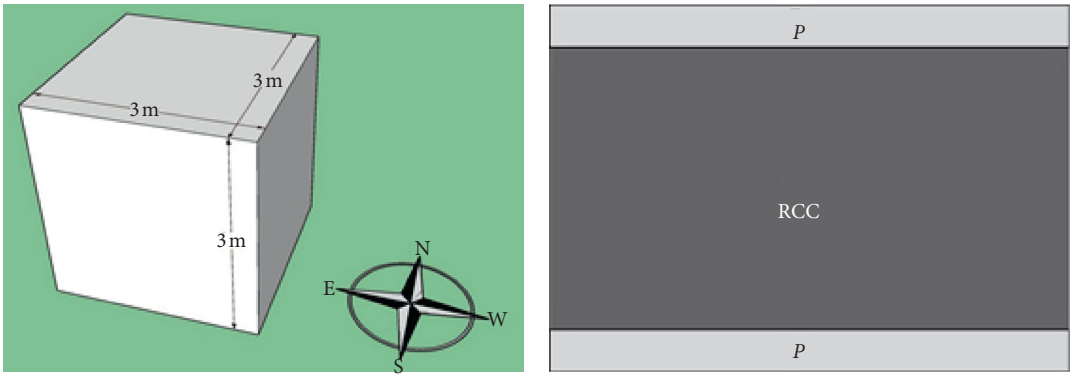

(a) (b)

Figure 3: (a) Cube-shaped building model; (b) RCC roof configuration.

(U_t) is the measure of both the thermal resistance and the thermal mass of building elements (walls, slabs, roofs, etc.), as it simultaneously takes into account the thermal conductivity, the specific heat capacity, and the density, under periodic thermal conditions. A lower unsteady-state thermal transmittance value signifies a higher thermal resistance and thermal mass [39–43]. The steady-state thermal transmittance U_s indicates the heat transfer rate through a building configuration. A lower value of steady-state transmittance implies better thermal resistance of its assembly. It is given by the following equation:

$$U_{\text{TB+PCMs}} = \left(\frac{1}{h_o} + \frac{X_p}{k_p} + \frac{X_{\text{tb}}}{k_{\text{cb}}} + \frac{X_{\text{pcm}}}{k_{\text{pcm}}} + \frac{1}{h_i}\right)^{-1}. \quad (1)$$

To determine the unsteady-state transmittance, the attenuation factor (decrement factor), and the time delay (time lag) of masonry walls settled with solid terracotta bricks and PCM stuffed terracotta bricks, a one-dimensional heat diffusion equation was solved by applying the admittance method to compute unsteady parameters:

$$\frac{\partial^2 T}{\partial x^2} = \frac{1}{\alpha}.\frac{\partial T}{\partial \tau},$$

$$\begin{bmatrix} T_e \\ q_e \end{bmatrix} = \begin{bmatrix} \cosh(m+im) & \dfrac{(\sinh(m+im))}{c} \\ c\,\sinh(m+im) & \cosh(m+im) \end{bmatrix} \begin{bmatrix} T_i \\ q_i \end{bmatrix}, \quad (2)$$

where T_e is the cyclic temperature, q_e is the cyclic heat flux, α indicates the thermal diffusivity ($\alpha = k/\rho C_p$), and m signifies the cyclic thickness ($m = x \cdot z$). In addition, x specifies the element thickness, while z refers to the finite thickness of the element ($z = \sqrt{\rho c_p / kn}$), and n is the cyclic period.

The characteristic admittance of an element is derived by $(c) = \sqrt{j}\ 2\pi k \rho c_p / n$ and therefore it is

$$\begin{bmatrix} f_1 & f_2 \\ f_3 & f_1 \end{bmatrix} = \begin{bmatrix} b_1 + ib_2 & \dfrac{(b_3 + ib_4)}{c} \\ c(-b_4 + ib_3) & b_1 + ib_2 \end{bmatrix},$$

$$\begin{aligned} b_1 &= \cosh m \cos m, \\ b_2 &= \sinh m \sin m, \\ b_3 &= (\cosh m \sin m + \sinh n \cos m)\left(\frac{1}{\sqrt{2}}\right), \\ b_4 &= (\cosh m \sin m + \sinh m \cos m)\left(\frac{1}{\sqrt{2}}\right). \end{aligned} \quad (3)$$

Moreover, it is

The matrices for internal and external surface resistances are given by

$$r_{st} = \begin{bmatrix} 1 & h_i^{-1} \\ 0 & 1 \end{bmatrix} \cdot r_{so} = \begin{bmatrix} 1 & h_o^{-1} \\ 0 & 1 \end{bmatrix}. \quad (4)$$

The transmission matrix for conventional walls with convection resistance is given by

$$\begin{bmatrix} T_e \\ q_e \end{bmatrix} = \begin{bmatrix} 1 & h_i^{-1} \\ 0 & 1 \end{bmatrix} \begin{bmatrix} m_1 & m_2 \\ m_3 & m_1 \end{bmatrix} \begin{bmatrix} n_1 & n_2 \\ n_3 & n_1 \end{bmatrix} .. \begin{bmatrix} 1 & h_o^{-1} \\ 0 & 1 \end{bmatrix} \begin{bmatrix} T_i \\ q_i \end{bmatrix}, \quad (5)$$

where m and n indicate different building materials:

$$\begin{bmatrix} T_e \\ q_e \end{bmatrix} = \begin{bmatrix} A_1 & A_2 \\ A_3 & A_4 \end{bmatrix} \begin{bmatrix} T_i \\ q_i \end{bmatrix}. \quad (6)$$

The unsteady-state transmittance U_t is the heat flow at the inner surface when the exterior surface is exposed to a periodic temperature variation, while the room temperature is maintained at a constant temperature. It can be computed by the following equation:

$$U_t = \left|\frac{1}{A_2}\right|. \tag{7}$$

The attenuation of the sinusoidal heatwave through the wall/roof is called the decrement factor (f) or attenuation factor. It is the ratio of the unsteady transmittance to the steady transmittance:

$$f = \frac{U_t}{U_s}. \tag{8}$$

Then again, the time lag (φ) specifies the time it takes for a heatwave to propagate from the exterior to the interior surface, with respect to the temperature peaks. Its value is given by

$$\varphi = \frac{12}{\pi}\arctan\left(\frac{im(f)}{\mathrm{Re}(f)}\right). \tag{9}$$

A MATLAB code was developed to compute unsteady-state transmittance, decrement factor, and time lag of various masonry walls settled with terracotta bricks. In a second step, the determined unsteady-state transmittance was utilized to estimate the potential for air-conditioning cost-saving and carbon emission mitigation potential, as well as the payback periods of buildings.

2.5. Cost Assessment Methodology. The temperature differences between the external environment and the constant reference temperature within the internal space of a building zone delineate the heating and cooling loads through building enclosures. The degree-hours approach is a feasible method to compute annual energy usage. The annual energy savings of building envelopes for heating and cooling can be estimated by using heating degree-hours (HDH) and cooling degree-hours (CDH). According to the ASHRAE requirements, 18°C is assumed as the base temperature for both cooling and heating of buildings. ASHRAE meteorological data have been utilized for cooling and heating degree-hours in Ahmedabad (23.07°N 72.63°E) and Lucknow (26.75°N 80.88°E), in India [44]. Figure 4 shows the monthly cooling and heating degree-hours for both mentioned cities. Table 2 shows the elements considered for the corresponding thermoeconomic analysis. The sol-air temperature is the temperature which gives the combined effect of outdoor temperature distribution and incident solar radiation. The CDH can be computed by multiplying the number of cooling hours with the difference in sol-air temperature and base temperature. Similarly, HDH can be computed by multiplying the number of heating hours with the difference in sol-air temperature and base temperature as shown in equations (10) and (11), respectively:

$$\mathrm{CDH} = N_C(T_S - T_b), \tag{10}$$

$$\mathrm{HDH} = N_H(T_b - T_S), \tag{11}$$

where N_C and N_H are the number of cooling and heating hours, T_b is the constant-base temperature, and T_s is the sol-air temperature.

The thermoeconomic analysis can be performed to compute parameters such as cooling and heating cost savings (C_c and C_h), total air-conditioning cost-savings (C_t), payback period (PB), and carbon emission mitigation (CM) [45–47]. The cooling and heating cost-saving findings provide information about the beneficial impact of inserting PCMs in terracotta bricks, compared with conventional solid terracotta brick assemblies in buildings. They can be computed by using the following equations:

$$C_c = \left(\frac{10^{-3}.C_e.\mathrm{CDH}.\Delta U_t^l}{\mathrm{COP}}\right), \tag{12}$$

$$C_h = \left(\frac{10^{-3}.C_n.\mathrm{HDH}.\Delta U_t^s}{\eta}\right). \tag{13}$$

Moreover, the total air-conditioning cost savings can be obtained from the following equation:

$$C_t = C_c + C_h. \tag{14}$$

It should be noted that C_h and C_c refer to the heating and cooling cost savings, while ΔU_t is the difference in unsteady-state thermal transmittance between the solid terracotta brick scenario and the filled with PCMs terracotta brick scenario.

Saving of electricity leads to a wanted carbon mitigation effect. This effect can be obtained from

$$M_c = 10^{-3}\left(\Delta U_t^l.p_1.\frac{CDH}{COP} + \Delta U_t^s.p_2.\frac{HDH}{\eta}\right). \tag{15}$$

where p_1 is the mass of carbon emission per unit energy production by the coal power plant and p_2 is the mass of carbon emission per unit energy production by natural gas.

Finally, the payback period highlights the time it takes for PCMs to recover the funds invested (the initial investment cost). It is derived by the following equation:

$$pp = \frac{\ln\left[C_i.(i-d)/C_t + t1\right]}{\ln(1+i)/(1+d)}. \tag{16}$$

The inflation rate (i) and discount rate (d) values are considered as per the Indian scenario. This payback period method considers inflation rate and discount rates, but it does not consider the escalation rate of energy.

3. Results and Discussion

3.1. Unsteady Parameters of Various PCM-Stuffed Terracotta Bricks. Equations (1) and (7) are applied to assess steady and unsteady transmittances of bricks, respectively. Figure 5(a) depicts the steady and unsteady transmittances of solid and terracotta bricks stuffed with PCMs. From these results, it is noted that the unsteady transmittance is lower than the steady transmittance for all the studied bricks. On the other hand, the unsteady transmittance depends on the fundamental thermophysical properties of bricks, such as thermal conductivity, specific heat capacity, and density. Unsteady transmittance is the finest measure to assess the thermal mass and thermal resistance of a structure, while it allows an

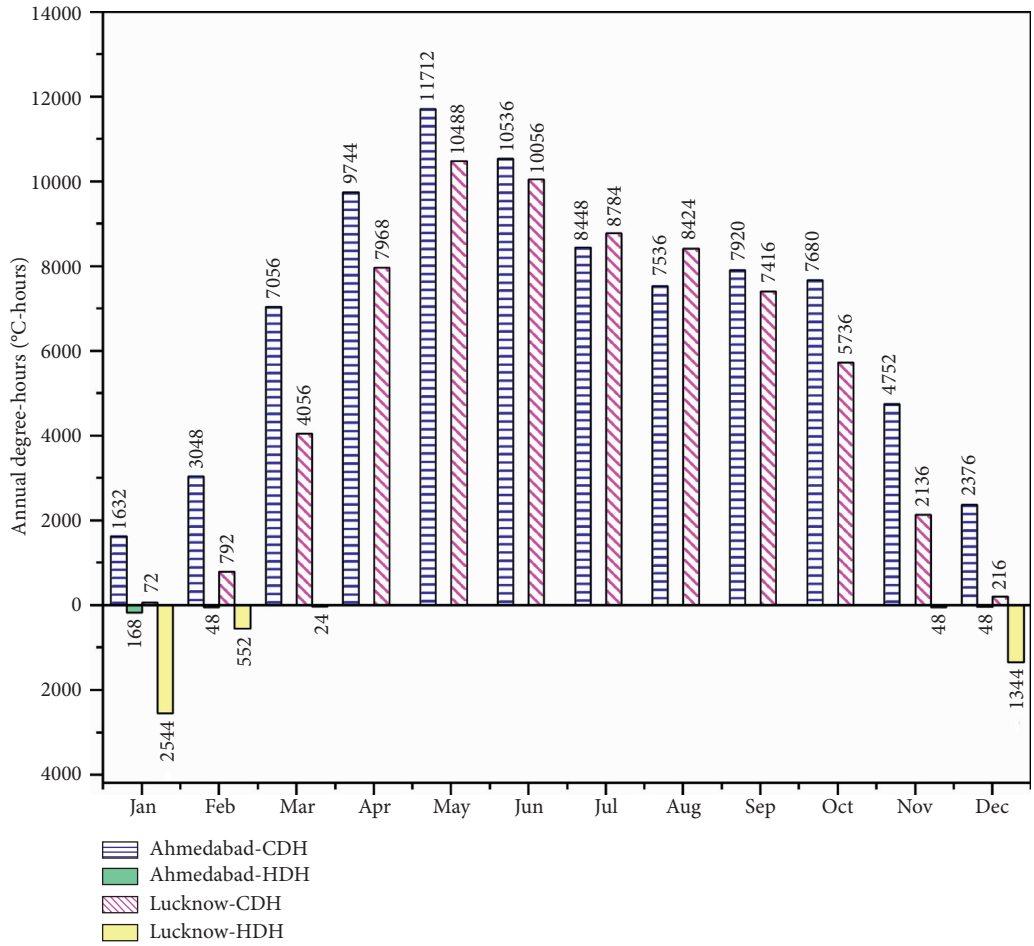

Figure 4: Annual cooling and heating degree-hours in Ahmedabad and Lucknow.

Table 2: Elements used for the thermoeconomic analysis.

S. No.	Elements	Value
1	Annual cooling degree-hours ($CDH_{18}{}^{o}{}_{C}$) (°C-hours) in ahmedabad and lucknow	82440 and 6614
2	Annual heating degree-hours ($HDH_{18}{}^{o}{}_{C}$) (°C-hours) in ahmedabad and lucknow	264 and 4512
3	Outside and inside heat transfer coefficients (h_o *and* h_i) (W/m^{2}K)	25.00 and 7.70
4	Coefficient of performance (*COP*)	2.50
5	Unit cost of electricity (C_e) ($/kWh)	0.082
6	Unit cost of natural gas (C_n) ($/kWh)	0.014
7	Efficiency (η)	0.80
8	Mass of CO_2 emission rates per unit usage of electricity (p_1) (kg//kWh)	0.98 x 1.60
9	Mass of CO_2 emission rates per unit usage of natural gas (p_2) (kg//kWh)	0.18
10	Material cost of PCMs (C_i) ($/kg) C_{OM18}, C_{HS22}, C_{OM29}, C_{OM32}, and C_{OM37}	3.75, 1.26, 4.29, 2.68, and 2.86
11	Inflation rate (i)	7.6%
12	Discount rate (d)	6.6%

accurate calculation of air-conditioning cost-saving potential of various terracotta bricks stuffed with PCMs. As it is already mentioned, a lower value of unsteady transmittance indicates a better thermal performance of terracotta bricks (in relation to the thermal mass and the thermal resistance). PCMs in the liquid phase provide the least values of steady and unsteady transmittance compared to the solid phase, due to their superior thermophysical properties in this state. In general, amongst all studied terracotta brick configurations (TB, PCMTB-A, PCMTB-B, and PCMTB-C), the PCMTB-C configuration has shown the best thermal behaviour due to its lowest unsteady transmittance value. Furthermore, in relation to the optimal PCM (OM18, HS22, OM29, OM32, and OM37), it is revealed that the OM32 shows the lowest steady and unsteady transmittance values. The order of preference of the examined PCMs from the

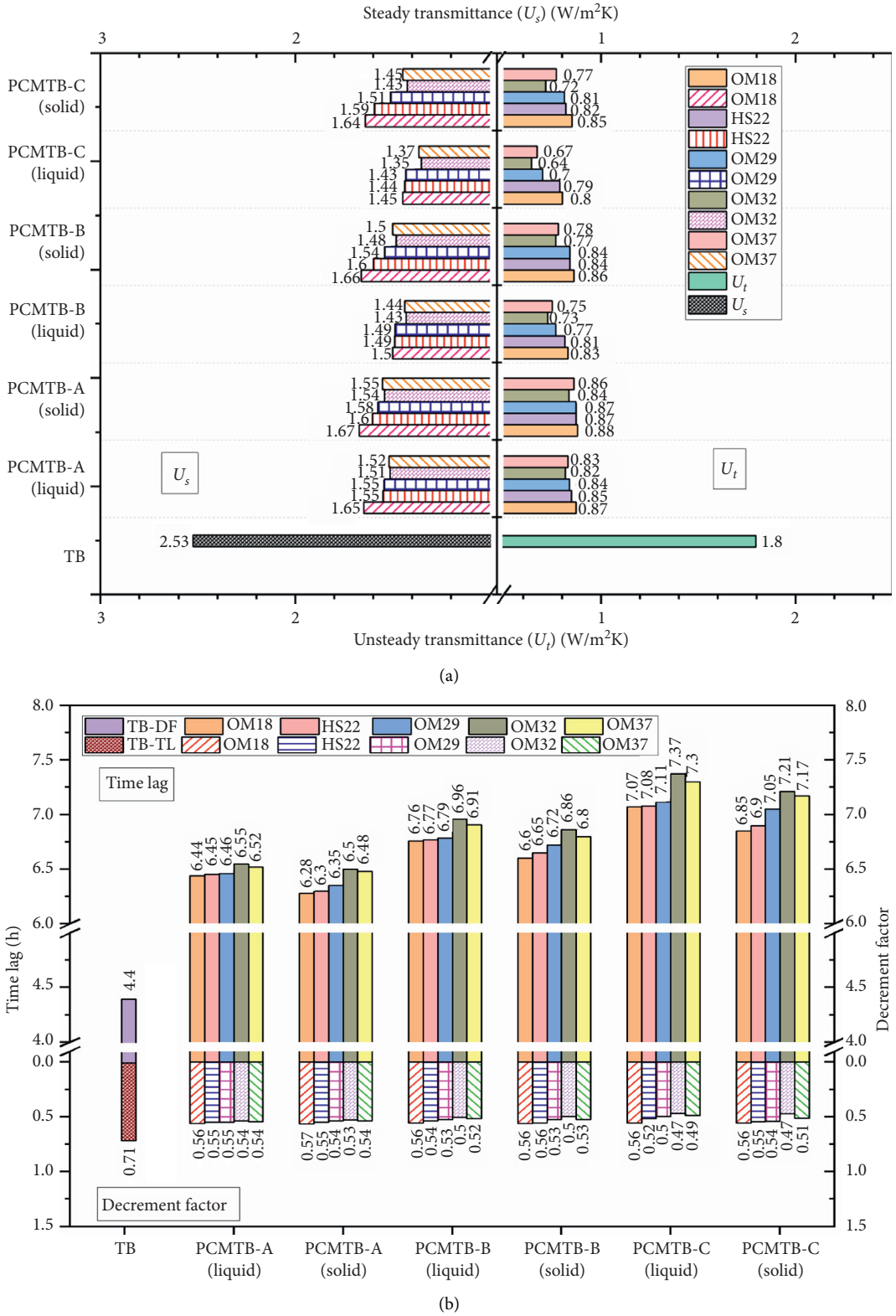

Figure 5: Thermal characteristics of terracotta bricks integrated with PCMs: (a) Steady and unsteady transmittance variations; (b) decrement factor and time lag variations.

least steady and unsteady transmittance to the highest steady and unsteady transmittance is OM32 < OM37 < OM29 < HS22 < OM18.

The decrease of the decrement factor, as well as the increase of the time lag by selecting terracotta brick, can affect substantially the indoor thermal comfort conditions in buildings; in that respect, temperature peaks due to the heatwave can be attenuated and shifted from peak hours to nonpeak hours. To assess the decrement factor and time lag values, one can apply equations (8) and (9), respectively. To improve the thermal performance of terracotta brick, the attenuation factor should be as low as possible, while the time lag should receive a high value. Figure 5(b) shows the attenuation factor and its time lag of various terracotta bricks stuffed with PCMs. PCMs in the liquid phase lead to the lowest values of the attenuation factor and the highest values of time lag, in relation to the solid phase. PCMTB-A and PCMTB-B configurations are designed with one and two layers of PCMs, respectively. The PCMTB-C is designed with three layers of PCM, and therefore the PCMTB-C offers the highest thermal mass compared to PCMTB-A and B. As it is expected, with regard to all analysed terracotta brick configurations (TB, PCMTB-A, PCMTB-B, and PCMTB-C), the PCMTB-C configuration has shown the lowest attenuation factor and the highest time lag values due to enhanced thermal mass. In addition, for the optimal PCM (OM18, HS22, OM29, OM32, and OM37), it is exposed that the OM32 shows the lowest attenuation factor and the highest time lag. To conclude, the thermal performance of all analysed terracotta brick walls stuffed with a certain PCM is clarified by $f_{OM32} < f_{OM37} < f_{OM29} < f_{HS22} < f_{OM18}$ and $\varphi_{OM32} > \varphi_{OM37} > \varphi_{OM29} > \varphi_{HS22} > \varphi_{OM18}$.

3.2. Cooling and Heating Cost saving of Terracotta Brick Buildings Integrated with PCMs. Equations (12) and (13) are applied to compute cooling and heating cost saving of various PCM stuffed terracotta brick buildings compared to solid terracotta brick buildings. Figures 6(a) and 6(b) illustrate the cooling and heating cost saving of various buildings, arranged with masonry walls (solid terracotta walls and terracotta walls integrated with PCMs) in Ahmedabad and Lucknow climates.

In Ahmedabad, terracotta brick wall configurations PCMTB-A stuffed with a certain PCM of OM18, HS22, OM29, OM32, and OM37 have shown a cooling cost saving of $ 59.92, $ 61.34, $ 62.00, $ 63.34, and $ 62.35, respectively. Likewise, the heating cost saving is $ 0.1, $ 0.1, $ 0.1, $ 0.11, and $ 0.1. Evidently, amongst all examined PCMs in the PCMTB-A assembly, the OM32 shows the highest cooling and heating cost saving. Furthermore, the terracotta brick wall configuration PCMTB-B stuffed with OM32 PCM shows the highest cooling and heating cost saving of $ 69.27 and $ 0.11, respectively. Similarly, with respect to all simulated terracotta brick wall configurations, the PCMTB-C stuffed with OM32 showed the highest cooling and heating cost saving of $ 74.58 and $ 0.12, respectively.

Similarly in Lucknow, terracotta brick wall configuration PCMTB-C stuffed with OM32 PCM shows the highest cooling and heating cost saving of $ 59.8 and $ 2.04, respectively. As seen, the cooling cost saving is more evident in Ahmedabad than in Lucknow, due to its hot-dry climatic conditions. Nevertheless, the heating cost saving is predominant in Lucknow in comparison to Ahmedabad, due to its exposed composite climate.

The most influencing thermal characteristic for enhancing cooling and heating cost savings is the unsteady transmittance of PCM integrated terracotta bricks. A lower value of unsteady transmittance contributes to higher cooling and heating cost savings. The best order of PCMs as per the highest cooling and heating cost-saving is OM32 > OM37 > OM29 > HS22 > OM18. The preferred order of PCM stuffed terracotta brick configuration as per the highest cooling and heating cost-saving is PCMTB-C > PCMTB-B > PCMTB-A.

3.3. Total Building Air-Conditioning Cost Saving of Terracotta Brick Buildings Integrated with PCMs. Equation (14) is used to estimate the total building air-conditioning cost saving of terracotta brick buildings integrated with PCMs compared to conventional terracotta brick buildings. Figure 7 shows the total building air-conditioning cost saving of terracotta brick buildings stuffed with PCMs compared to solid terracotta brick buildings in Ahmedabad and Lucknow climates.

In Ahmedabad, terracotta brick wall configurations PCMTB-A, stuffed with PCMs of OM18, HS22, OM29, OM32, and OM37 have shown an overall total building air-conditioning cost saving of $ 60.02, $ 61.44, $ 62.1, $ 63.45, and $ 62.63, respectively. Amongst all PCMs in the PCMTB-A, the OM32 underlines the highest total building air-conditioning cost saving. The terracotta brick wall configuration PCMTB-B stuffed with OM32 PCM shows the highest total building air-conditioning cost saving of $ 69.4 among all examined configuration in this category. In overall, among all assumed terracotta brick wall configurations stuffed with PCMs (PCMTB-A, PCMTB-B, and PCMTB-C), the PCMTB-C configuration with PCM corresponding to OM32 shows the maximum total building air-conditioning cost saving of $ 74.7.

In Lucknow, amongst all the examined terracotta brick wall configurations, the PCMTB-C stuffed with OM32 reveals the highest total building air-conditioning cost saving of $ 61.9. In Ahmedabad and Lucknow, the terracotta brick wall configuration PCMTB-B with OM32 shows a 9.35% increase in total building air-conditioning cost saving compared to PCMTB-A with OM32. The terracotta brick wall configuration PCMTB-C with OM32 shows an increment of 17.73% in total building air-conditioning cost saving compared to PCMTB-A with OM32.

3.4. Carbon Emission Mitigation Potential of Terracotta Brick Buildings Integrated with PCMs. Equation (15) was used to determine the carbon emission mitigation of terracotta brick buildings stuffed with PCMs compared to solid terracotta brick buildings. Figure 8 shows the carbon emission

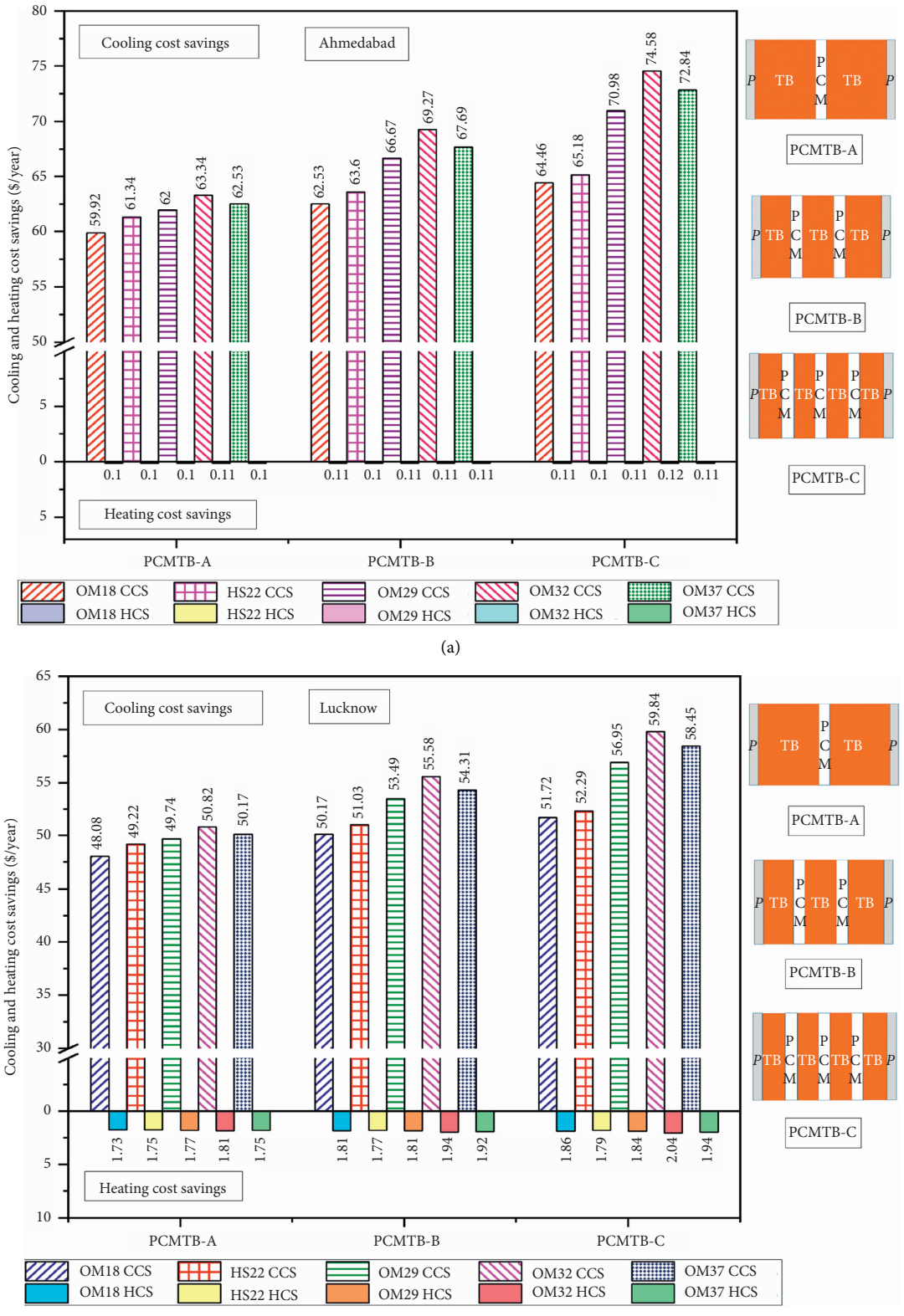

Figure 6: Annual cooling and heating cost of terracotta brick buildings integrated with PCMs: (a) Ahmedabad; (b) Lucknow.

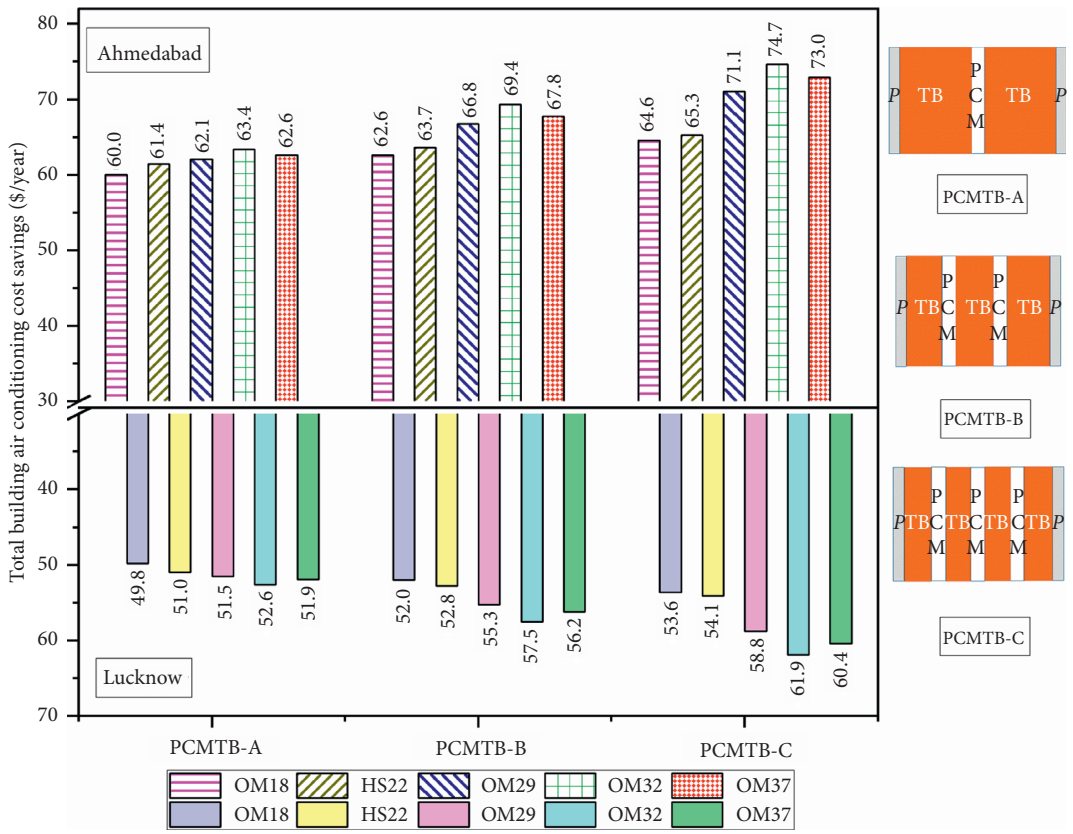

Figure 7: Total building air-conditioning cost saving of terracotta brick buildings integrated with PCMs in Ahmedabad and Lucknow.

mitigation potential of terracotta brick buildings integrated with PCMs in Ahmedabad and Lucknow climates.

In Ahmedabad, terracotta brick wall configurations PCMTB-A stuffed with PCMs of OM18, HS22, OM29, OM32, and OM37 have shown a carbon emission mitigation of 1.15 ton/kWh, 1.17 ton/kWh, 1.19 ton/kWh, 1.21 ton/kWh, and 1.20 ton/kWh, respectively. Amongst all PCMs in the PCMTB-A assembly, the OM32 shows the highest carbon emission mitigation; the findings have led to a 1.21 ton/kWh mitigation effect due to the significant air-conditioning cost saving for this selection. The terracotta brick wall configuration PCMTB-B stuffed with OM32 shows the highest carbon emission mitigation of 1.33 ton/kWh among all studied PCMs. Within the framework of all analysed terracotta brick wall configurations stuffed with PCMs (PCMTB-A, PCMTB-B, and PCMTB-C), the PCMTB-C configuration with PCM corresponding to OM32 shows the highest carbon emission mitigation of 1.43 ton/kWh.

Then again, in Lucknow, amongst all the terracotta brick wall configurations (PCMTB-A, PCMTB-B, and PCMTB-C) stuffed with PCMs, the PCMTB-C formations with PCM corresponding to OM32 highlights the highest carbon emission mitigation of 1.17 ton/kWh. In Ahmedabad and Lucknow, the terracotta brick wall configuration PCMTB-B with OM32 shows an increment of 9.35% in carbon emission mitigation compared to PCMTB-A with OM32. The terracotta brick wall configuration PCMTB-C with OM32 shows an increment of 17.73% in carbon emission mitigation compared to PCMTB-A with OM32.

3.5. Payback Periods of Terracotta Brick Buildings Integrated with PCMs. Equation (16) was used to calculate the payback period of terracotta brick buildings stuffed with PCMs. Figure 9 shows the payback periods of terracotta brick buildings integrated with PCMs compared to conventional terracotta bricks in Ahmedabad and Lucknow.

In Ahmedabad, terracotta brick wall configurations PCMTB-A stuffed with PCMs of OM18, HS22, OM29, OM32, and OM37 have resulted in a payback period of 13.6 years, 8.1 years, 15 years, 9.4 years, and 10 years, respectively. Amongst all PCMs in the PCMTB-A assembly, the HS22 shows the least payback period of 8.1 years followed by 9.4 years for OM32. The payback periods increase from the configurations PCMTB-A to PCMTB-C due to the increased cost of incorporating PCMs in terracotta bricks. Accordingly, the PCMTB-A and PCMTB-B configurations are more profitable from an economic point of view, while they present rational payback periods in contrast to PCMTB-C. For the lower payback periods, the following PCM materials are preferred in sequence: HS22, OM32, OM37, OM18, and OM29. The preferred sequential order of PCM is the same as material cost sequential order of PCM from low cost to high cost. The material cost of PCM is the most influential parameter in the payback period of PCM integrated terracotta bricks. From the lowest payback periods perspective, the configurations PCMTB-A and PCMTB-B are preferred over PCMTB-C.

The results of the above research findings apply to hot-dry and composite climatic conditions. The research can be

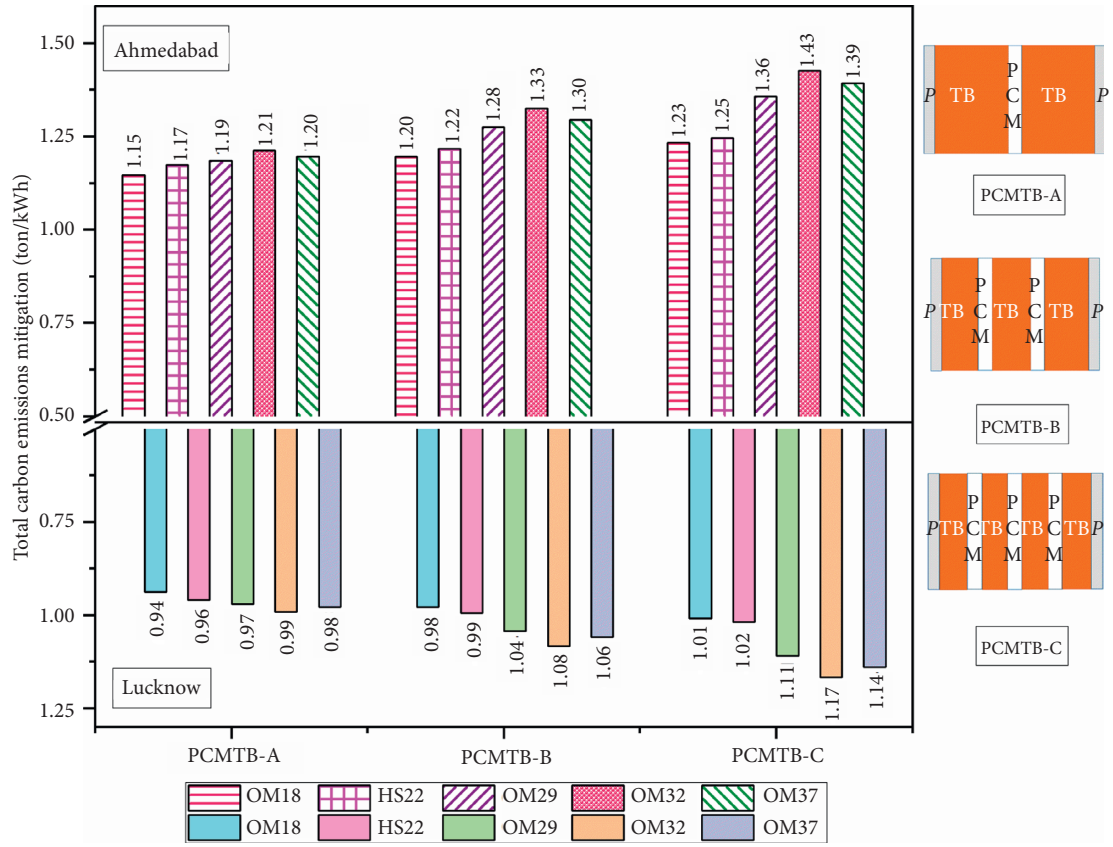

Figure 8: Carbon emission mitigation of terracotta brick buildings integrated with PCMs in Ahmedabad and Lucknow climates.

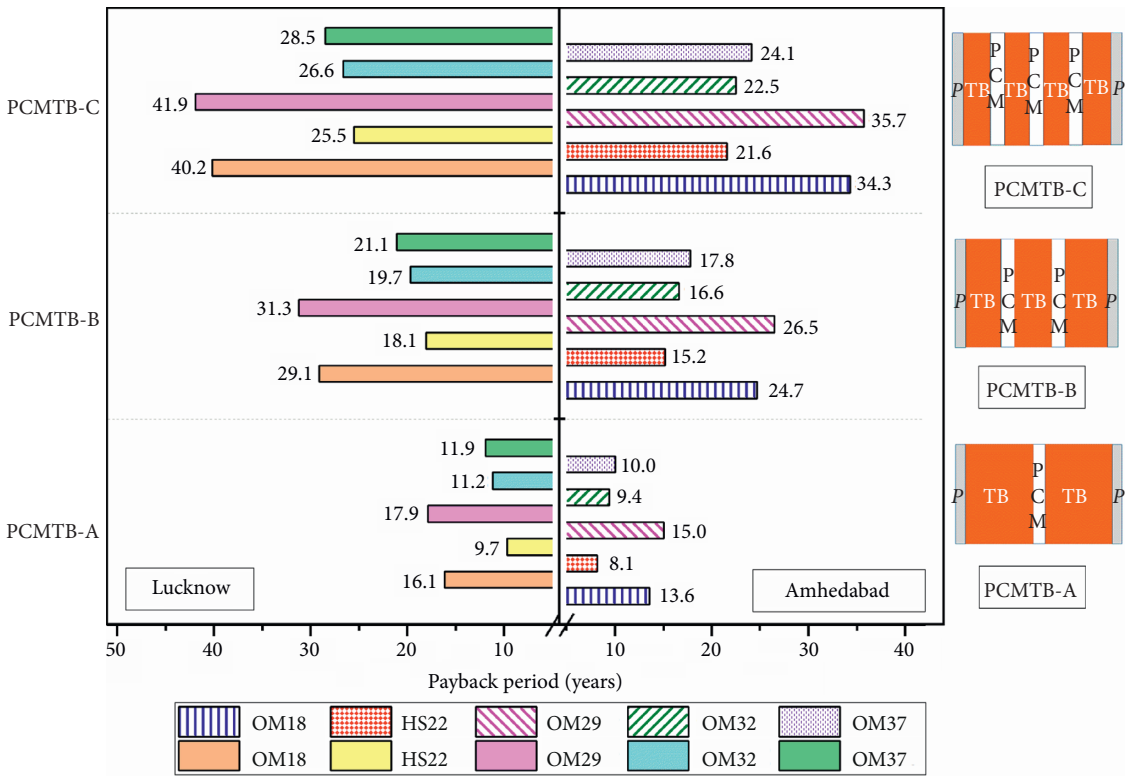

Figure 9: Payback periods of terracotta brick buildings integrated with PCMs in Ahmedabad and Lucknow.

extended to other climatic regions as well. Future research can be carried out on energy-efficient building envelopes integrated with various combinations of new PCMs.

4. Conclusions

This work evaluates the unsteady heat transfer characteristics, air-conditioning cost-saving, carbon emission mitigation, and payback periods of various PCM stuffed terracotta bricks compared to conventional terracotta bricks. In that respect, the thermophysical properties of five different PCMs (OM18, HS22, OM29, OM32, and OM37) in both solid and liquid phases were measured. This paper presents a mathematical model to compute unsteady thermal parameters which are further utilized for computing the air-conditioning cost-saving potential of PCM stuffed terracotta brick buildings in hot-dry and composite climates of India.

(i) The buildings of PCMTB-C configuration stuffed with OM32 saves the highest yearly air-conditioning costs of $ 74.70 and $ 61.9, respectively, in hot-dry and composite climates of India among all three terracotta brick configurations (PCMTB-A, B, and C) with five PCMs (OM18, HS22, OM29, OM32, and OM37) studied.

(ii) The buildings of PCMTB-C configuration stuffed with OM32 saves the highest carbon emission mitigation of 1.43 ton/kWh and 1.17 ton/kWh, respectively, in hot-dry and composite climates of India among all three terracotta brick configurations (PCMTB-A, B and C) with five PCMs (OM18, HS22, OM29, OM32, and OM37) studied.

(iii) The steady and unsteady transmittances reduce with the increase in the PCM layers in the terracotta bricks. PCMTB-C configuration stuffed with OM32 PCM gives the least steady and unsteady transmittance due to its improved thermal mass and thermal resistance compared to all studied configurations with five PCMs.

(iv) The attenuation factor reduces and time lag enhances with the increase in the PCM layers in the terracotta bricks. PCMTB-C configuration stuffed with OM32 PCM gives the least attenuation factor and the highest time lag due to its improved thermal mass and thermal resistance compared to all studied configurations with five PCMs.

(v) The best order of PCMs as per the desirable unsteady parameters, highest air-conditioning cost-saving, highest carbon emission mitigation potential is OM32 > OM37 > OM29 > HS22 > OM18. The preferred order of PCM stuffed terracotta brick configuration as per the desirable unsteady parameters, highest air-conditioning cost-saving, and highest carbon emission mitigation potential is PCMTB-C > PCMTB-B > PCMTB-A.

(vi) The payback period of the building increases with the increase in the PCM layers in the terracotta brick. PCMTB-A stuffed with HS22 buildings in hot-dry climate shows the least payback period of 8.1 years among all three terracotta brick configurations (PCMTB-A, B, and C) with five PCMs (OM18, HS22, OM29, OM32, and OM37) studied. For the lower payback periods in hot-dry and composite climates, the following PCM materials are preferred in sequence: HS22, OM32, OM37, OM18, and OM29. From the lowest payback periods perspective, the configurations PCMTB-A and PCMTB-B are preferred over PCMTB-C.

(vii) It is recommended to use PCMTB-B configuration with OM32 for buildings to have desirable unsteady parameters, higher air-conditioning cost-saving, higher carbon emission mitigation potential, and acceptable payback periods. It is not advisable to go for PCMTB-C configuration due to its long payback period of about 20 years.

The results of this study are useful in designing energy-conscious buildings with PCM-integrated terracotta bricks.

Nomenclature

C_c: Cooling cost saving ($)
C_e: Unit cost of electricity ($/kWh)
C_h: Heating cost-saving ($)
C_i: Material cost of PCM ($/kg)
C_n: Unit cost of natural gas ($/kWh)
C_p: Specific heat (kJ/(kg·K))
C_t: Annual air-conditioning cost-saving ($)
d: Discount rate (%)
f: Decrement factor (-)
h: Heat transfer coefficient (W/(m^2·K))
i: Inflation rate (%)
k: Thermal conductivity (W/(m·K))
M_c: Mass of CO_2 emission reduction (ton/kWh)
N_C: Number of cooling hours (h)
N_H: Number of heating hours (h)
p_1, p_2: Mass of CO_2 emission due to energy production (kg/kWh)
T_b: Base temperature (°C)
T_s: Sol air temperature (°C)
U: Thermal transmittance (W/(m^2·K))
U_t: Unsteady transmittance (W/(m^2·K))
X: Building material thickness (m)

Greek letters

α: Thermal diffusivity
η: Efficiency of natural gas power generation
φ: Time lag (h)
ρ: Density (kg/m^3)

Acronyms

CDH: Cooling degree-hours (°C-hours)
COP: Coefficient of performance
HDH: Heating degree-hours (°C-hours)
HS: Hydrated salt

OM: Organic mixture
P: Plaster
PP: Simple payback period
PCM: Phase change material
PCMTB: PCM-stuffed terracotta brick
TB: Terracotta brick.

Data Availability

The data used to support the findings of this study are included within the article.

Disclosure

This research received no specific grant from any funding agency (public/commercial).

Conflicts of Interest

The authors declare that they have no conflicts of interest.

References

[1] P. Nejat, F. Jomehzadeh, M. M. Taheri, M. Gohari, and M. Z. Abd. Majid, "A global review of energy consumption, CO 2 emissions and policy in the residential sector (with an overview of the top ten CO 2 emitting countries)," *Renewable and Sustainable Energy Reviews*, vol. 43, pp. 843–862, 2015.

[2] R. Qi, L. Lu, and H. Yang, "Investigation on air-conditioning load profile and energy consumption of desiccant cooling system for commercial buildings in Hong Kong," *Energy and Buildings*, vol. 49, pp. 509–518, 2012.

[3] D. G. L. Samuel, S. M. S. Nagendra, and M. P. Maiya, "Passive alternatives to mechanical air conditioning of building: a review," *Building and Environment*, vol. 66, pp. 54–64, 2013.

[4] K. J. Kontoleon, "Glazing solar heat gain analysis and optimization at varying orientations and placements in aspect of distributed radiation at the interior surfaces," *Applied Energy*, vol. 144, pp. 152–164, 2015.

[5] V. A. A. Raj and R. Velraj, "Review on free cooling of buildings using phase change materials," *Renewable and Sustainable Energy Reviews*, vol. 14, no. 9, pp. 2819–2829, 2010.

[6] A. Pasupathy, R. Velraj, and R. V. Seeniraj, "Phase Change Material-based building architecture for thermal management in residential and commercial establishments," *Renewable and Sustainable Energy Reviews*, vol. 12, no. 1, pp. 39–64, 2008.

[7] S. S. Chandel and T. Agarwal, "Review of current state of research on energy storage, toxicity, health hazards and commercialization of Phase Changing Materials," *Renewable and Sustainable Energy Reviews*, vol. 67, pp. 581–596, 2017.

[8] H. Akeiber, P. Nejat, M. Z. A. Majid et al., "A review on phase change material (PCM) for sustainable passive cooling in building envelopes," *Renewable and Sustainable Energy Reviews*, vol. 60, pp. 1470–1497, 2016.

[9] P. K. S. Rathore and S. K. Shukla, "Potential of macro-encapsulated pcm for thermal energy storage in buildings: a comprehensive review," *Construction and Building Materials*, vol. 225, pp. 723–744, 2019.

[10] F. Souayfane, F. Fardoun, and P.-H. Biwole, "Phase Change Materials (PCM) for cooling applications in buildings: a review," *Energy and Buildings*, vol. 129, pp. 396–431, 2016.

[11] R. Jacob and F. Bruno, "Review on shell materials used in the encapsulation of phase change materials for high temperature thermal energy storage," *Renewable and Sustainable Energy Reviews*, vol. 48, pp. 79–87, 2015.

[12] H. J. Akeiber, M. A. Wahid, H. M. Hussen, and A. T. Mohammad, "Review of development survey of phase change material models in building applications," *Scientific World Journal*, vol. 2014, pp. 1–11, 2014.

[13] S. R. L. da Cunha and J. L. B. de Aguiar, "Phase Change Materials and energy efficiency of buildings: a review of knowledge," *Journal of Energy Storage*, vol. 271260 pages, 2020.

[14] S. Mengjie, N. Fuxin, M. Ning, H. Yanxin, and D. Shiming, "Review on building energy performance improvement using Phase Change Materials," *Energy and Buildings*, vol. 158, pp. 776–793, 2018.

[15] A. Waqas and Z. Ud Din, "Phase change material (PCM) storage for free cooling of buildings-A review," *Renewable and Sustainable Energy Reviews*, vol. 18, pp. 607–625, 2013.

[16] S. Ben Romdhane, A. Amamou, R. Ben Khalifa, N. M. Saïd, Z. Younsi, and A. Jemni, "A review on thermal energy storage using phase change materials in passive building applications," *Journal of Building Engineering*, vol. 32, Article ID 101563, 2020.

[17] Y. Zhou, S. Zheng, Z. Liu et al., "Passive and active phase change materials integrated building energy systems with advanced machine-learning based climate-adaptive designs, intelligent operations, uncertainty-based analysis and optimisations: a state-of-the-art review," *Renewable and Sustainable Energy Reviews*, vol. 130, Article ID 109889, 2020.

[18] Y. Zhou, S. Zheng, and G. Zhang, "A review on cooling performance enhancement for phase change materials integrated systems-flexible design and smart control with machine learning applications," *Building and Environment*, vol. 174, Article ID 106786, 2020.

[19] F. Kuznik and J. Virgone, "Experimental investigation of wallboard containing phase change material: data for validation of numerical modeling," *Energy and Buildings*, vol. 41, no. 5, pp. 561–570, 2009.

[20] I. Mandilaras, M. Stamatiadou, D. Katsourinis, G. Zannis, and M. Founti, "Experimental thermal characterization of a mediterranean residential building with pcm gypsum board walls," *Building and Environment*, vol. 61, pp. 93–103, 2013.

[21] D. Mazzeo and G. Oliveti, "Parametric study and approximation of the exact analytical solution of the stefan problem in a finite PCM layer in a steady periodic regime," *International Communications in Heat and Mass Transfer*, vol. 84, pp. 49–65, 2017.

[22] D. Mazzeo, G. Oliveti, and N. Arcuri, "Definition of a new set of parameters for the dynamic thermal characterization of PCM layers in the presence of one or more liquid-solid interfaces," *Energy and Buildings*, vol. 141, pp. 379–396, 2017.

[23] Y. Zhou, C. W. F. Yu, and G. Zhang, "Study on heat-transfer mechanism of wallboards containing active phase change material and parameter optimization with ventilation," *Applied Thermal Engineering*, vol. 144, pp. 1091–1108, 2018.

[24] S. G. Yoon, Y. K. Yang, T. W. Kim, M. H. Chung, and J. C. Park, "Thermal performance test of a phase-change-material cool roof system by a scaled model," *Advances in Civil Engineering*, vol. 2018, 11 pages, 2018.

[25] X. Jin, M. A. Medina, and X. Zhang, "On the importance of the location of pcms in building walls for enhanced thermal performance," *Applied Energy*, vol. 106, pp. 72–78, 2013.

[26] E. Tunçbilek, M. Arıcı, M. Krajčík, S. Nižetić, and H. Karabay, "Thermal performance based optimization of an office wall containing PCM under intermittent cooling operation," *Applied Thermal Engineering*, vol. 179, Article ID 115750, 2020.

[27] Z. Liu, Z. Yu, T. Yang et al., "A review on macro-encapsulated phase change material for building envelope applications," *Building and Environment*, vol. 144, no. April, pp. 281–294, 2018.

[28] J. Lei, J. Yang, and E.-H. Yang, "Energy performance of building envelopes integrated with phase change materials for cooling load reduction in tropical Singapore," *Applied Energy*, vol. 162, pp. 207–217, 2016.

[29] E. Tunçbilek, M. Arıcı, S. Bouadila, and S. Wonorahardjo, "Seasonal and annual performance analysis of PCM-integrated building brick under the climatic conditions of Marmara region," *Journal of Thermal Analysis and Calorimetry*, vol. 141, no. 1, pp. 613–624, 2020.

[30] K. Lee Ok, M. A. Medina, E. Raith, and X. Sun, "Assessing the integration of a thin phase change material (pcm) layer in a residential building wall for heat transfer reduction and management," *Applied Energy*, vol. 137, pp. 699–706, 2014.

[31] X. Mi, R. Liu, H. Cui, S. A. Memon, F. Xing, and Y. Lo, "Energy and economic analysis of building integrated with pcm in different cities of China," *Applied Energy*, vol. 175, pp. 324–336, 2016.

[32] B. Y. Yun, J. H. Park, S. Yang, S. Wi, and S. Kim, "Integrated analysis of the energy and economic efficiency of pcm as an indoor decoration element: application to an apartment building," *Solar Energy*, vol. 196, pp. 437–447, 2019.

[33] E. Solgi, S. Memarian, and G. N. Moud, "Financial viability of pcms in countries with low energy cost: a case study of different climates in Iran," *Energy and Buildings*, vol. 173, pp. 128–137, 2018.

[34] ASTM:D5334-14, *Standard Test Method for Determination of Thermal Conductivity of Soil And Soft Rock by Thermal Needle Probe Procedure*, vol. 04, no. November, pp. 6–13, 2016.

[35] R. Cheng, M. Pomianowski, X. Wang, P. Heiselberg, and Y. Zhang, "A new method to determine thermophysical properties of PCM-concrete brick," *Applied Energy*, vol. 112, pp. 988–998, 2013.

[36] J. P. Holman, *Experimental Methods for Engineers*, McGraw-Hill Companies, New York, NY, USA, 2012.

[37] X. Sun, K. O. Lee, M. A. Medina, Y. Chu, and C. Li, "Melting temperature and enthalpy variations of phase change materials (PCMs): a differential scanning calorimetry (DSC) analysis," *Phase Transitions*, vol. 91, no. 6, pp. 667–680, 2018.

[38] D. Mazzeo, G. Oliveti, A. de Gracia, J. Coma, A. Solé, and L. F. Cabeza, "Experimental validation of the exact analytical solution to the steady periodic heat transfer problem in a PCM layer," *Energy*, vol. 140, pp. 1131–1147, 2017.

[39] S. Shaik and A. B. Talanki Puttaranga Setty, "Influence of ambient air relative humidity and temperature on thermal properties and unsteady thermal response characteristics of laterite wall houses," *Building and Environment*, vol. 99, pp. 170–183, 2016.

[40] CIBSE, *CIBSE Environmental Design Guide A. The Chartered Institution of*, Building Services Engineers London, London, UK, 2006.

[41] K. J. Kontoleon and D. K. Bikas, "The effect of south wall's outdoor absorption coefficient on time lag, decrement factor and temperature variations," *Energy and Buildings*, vol. 39, no. 9, pp. 1011–1018, 2007.

[42] S. Shaik and A. B. P. S. Talanki, "Optimizing the position of insulating materials in flat roofs exposed to sunshine to gain minimum heat into buildings under periodic heat transfer conditions," *Environmental Science and Pollution Research*, vol. 23, no. 10, pp. 9334–9344, 2016.

[43] G. M. Soret, P. Vacca, J. Tignard et al., "Thermal inertia as an integrative parameter for building performance," *Journal of Building Engineering*, vol. 33, Article ID 101623, 2020.

[44] ASHRAE, *American Society Of Heating, Refrigerating and Air-Conditioning Engineers*, Climatic Design Information, Atlanta, USA, Chapter 14, 2009.

[45] A. Bolattürk, "Optimum insulation thicknesses for building walls with respect to cooling and heating degree-hours in the warmest zone of Turkey," *Building and Environment*, vol. 43, no. 6, pp. 1055–1064, 2008.

[46] K. G. Kumar, S. Saboor, V. Kumar, K. H. Kim, and T. P. A. Babu, "Experimental and theoretical studies of various solar control window glasses for the reduction of cooling and heating loads in buildings across different climatic regions," *Energy and Buildings*, vol. 173, pp. 326–336, 2018.

[47] J. A. Duffie and W. A. Beckman, *Solar Engineering of Thermal Processes*, John Wiley and Sons, New York, NY, USA, 2013.

Hindawi
Advances in Civil Engineering
Volume 2020, Article ID 8867558, 21 pages
https://doi.org/10.1155/2020/8867558

Research Article

Energy and Daylighting Evaluation of Integrated Semitransparent Photovoltaic Windows with Internal Light Shelves in Open-Office Buildings

Abdelhakim Mesloub,[1] Artira Ghosh ,[2,3,4] Ghazy Abdullah Albaqawy,[1] Emad Noaime,[1] and Badr M Alsolami[5]

[1]*Department of Architectural Engineering, Ha'il University, Ha'il 2440, Saudi Arabia*
[2]*Environment and Sustainability Institute, University of Exeter, Penryn TR10 9FE, UK*
[3]*College of Engineering, Mathematics and Physical Sciences, Renewable Energy, University of Exeter, Penryn TR10 9FE, UK*
[4]*Renewable Energy, Stella Turk Building, University of Exeter, Penryn TR10 9FE, UK*
[5]*Islamic Architecture Department, College of Engineering and Islamic Architecture, Umm Al-Qura University, Mecca, Saudi Arabia*

Correspondence should be addressed to Artira Ghosh; a.ghosh@exeter.ac.uk

Received 28 September 2020; Revised 11 November 2020; Accepted 26 November 2020; Published 21 December 2020

Academic Editor: Dong Zhao

In modern architecture, highly glazed commercial buildings account for considerable amount of energy, specifically in cold and hot climates because of heating, cooling, and lighting energy load demand. Abatement of this high building energy is possible by employing semitransparent photovoltaic (STPV) window which has triple point advantages as they control the admitted solar gain and daylight and generates benign electricity. Integration of internal light shelves (ILS) to this STPV window assists in controlling visual comfort. Thus, this study aims to evaluate the impact of a nonuniform layout of double-glazing (DG) low-e STPV and DG low-E argon-filled clear glass integrated into a fully glazed open-office facade combined with ILS in cardinal orientations under Riyadh, London, Kuala Lumpur, and Algiers climates. Comprehensive energetic and radiance simulations were conducted to evaluate three groups of STPV configurations. The first group replaced the glazing area with amorphous silicon (a-Si) modules with different transparencies; the second and third groups changed only 75% and 50% of the glazing area, respectively, with STPVs integrated with the ILS. The results revealed that the integration of a-Si modules did not meet the visual comfort requirements but obtained the maximum saving in the east-west axis. It was also found that the optimum design on the south-facing facade with the nonuniform facade achieved 50% of STPV10 coverage in clear glazing windows combined with ILS; the energy saving ratios comparing the reference models were 76%, 83%, 65%, and 70% in Riyadh, London, Kuala Lumpur, and Algiers, respectively. Thus, the integration of STPVs with ILS is considered a more efficient way and effective solution to reduce the possibility of glare discomfort.

1. Introduction

Currently, the overall energy consumption in the buildings sector is responsible for almost one-third of the energy used worldwide. Heating, cooling, and artificial lighting load demands are the reason for this high consumption. Energy loss and gain both incur in higher order through the transparent building window envelopes [1, 2]. Traditional buildings windows are highly transparent single- or double-glazing type which allows excessive amount of solar heat and daylight both into a building interior. In modern architecture, percentages of fully glazed facades are gaining importance which can increase further the energy demand. Controlling this entering light is of utmost importance to reduce the building energy demand and enhance the occupants' comfort [3]. However, daylight in a fully glazed

building design provides tremendous psychological benefits to building occupants and reduces electrical lighting energy [4]. Hence, suitable light control mechanism is required which will control the solar heat and by employing proper daylighting overall energy cost can be reduced. Previously, light shelves [5] were often employed to building to obtain visual and thermal for occupants. Light shelves can be static flat or curved reflective shaped and can easily be mounted on the external or internal part of vertical opening. They can offer shading, redirect incoming light flux towards the ceiling, and improve uniform daylight penetration [6–8]. However, it has some limitations such as increase of solar gain may offset the lighting energy saving potential, issues created from glare, and maintenance requirement for dynamic light shelves [7].

Recent trend is to employ semitransparent window over fully transparent window to control the entering solar light. Semitransparent photovoltaic (STPV) windows are specially gaining importance as they have ability to abate the energy demand being energy efficient over conventional windows [9]. They are considered a promising fenestration technology that can preserve energy and provide thermal and visual comfort [10]. Thin-film a-Si (amorphous silicon), cadmium telluride (CdTe) [11], and copper indium gallium selenide (CIGS) PVs have the ability to modulate the entering light and produce benign power [12, 13]. Also third-generation DSSC [14] and perovskites [15, 16] are able to tune the transparency. Some of them are integrated in commercialised products with module effectiveness of up to 10% and cell efficiency of up to 13.6% [17] on the basis of the optical (visible light transmittance) and thermal characteristics and PV system used [18].

The most significant rating indices used for evaluating the thermal performance of an STPV fenestration system are the solar heat gain coefficient (SHGC) and thermal transmission (U-value) [19]. In short, the U-value measures the overall heat transfer from a material and is expressed between the values of 0.1 and 1, where lower U-value indicates high thermal insulation. It is considered an important factor in cold climate [11], but has less effect than the SHGC in warmer climate due to direct solar radiation [20]. Fung and Yang [21] found that the area of solar cells in the PV module significantly affect the total heat gain, since nearly 70% of the total heat gain was reduced when the solar cell area ratio, defined as PV module area covered by solar cells, was set at 0.8. However, other parameters, such as solar cells' efficiency and the PV module thickness, had only limited influence. He et al. [22] compared the performance of a-Si PV single- and double-glazing windows in east China both numerically and experimentally. The double-glazing solution was found to be able to decrease indoor heat gains to 46%, enhancing indoor thermal comfort. Didoné and Wagner [23] carried out a numerical simulation to assess the potential energy savings of STPVs in tropical climates. The results revealed that the use of an appropriate control system and an energy production could achieve 17% to 43% potential energy savings. In the same climate, Ng and Mithraratne [24] evaluated the overall energy performance of six commercially available STPV modules by calculating net electrical benefits (NEB) for different WWR window designs in Singapore. They found that the integration of all STPVs with appropriate WWR performed better than conventional windows in terms of energy saving. Elsewhere, the possible benefits of integrating STPVs in Mediterranean climates was explored by Olivieri et al. and Mesloub et al. who suggested that the technology potential is high [25, 26]. While Huang et al. [27] proved that double-glazing Low-e STPVs performed better than conventional double-glazing windows on the west and east orientation in cooling dominant climate. Kapsis and Athienitis [28, 29] investigated the effect of optical parameters of STPV windows by using the first-generation module on the energy performance of using the concept of a three-section facade. The results revealed that STPVs with 10% transmittance could save up to 53.1% electricity and daylight requirements achieved with an effective transmittance of more than 30% and 40%. Li et al. [30] recommended that the ratio of PV cells for double-skin STPV facades can be less than 60% to achieve the requirements of indoor daylighting in Tianjin, China. Chang et al. [1] developed a novel dynamic daylighting metric to assess STPVs by considering the effect of window sizes and orientations within the same context. The results revealed that the optimal orientation is the south to achieve the lowest annual net energy and daylighting quantity and quality.

However, power generation from STPV is strongly correlated with the transmittance level of PV. Lower transmittance generates higher power while stops viewing from interior to exterior while higher transmittance generates lower power and allows viewing. The current practice of STPVs is applied to uniform layouts for the whole window area. Only a few studies have investigated the spatial distribution of glazing types [31], as well as the application of STPV with different transparencies and window-to-wall ratio (WWR), which is considered an effective daylighting strategy to control the quantity of daylight and produce energy [32]. However, for large STPV facades, the lower part of the window can reduce the light transmission but the upper part still allows higher light [33] which further needs to be abated. To limit the light transmission from the upper part of the window inclusion of light shelves can be an option. For the first time, this study will evaluate the impact of nonuniform layouts of DG low-e STPV and DG low-e argon-filled clear glass integrated in fully glazed open-office facades, combined with internal light shelves in cardinal orientations in different climates. The outcome will propose an optimum balance solution in terms of energy saving and visual comfort in the application of future buildings.

2. Materials and Methods

A comprehensive numerical parametric simulation of integrated STPVs combined with ILS was conducted based on EnergyPlus and Diva-for-Rhino simulation tools. All STPV configurations were simulated in four diverse climates to analyze the influence of different latitude and climatic conditions on the optimal configuration of the combined systems. The Meteonorm meteorological database corresponding to Riyadh was used for the subtropical desert

climate, while the Typical Meteorological Year (TMY) files of London, Algiers, and Kuala Lumpur were used for the marine west coast (temperate) and Mediterranean climates and tropical rainforest, respectively. Among the most important reasons for selecting these cities are the differences in external temperature (either too cold, too hot or average) and the amount of solar radiation that affect the solar panel performance and external illuminance in each zone based on the sky condition. Table 1 shows the location and climatic conditions of each zone based on Köppen Climate Classification.

2.1. Perimeter Zone Configuration. An open-plan perimeter office zone was modelled using the Diva-for-Rhino simulation software in cardinal orientations as shown in Figure 1. The area of the open-office is based on the US Department of Energy (DOE) large commercial building prototype [34], which is a 180 m^2 furnished area that is 20 m wide by 9 m deep with a 3 m high ceiling. The height of the furniture was taken into account to provide all occupants with access to outdoor views and no exterior obstructions.

2.2. STPV Configurations. In this study, a total of nine STPV configurations and reference models were examined referring to the level of transmittance (10%, 20%, and 30%) and the height and length of flat internal light shelves. The spatial combination of STPVs, glazing surfaces, and internal light shelves is based on the principle of dividing the facade into upper daylight and the lower part for viewing [31]. Meanwhile, the length of ILS is equal to the distance to the clerestory [7]. The STPV configurations can be divided into three main groups. The first group replaces the full clear glazing (100% WWR) by STPVs with variant transparencies. The second group considers the glazing divided into two continuous stripes. The lower part of the glazing is integrated with the STPVs with 75% of total area of glazing. The upper daylight part utilises the clear glass as well as sets up flat ILS 0.75 m in length and 2.25 m in height. The third group divides the glazing into two equal continuous stripes, with a 1.5 m ILS length, while keeping STPVs on the bottom and clear glass on top, as clearly shown in Figure 2.

The chosen STPVs were amorphous silicon (a-Si) types that were obtained from Onyx in Spain and had a range of visible light transmittance (10%, 20%, and 30%), suitable for building residents with an excellent outdoor view. The performance of ordinary a-Si PV thin-film modules becomes distinctly low (less than 5%). As a result, a change between the energy and daylighting performances ought to be affected to maximise the benefits of energy. A better PV module transmittance could result in a decline of energy conversion efficiency as well as an upgrade of the solar heat benefit coefficient. Table 2 describes the thermooptical properties of various STPV models used in the analysis.

2.3. Energy and Radiance Simulation. The energy modelling of EnergyPlus makes it possible to simulate the energy production of the STPV system by means of an equivalent one-diode model [35]. This model uses an empirical relationship to predict the operating performance of the PV based on conditions such as PV cell temperature and estimation of conversion efficiency for each time step. Nevertheless, a comprehensive validation was performed in previous studies [25, 36]. The electrical properties of various STPV transparencies applied in this study are summarised in Table 3.

On the other hand, an ideal HVAC system is also assumed to supply the required heating or cooling air to the related zone to meet the set point indoor air temperature of 26°C in the summer and 20°C in the winter season based on international standard (ASHRAE 55, ISO 7730), with a heating and cooling coefficient performance of 1. Taking into account that the simulated open-office components are in cardinal orientation, the floor, the ceiling, and the internal walls were adiabatic. The HVAC system was turned on only during the occupancy schedule, which was from 8.00 AM to 5.00 PM.

A flat LED ceiling surface-mounted luminaire with an input power of 17.4 W was installed in regular distances of 1.5 m by 2 m in columns and rows, respectively. This arrangement is for illuminating the whole work plane with a sufficient quantity of light in the case of an absence of daylight based on the lumen method [37].

The quantitative results derived from the radiance simulation (Diva-for-Rhino program) depend significantly on the successful configuration of the input parameters according to the specification of the STPV and ILS design. The radiance parameters such as materials reflection as depicted in Table 4 were specified to ensure the photometric accuracy of the results, which can be categorised as a ray-tracing algorithm, which tracks rays of light backwards from the eye to the focus of the scene [38]. The simulation radiance parameters used in the daylighting simulation is depicted in Table 5.

In this context, the annual climate-based daylight metrics were applied to evaluate the daylighting performance and were compared with the reference model under various sky and external illuminance conditions. The first metric is daylight autonomy (DA), which was evaluated based only on a minimum illuminance level of 300 lux, but this metric alone failed to consider the effect of glare under excessive daylighting [1, 39]. The second metric was the useful daylight illuminance (UDI), which required upper and lower thresholds from 100 lux to 2000 lux to provide an effective mechanism to indicate high levels of illumination linked with discomfort glare and heat gains [40]. Furthermore, the Daylight Glare Probability (DGP) is for glare assessments [41]. The criteria of assessments for each metric are summarised in Table 6.

3. Results and Discussion

3.1. Energy Performance Evaluation. The impacts of spatial distribution transparencies and integrated ILS on the STPV performance set up in open-office buildings in different climates were numerically investigated in terms of annual net energy consumption. Hereafter, the net energy consists

Table 1: Climatic conditions of different cities used in this study.

Cities (climate)	Latitude	Longitude	Average air temperature in winter and summer (°C)	Annual average solar irradiance (kWh/m^2)	Sky condition	External illuminance (klx)
Riyadh (subtropical desert climate)	24.43°N	46.43°E	14.4–36.1	2200	Clear	19 to 35
London (marine west coast climate) "Cfb"	51.09°N	0.11°W	4.3–17.3	1000	Overcast	03 to 20
Kuala Lumpur (tropical rainforest) "Af"	03.07°N	101.33°E	27.2–28.3	1600	Intermediate	18 to 23
Algiers Mediterranean "Csa"	36.43°N	3.15°E	11.1–25.6	1900	Clear-overcast	10 to 36

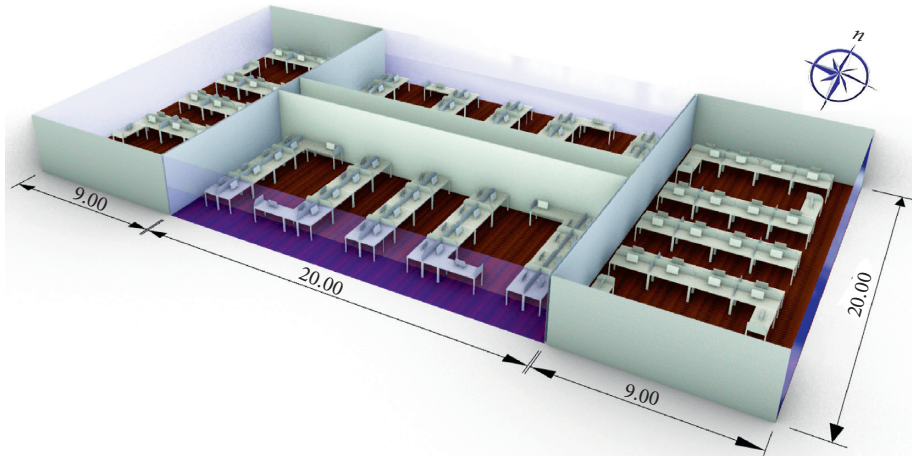

Figure 1: 3D model of perimeter open-office zone and furniture arrangements in cardinal orientation.

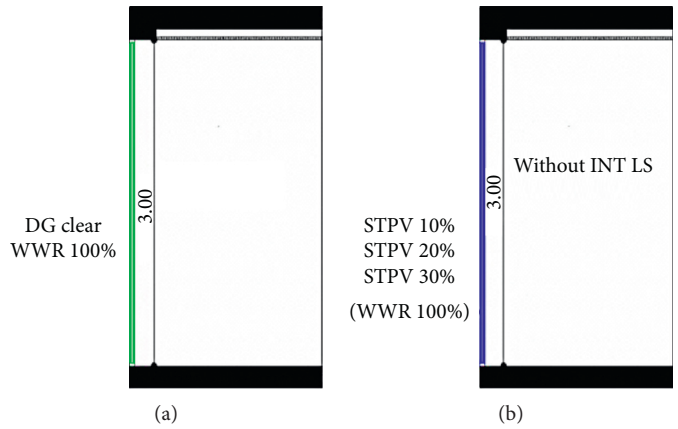

Figure 2: Continued.

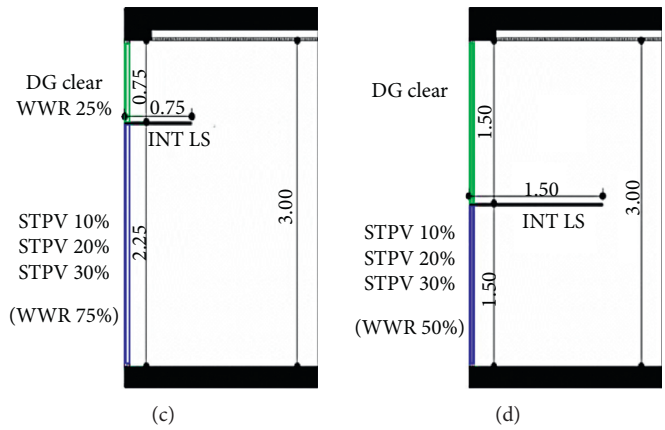

Figure 2: STPV configurations applied in each part of the simulation. (a) Reference model. (b) First Group. (c) Second Group. (d) Third Group.

Table 2: Thermooptical properties of various STPV (10%, 20%, and 30% VLT) and reference glazing models.

Glazing configurations	SHGC (%)	U-value (W/m^2K)	External light reflection (%)	Transmittance VLT (%)	Peak power (Wp/m^2)
Double-glazing low-E argon-filled	0.65	1.1	13	79	—
STPV DG low-E 10%	0.09	1.6	7.3	**10**	40
STPV DG low-E 20%	0.12	1.6	7.3	**20**	34
STPV DG low-E 30%	0.17	1.6	7.3	**30**	28

Table 3: Input electrical parameters of various STPV transparencies.

Parameters of PV	STPV 10%	STPV 20%	STPV 30%
Efficiency of module ($\eta_\circ$)	**4%**	**3.4%**	**2.8%**
Max power (Pmax)	123 watts	104 watts	86 watts
Max power voltage (Vpm)	132 V	132 V	132 V
Max power current (Ipm)	0.93 A	0.79 A	0.65 A
Open circuit voltage	191 V	191 V	191 V
Short circuit current	1.15 A	0.97 A	0.77 A
Temperature coefficient of P_{mpp}	−0.19%/C°	−0.19%/C°	−0.19%/C°
Temperature coefficient of V_{oc}	−0.28%/C°	−0.28%/C°	−0.28%/C°
Temperature coefficient of I_{sc}	+0.09%/C°	+0.09%/C°	+0.09%/C°

Table 4: Material reflection coefficient percentage.

Material	Reflection coefficient (%)
Ceiling	80
Floor	40
Wall	70
Furniture	50
Light shelve	90

of cooling, heating, and lighting energy minus the energy produced with a-Si solar cells. It is expressed with kWh per year, as presented in Tables 7 and 8.

On an annual basis, the results revealed that the net energy consumption of all STPV configurations compared to the reference model has a significant reduction, in particular, the cooling load energy, except for the first group of STPV configurations with all transparencies in the south-north axis of London due to the counterproductive effect on the heating load, which almost doubled from 6568 kWh to 7435 kWh for STPV 30% and STPV 10%, respectively. Inversely, the net energy used by the first group was less than other configurations in the east-west axis because of the sharp decline of cooling energy, as depicted in Table 8. Although the lighting energy consumption recorded the highest values, it can reach up to 2600 kWh in overcast sky conditions in London. The trend of PV modules with various transparencies from 10% to 30% slightly reduced the heating and lighting energy; meanwhile, they increased the cooling energy due to the entrance of more solar radiance. Also, there was a remarkable decrease of energy production because of the low conversion energy efficiency.

As expected, the integration of STPVs in the southern facade acquired the maximum annual yield, while the eastern facade had the least lighting energy consumption. Nevertheless, the more transmittance glazing integrated into the upper part of the window with ILS obtained a lower lighting energy in the southern facade, as depicted in the third group. The south-north axis consumes more energy than the east-west axis within all climate contexts.

The integration of ILS and STPV (second and third groups) leads to a significant improvement in terms of energy in the south-north axis rather than the east-west axis because of the substantial impact of ILS with high transmittance of clear glass in the upper part of window, which

Table 5: Radiance parameters used in daylighting simulation.

Radiance parameter	Ambient bounces	Ambient divisions	Ambient sampling	Ambient accuracy	Ambient resolution
Value	7	1500	100	0.1	300

Table 6: The performance indicators of visual comfort used in this study.

Criteria	Performance indicator of delighting quantity and quality
UDI	100 lux < dark area (needs artificial light) 100 lux–2000 lux (comfortable), at least 50% of the time >2000 lux too bright with thermal discomfort
DA	Set up 300 lx
DGP	0.35 < imperceptible glare 0.35–0.40 perceptible glare 0.4–0.45 disturbing glare >0.45 intolerable glare

reflected the concentrated solar heat gain and daylight into the back area to reduce both cooling and lighting energy. Consequently, the optimum energy performance of various STPVs combined with ILS configurations achieved with the second group (75% of STPV10 with 0.75 m ILS) in the south-north axis and the first group (STPV10 without ILS) in the east-west axis. The variances of net energy consumption between the optimum and worst configurations in both axes are approximately 73% to 48% in Riyadh, 94% to 30% in London, 64% to 36% in Kuala Lumpur, and 73% to 50% in Algiers, which indicates the importance of balancing the spatial distribution of glazing and the significant role of ILS in the southern facade that directly affects energy savings.

3.2. Daylighting Performance Evaluation. The evaluation of the daylighting performance of various integrated transparencies of STPV a-Si windows combined with ILS scenarios was based on achieving a balance between climate-based daylight metrics (DA300 lux & UDI100 lux-2000 lux thresholds) and DGP for glare comfort. It is important to mention that a-Si windows modules were treated as uniform optical properties. Three effective visible transmittance values of the STPV window modules were simulated: 10%, 20%, and 30%. The minimum value of 10% was selected to ensure a certain minimum view to the outdoors.

The figures in Tables 9–12 present the DA300 lux distribution to quantify the daylighting performance of the reference model comparing various STPV configurations with and without ILS in cardinal orientation in different climates. The reference model achieves the DA300 lux requirements in all-sky conditions, at least 78% in cardinal orientation. On the contrary, the first group, which replaced the clear glazing with STPVs with all transparencies, did not meet the requirements of illuminance design in office 300 lux, the highest percentage obtained in the south orientation with less than 20% in the best scenario. The second group noted a remarkable improvement compared to the first group. Specifically, the south orientation reached up to 20%, 15%, 9%, and 34% in Riyadh, London, Kuala Lumpur, and Algiers, respectively; this is due to the reflection of daylight that occurs in the middle of the office because of the integration of ILS and 25% of clear glass. However, this enhancement in DA300 lux distribution still did not achieve the minimum target of 50%. The third group can effectively improve luminous environment and exceed 50% of DA300 lux in all the southern offices in all climate regions, increasing from 32% to 59% for (50% of STPV 30%) compared to (75% of STPV 30%) in Riyadh, 30% to 61%, 11% to 64%, and 40% to 73% in London, Kuala Lumpur, and Algiers, for the east-west axis only achieved in tropical climate.

Tables 13–16 display the three UDI bins of the same configurations mentioned with the first climate-based daylight metric. The results confirmed again that the reference model achieved higher than 50% UDI100 lux–2000 lux, but a considerable percentage of UDI >2000 lux exposed to glare thermal discomfort in the south facade due to high transmittance reached 25%, 28%, and 33% in Riyadh, London, and Algiers, respectively, and 24% in Kuala Lumpur east-orientation. It can be seen that UDI <100 in the first group configuration ranges from 100% for STPV10% to 66%, 62%, 55%, and 54% for STPV30% in in Riyadh, London, Kuala Lumpur, and Algiers, respectively. Consequently, these results indicated that the performance of daylighting is unsuitable for the integration in open-office buildings in all climates. The integration of ILS in the second and third groups revealed a significant proportion of the working hours of desirable levels of illumination (i.e., appearing in the UDI100–2000 lux threshold), while the UDI >2000 lux was barely neglectable.

3.3. Visual Glare Evaluation. Glare is one of the most disturbing side effects of lighting. High luminance or extreme luminance differences associated with the visual field cause this effect. Computation of glare indices is done based on equations that can correlate luminance values or luminance distributions relating to the field of view of the observer, with the human glare sensation. Therefore, the DGP metric was employed to evaluate the annual daylight glare of reference models compared to the optimum STPV combined with ILS configurations based on their net energy and climate-based daylight metrics performance in various orientations and climates as shown in the figures included in Table 17.

The temporal maps of the occupied hours of the reference model illustrated that the simulated office in tropical climates (low latitudes) has imperceptible glare through the year. This is because the solar altitude, which is higher at midday, caused a remarkable drop in cardinal orientation, especially when adopting ILS. In contrary, the remaining tested climates (medium and high latitudes) show intolerable glare in the east-west axis, which can be explained due to the solar altitude in the winter season being lower, which causes a direct penetration to the office. The integration of

Table 7: Overall energy consumptions and net energy of different STPV configurations oriented to south and north axis in Riyadh, London, Kuala Lumpur, and Algiers cities.

Southern facade	Northern facade
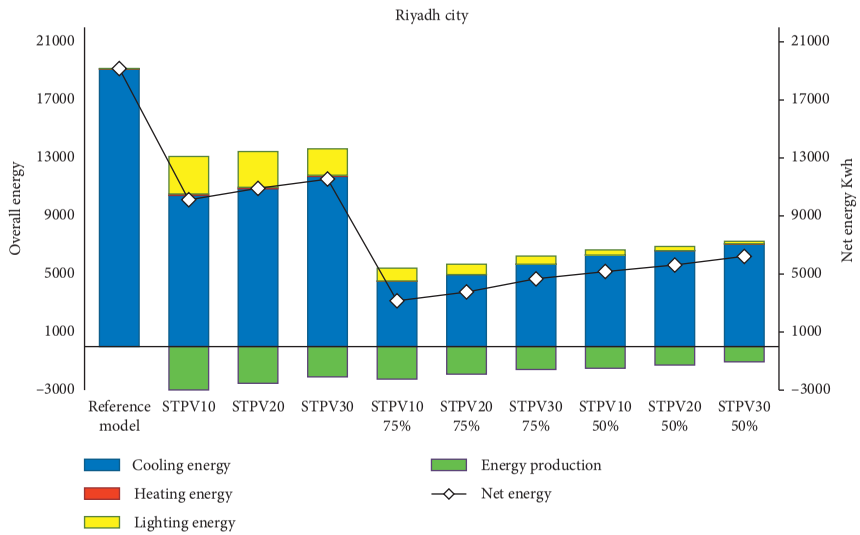	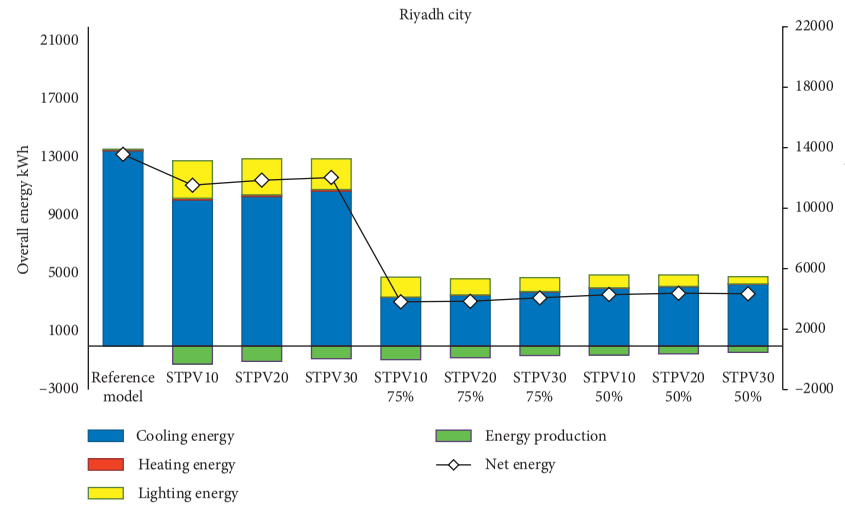
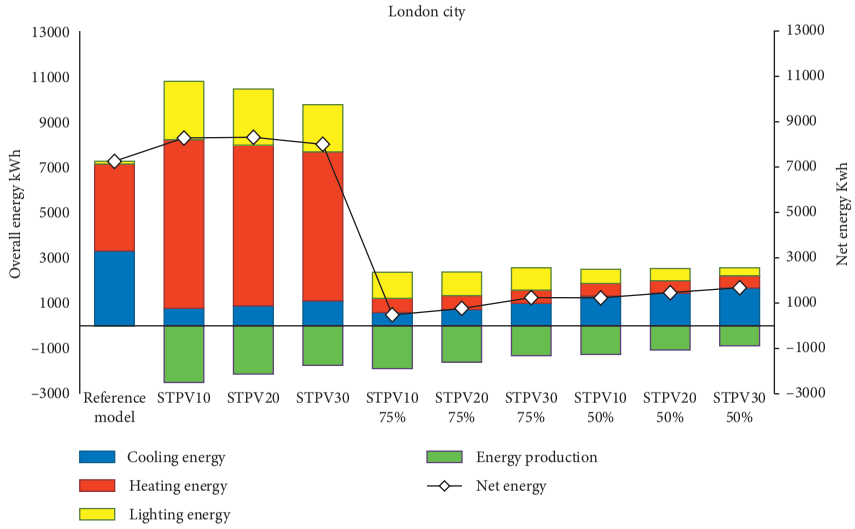	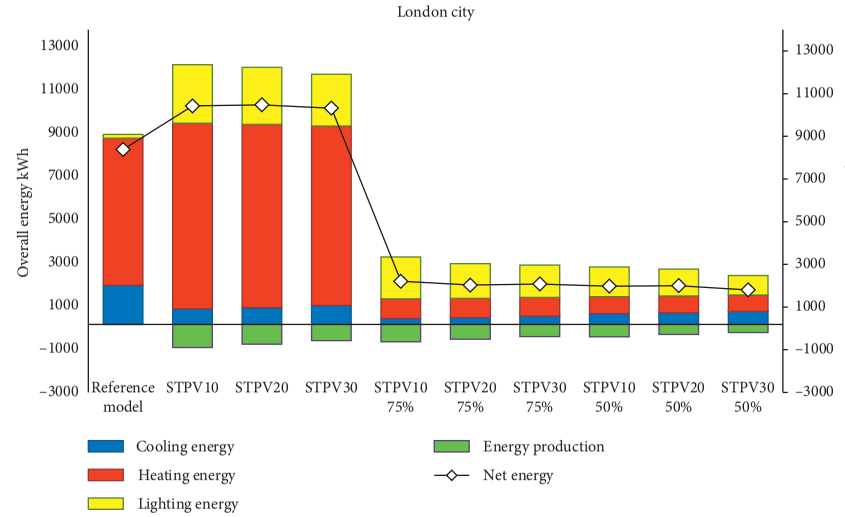

Table 7: Continued.

Southern facade	Northern facade
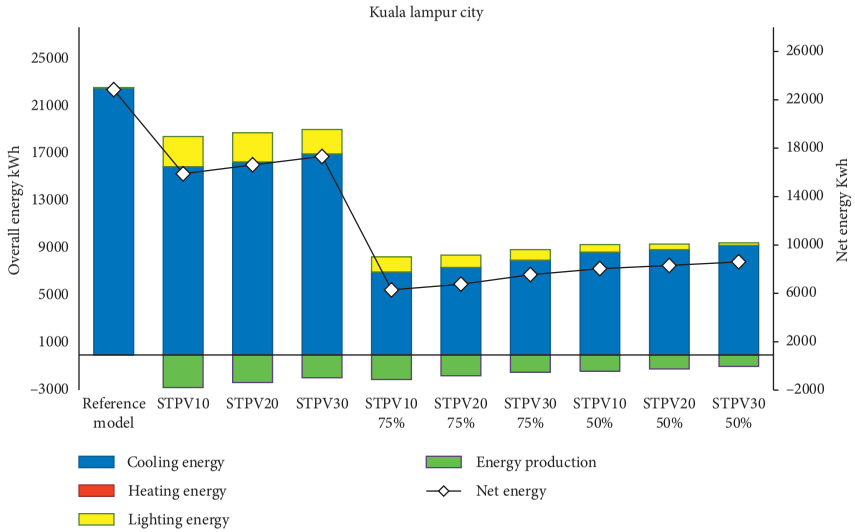	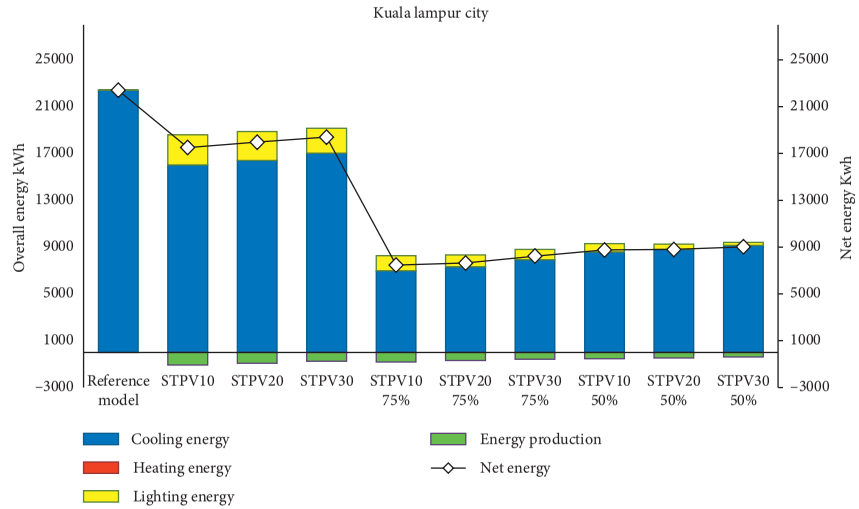
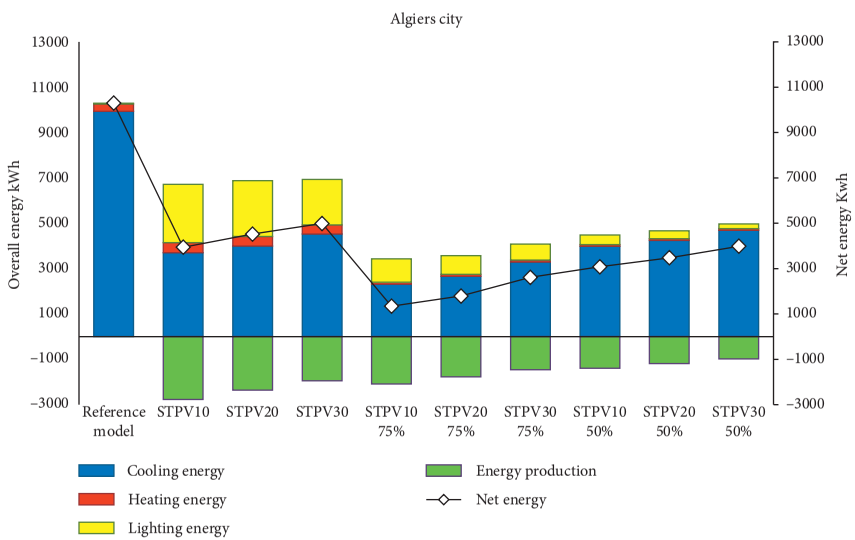	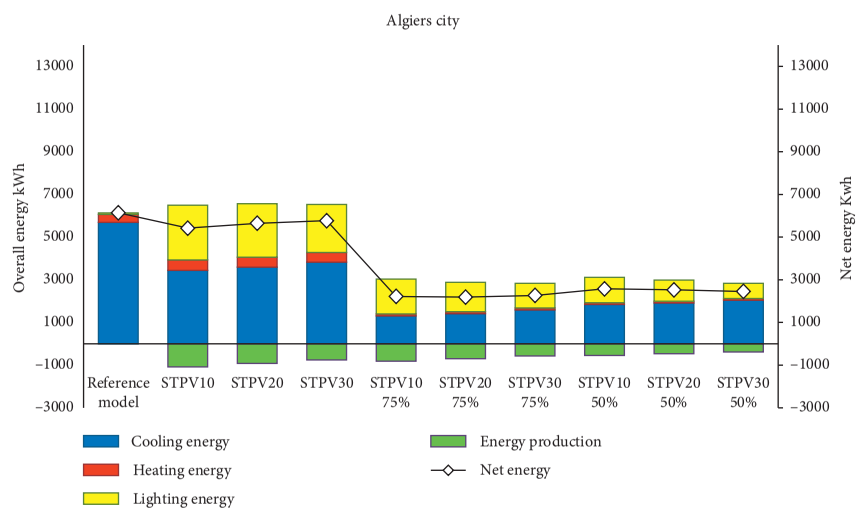

Table 8: Overall energy consumptions and net energy of different STPV configurations oriented to east and west axis in Riyadh, London, Kuala Lumpur, and Algiers cities.

Eastern facade	Western facade
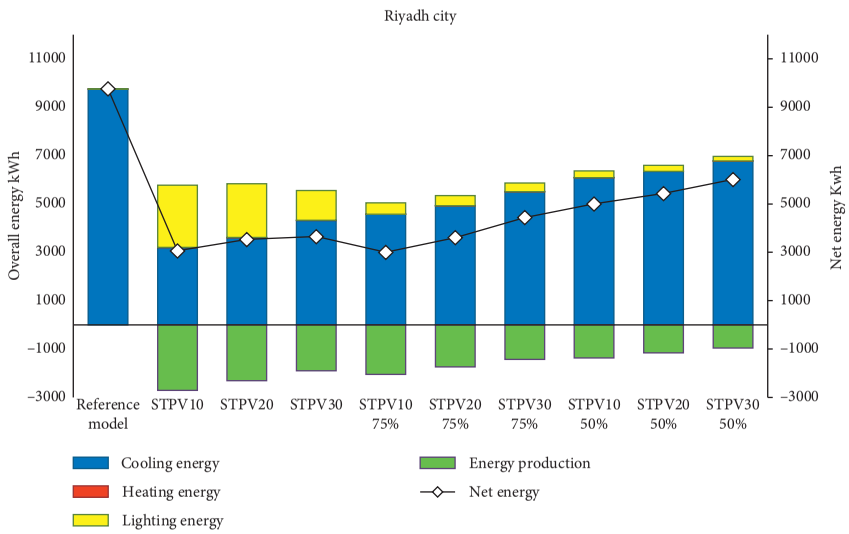	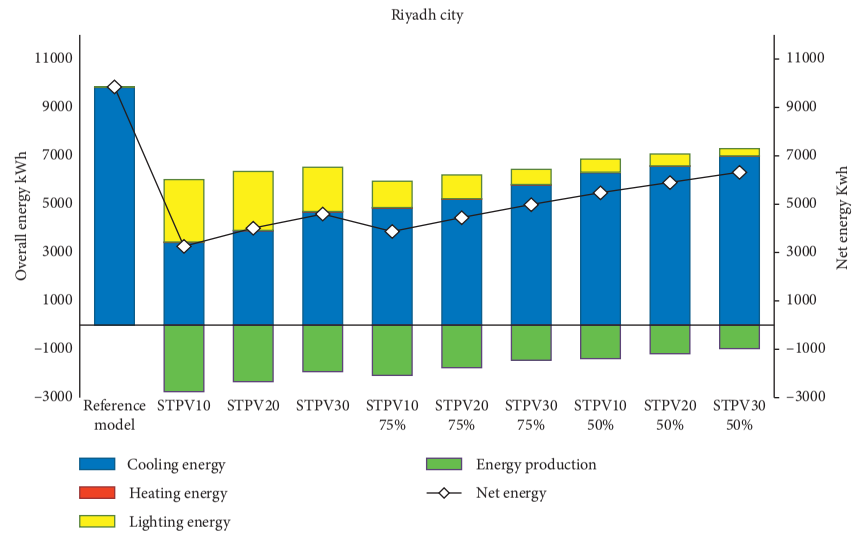
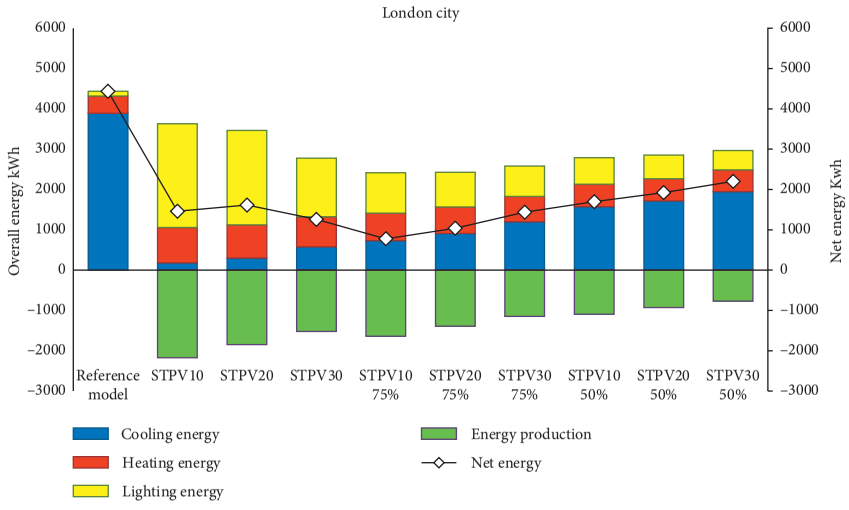	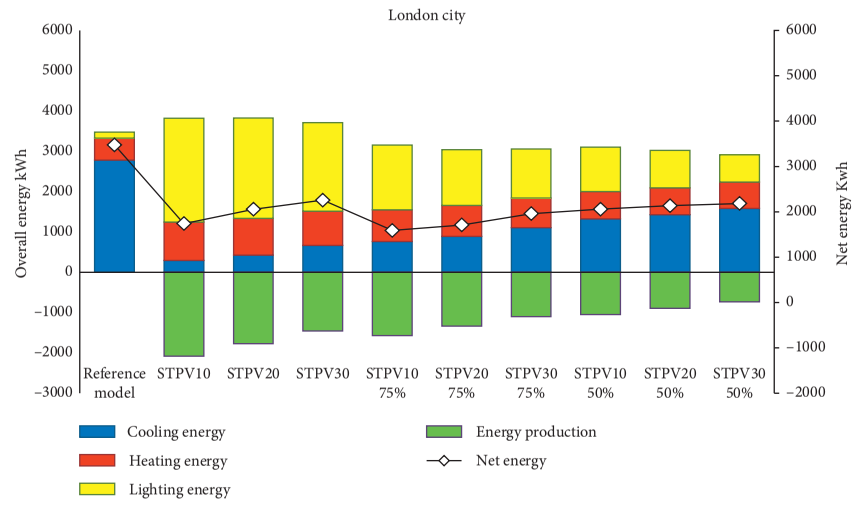

Table 8: Continued.

Eastern facade	Western facade
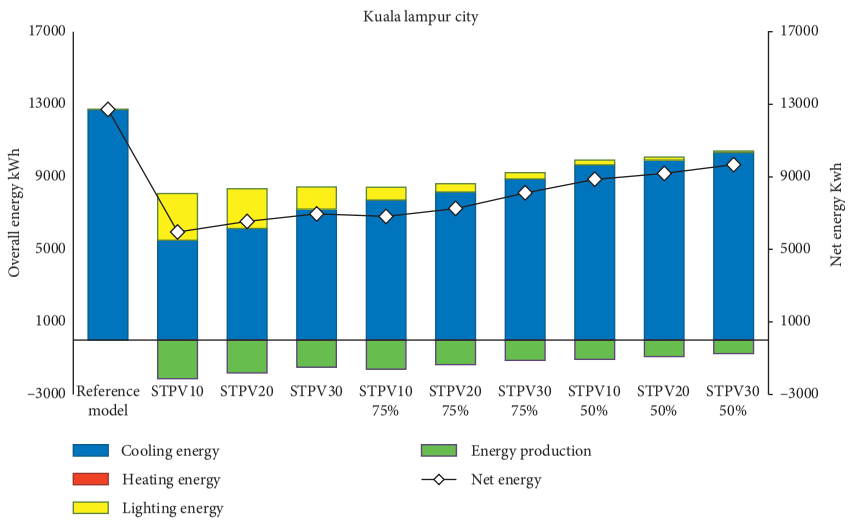	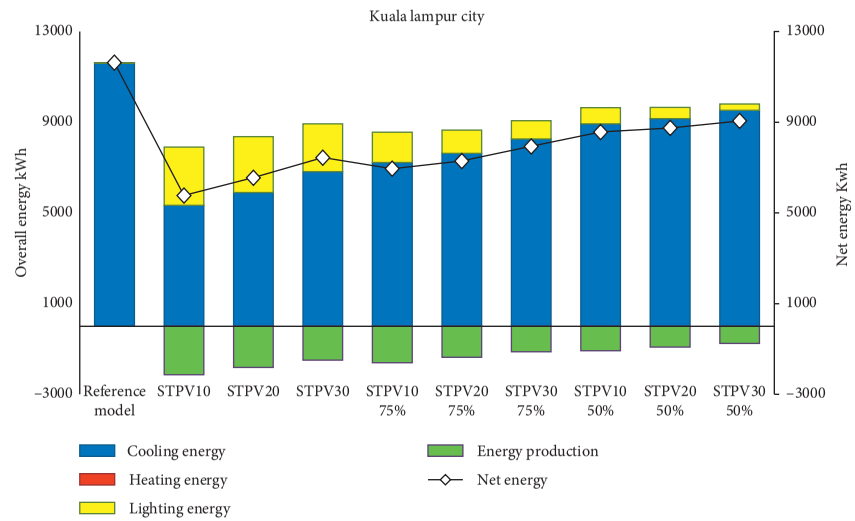
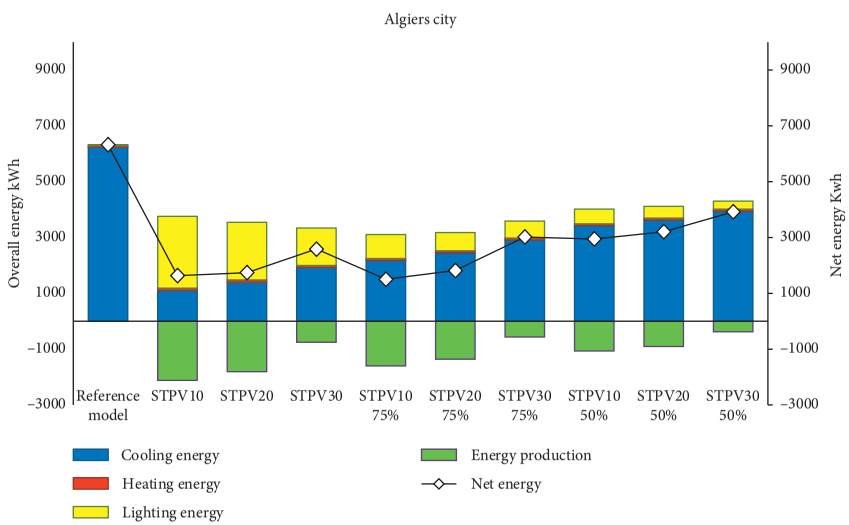	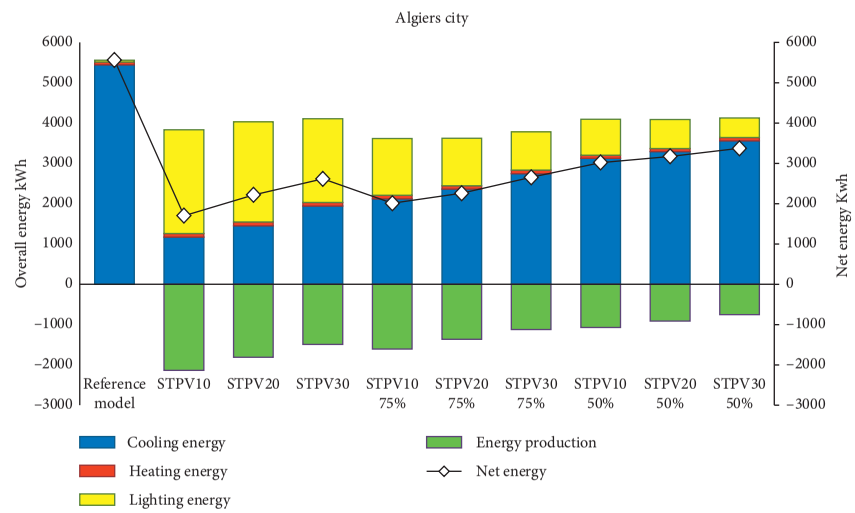

Table 9: DA300 lux distribution of fully glazed open office in cardinal orientations (Riyadh).

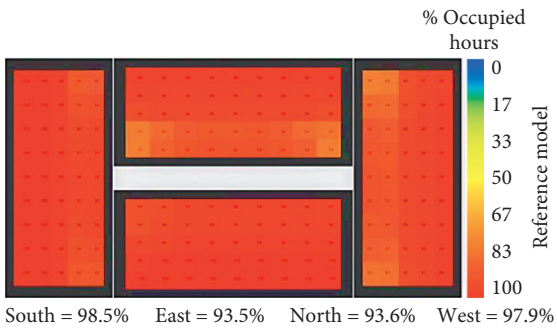 South = 98.5% East = 93.5% North = 93.6% West = 97.9% Reference model South = 98.5% East = 93.5% North = 93.6% West = 97.9%	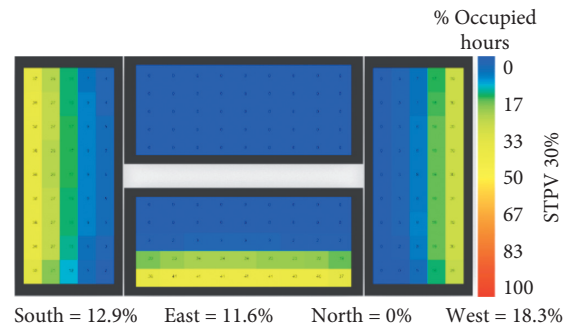 South = 12.9% East = 11.6% North = 0% West = 18.3% STPV 30% South = 12.9% East = 11.6% North = 0% West = 18.3%
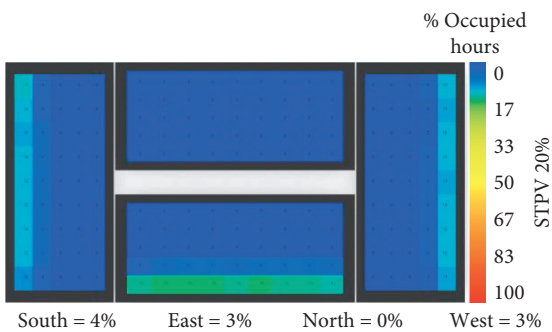 South = 4% East = 3% North = 0% West = 3% STPV 20% South = 4% East = 3% North = 0% West = 3%	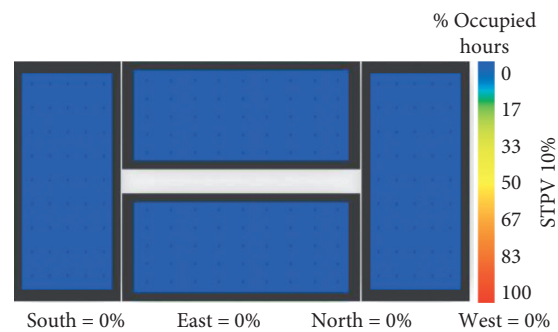 South = 0% East = 0% North = 0% West = 0% STPV 10% South = 0% East = 0% North = 0% West = 0%
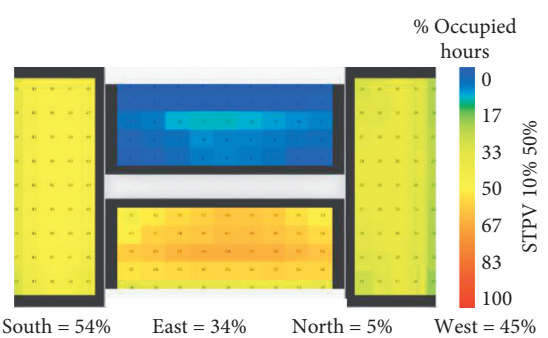 South = 54% East = 34% North = 5% West = 45% STPV 10% 50% South = 54% East = 34% North = 5% West = 45%	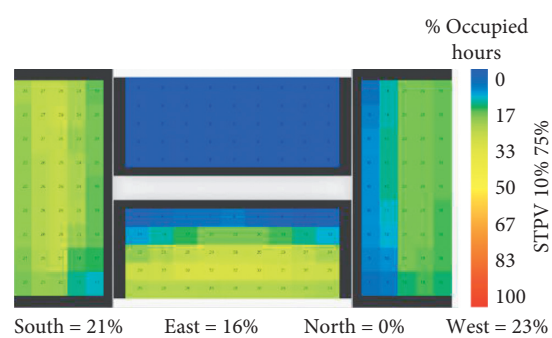 South = 21% East = 16% North = 0% West = 23% STPV 10% 75% South = 21% East = 16% North = 0% West = 23%
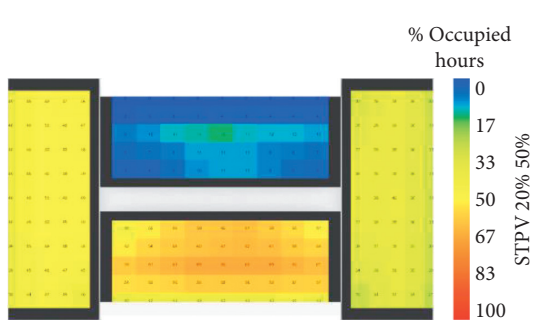 South = 55% East = 35% North = 6% West = 46% STPV 20% 50% South = 55% East = 35% North = 6% West = 46%	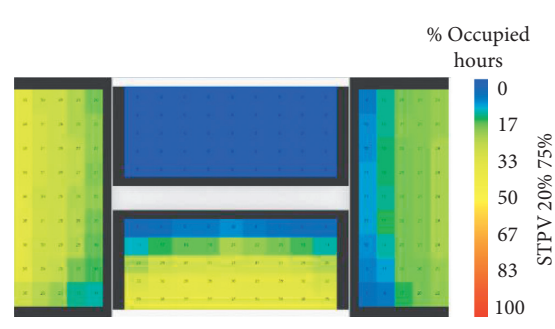 South = 26% East = 18% North = 0% West = 27% STPV 20% 75% South = 26% East = 18% North = 0% West = 27%

Table 9: Continued.

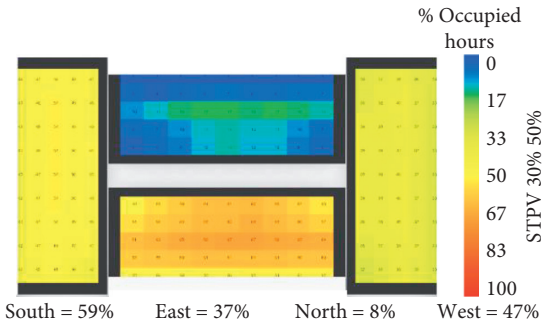	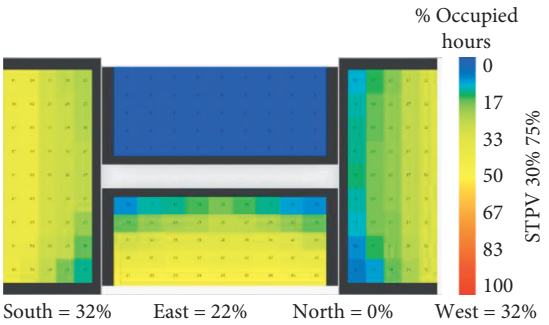
STPV 30% 50%	STPV 30%

Table 10: DA300 lux distribution of fully glazed open office in cardinal orientations (London).

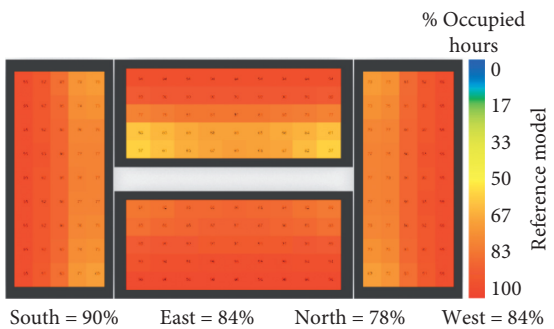	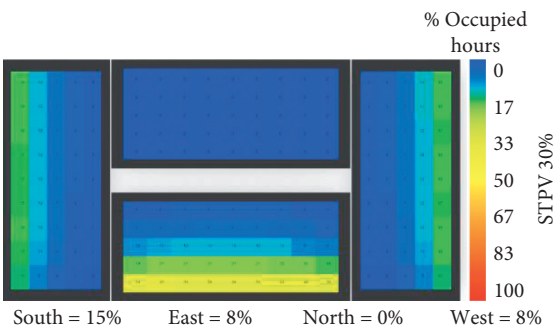
Reference model South = 90% East = 84% North = 78% West = 84%	STPV 30% South = 15% East = 8% North = 0% West = 8%
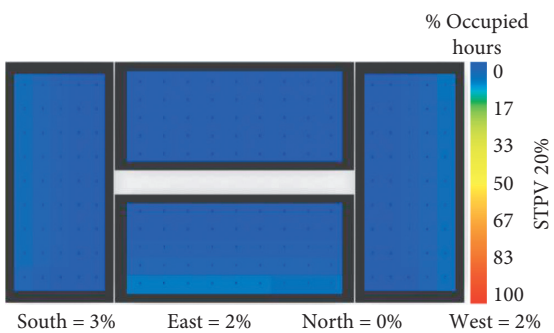	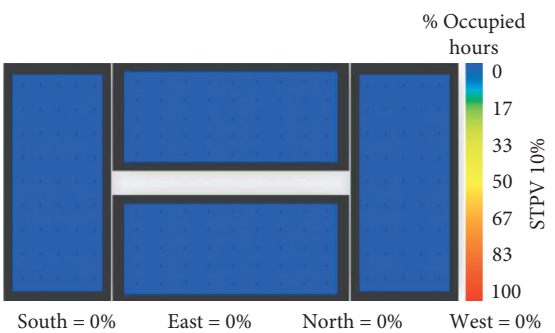
STPV 20% South = 3% East = 2% North = 0% West = 2%	STPV 10% South = 0% East = 0% North = 0% West = 0%
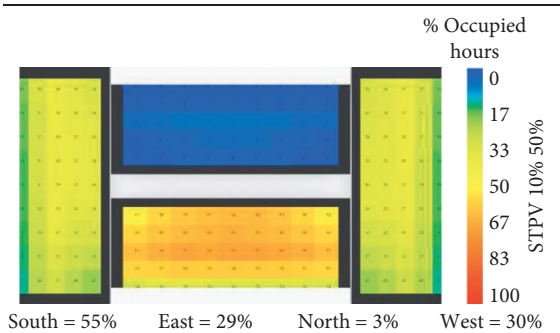	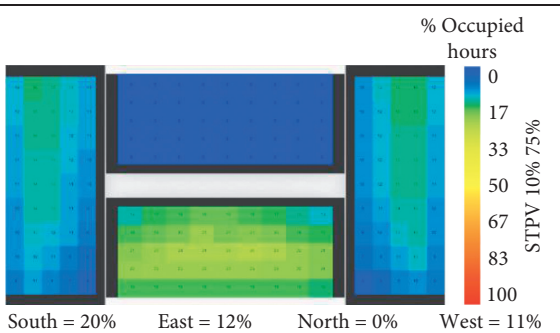
STPV 10% 50% South = 55% East = 29% North = 3% West = 30%	STPV10% 75% South = 20% East = 12% North = 0% West = 11%

Table 10: Continued.

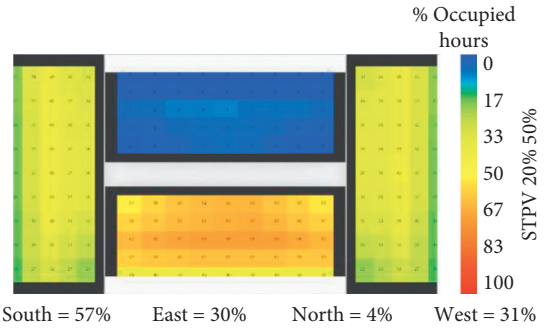 STPV 20% 50% South = 57% East = 30% North = 4% West = 31%	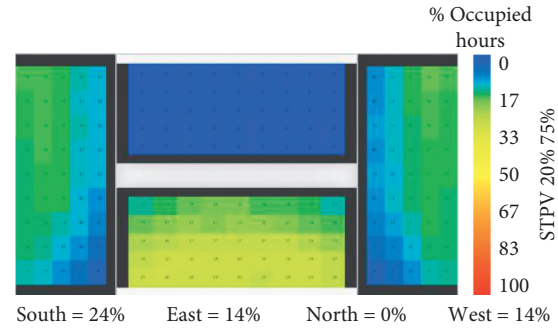 STPV20% 75% South = 24% East = 14% North = 0% West = 14%
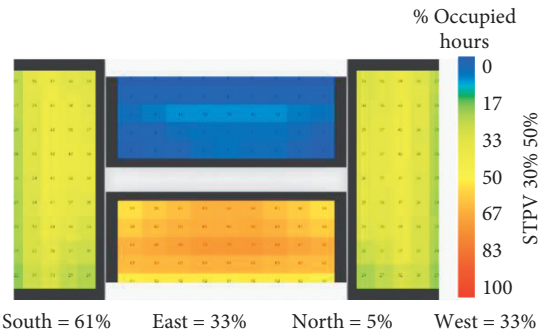 STPV 30% 50% South = 61% East = 33% North = 5% West = 33%	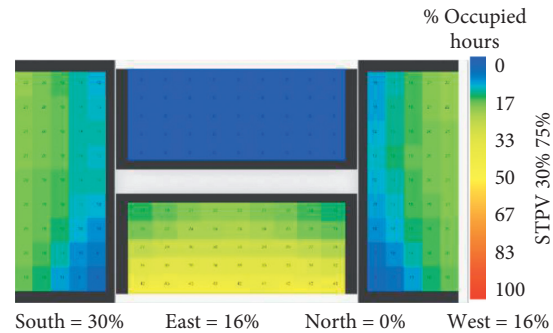 STPV 30% 75% South = 30% East = 16% North = 0% West = 16%

Table 11: DA300 lux distribution of fully glazed open office in cardinal orientations (Kuala Lumpur).

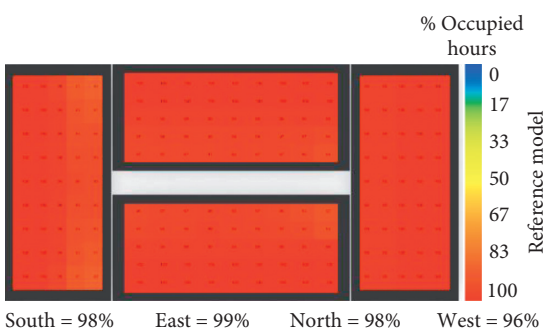 Reference model South = 98% East = 99% North = 98% West = 96%	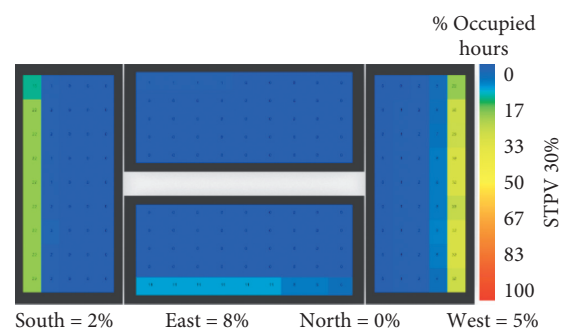 STPV 30% South = 2% East = 8% North = 0% West = 5%
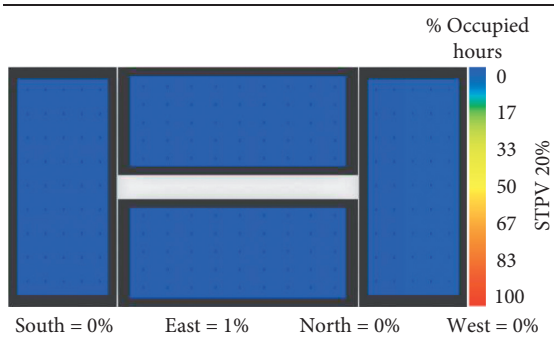 STPV 20% South = 0% East = 1% North = 0% West = 0%	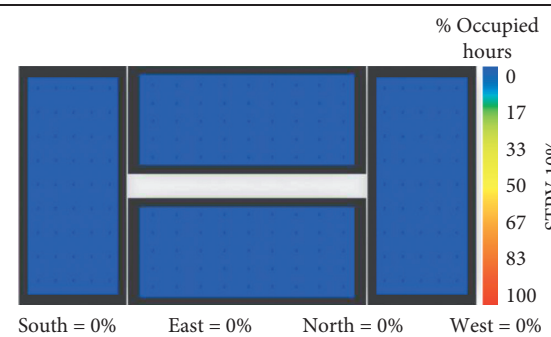 STPV10% South = 0% East = 0% North = 0% West = 0%

Table 11: Continued.

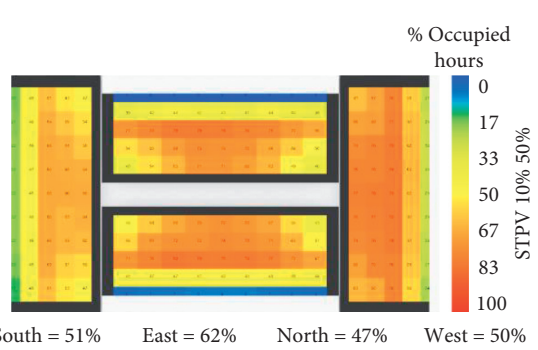	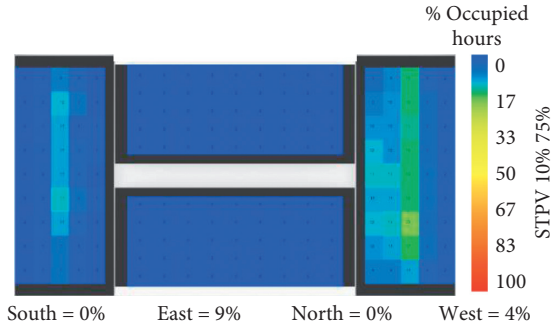
STPV 10% 50% South = 51% East = 62% North = 47% West = 50%	STPV 10% 75% South = 0% East = 9% North = 0% West = 4%
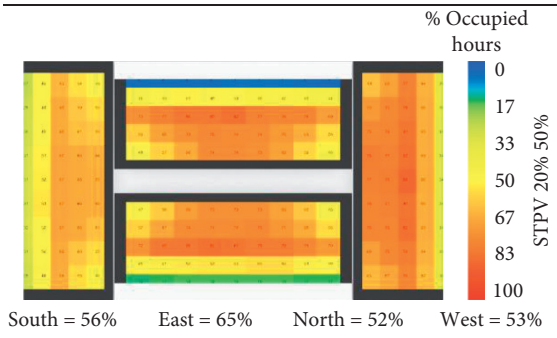	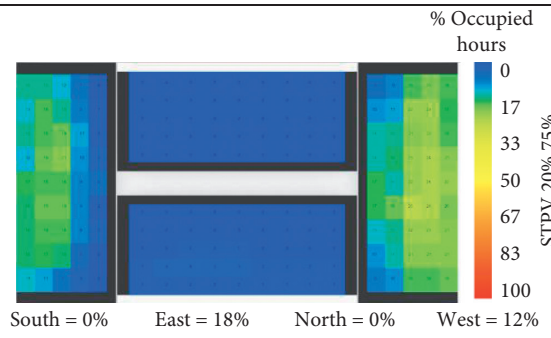
STPV 20% 50% South = 56% East = 65% North = 52% West = 53%	STPV 20% 75% South = 0% East = 18% North = 0% West = 12%
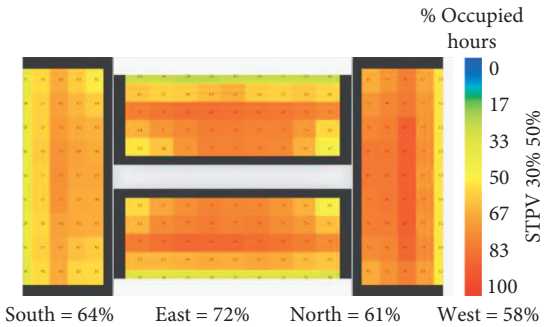	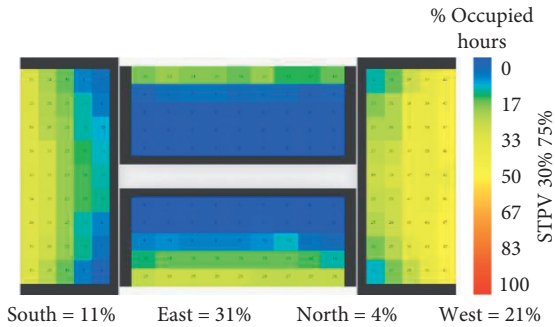
STPV 30% 50% South = 64% East = 72% North = 61% West = 58%	STPV 30% 75% South = 11% East = 31% North = 4% West = 21%

Table 12: DA300 lux distribution of fully glazed open office in cardinal orientations (Algiers).

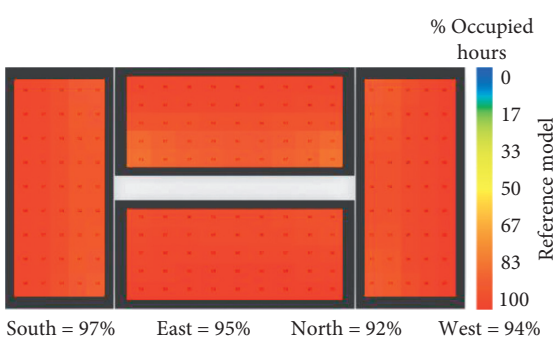	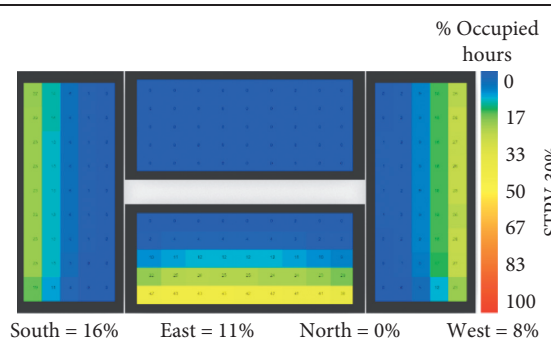
Reference model South = 97% East = 95% North = 92% West = 94%	STPV 30% South = 16% East = 11% North = 0% West = 8%

Table 12: Continued.

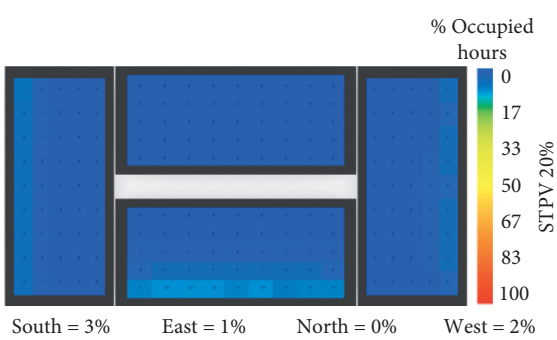	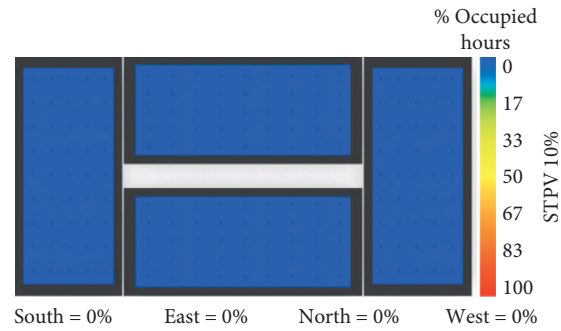
STPV 20% South = 3% East = 1% North = 0% West = 2%	STPV 10% South = 0% East = 0% North = 0% West = 0%
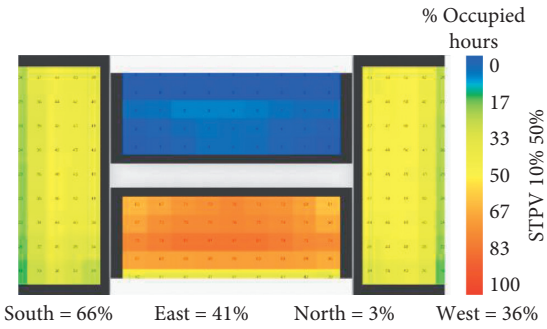	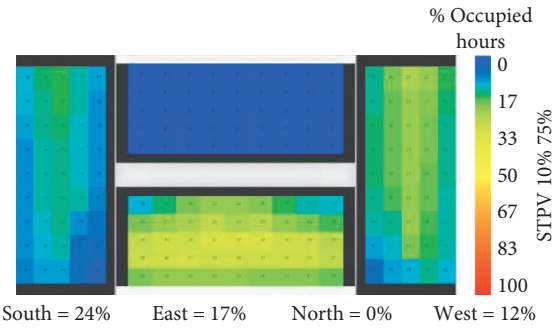
STPV 10% 50% South = 66% East = 41% North = 3% West = 36%	STPV 10% 75% South = 24% East = 17% North = 0% West = 12%
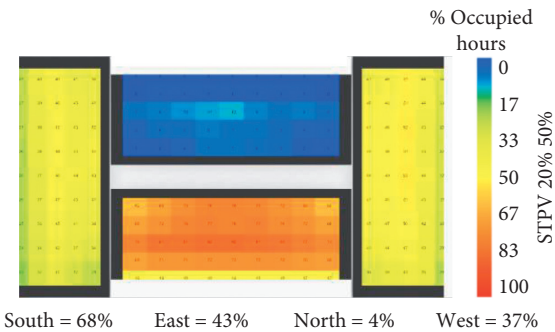	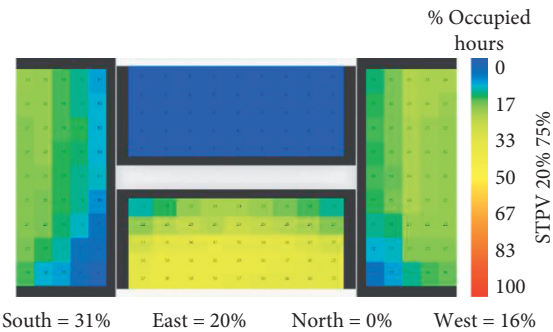
STPV 20% 50% South = 68% East = 43% North = 4% West = 37%	STPV20% 75% South = 31% East = 20% North = 0% West = 16%
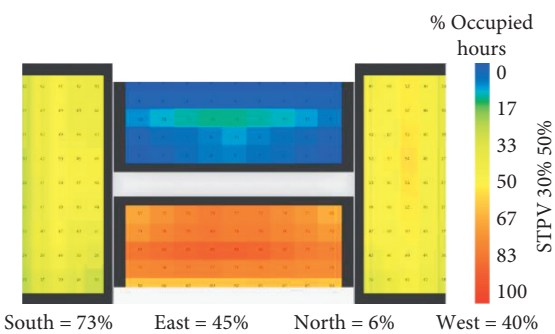	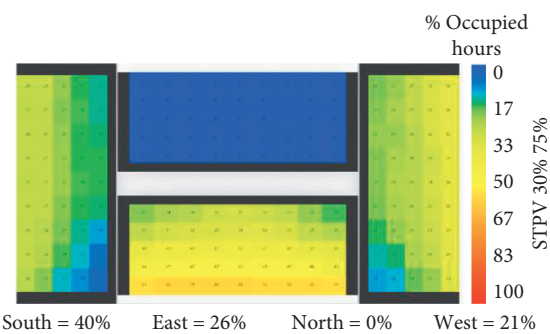
STPV 30% 50% South = 73% East = 45% North = 6% West = 40%	STPV 30% 75% South = 40% East = 26% North = 0% West = 21%

Table 13: UDI thresholds in cardinal orientations under clear sky condition (Riyadh city).

Orientation (Riyadh)	South	East	North	West	South	East	North	West	South	East	North	West
Configuration (STPV)	UDI <100				UDI 100–2000				UDI >2000			
R. model	0	0	0	0	75	82	99	73	25	18	1	27
STPV 10%	100	100	100	100	0	0	0	0	0	0	0	0
STPV 20%	88	89	100	82	12	11	0	18	0	0	0	0
STPV 30%	66	76	96	66	34	24	4	34	0	0	0	0
STPV 10% 75%	32	59	81	47	68	41	19	53	0	0	0	0
STPV 20% 75%	40	62	91	52	60	38	9	48	0	0	0	0
STPV 30% 75%	16	47	59	30	84	53	41	70	0	0	0	0
STPV 10% 50%	6	15	20	9	92	83	80	86	2	2	0	5
STPV 20% 50%	3	12	15	6	95	85	85	89	2	3	0	5
STPV 30% 50%	1	7	8	2	96	89	92	91	3	3	0	6

Table 14: UDI thresholds in cardinal orientations under overcast sky condition (London city).

Orientation (London)	South	East	North	West	South	East	North	West	South	East	North	West
Configuration (STPV)	UDI <100				UDI 100–2000				UDI >2000			
R. model	2	3	3	2	69	82	96	83	28	15	0	15
STPV 10%	100	100	100	100	0	0	0	0	0	0	0	0
STPV 20%	86	92	100	92	14	8	0	8	0	0	0	0
STPV 30%	62	78	97	78	38	22	3	22	0	0	0	0
STPV 10% 75%	37	65	95	64	62	35	5	35	1	0	0	0
STPV 20% 75%	31	59	89	57	69	41	11	42	0	0	0	0
STPV 30% 75%	25	49	73	48	74	51	27	52	1	0	0	0
STPV 10% 50%	12	21	32	21	84	76	68	77	4	3	0	3
STPV 20% 50%	11	19	27	18	85	79	73	80	4	3	0	2
STPV 30% 50%	9	14	20	14	86	83	80	83	5	3	0	0

Table 15: UDI thresholds in cardinal orientations under intermediate sky condition (Kuala Lumpur city).

Orientation (Kuala Lumpur)	South	East	North	West	South	East	North	West	South	East	North	West
Configuration (STPV)	UDI <100				UDI 100–2000				UDI >2000			
R. model	0	0	0	0	85	76	88	82	15	24	12	18
STPV 10%	100	100	100	100	0	0	0	0	0	0	0	0
STPV 20%	100	93	100	96	0	7	0	4	0	0	0	0
STPV 30%	71	55	75	70	29	45	25	30	0	0	0	0
STPV 10% 75%	32	25	34	39	68	74	66	61	0	1	0	0
STPV 20% 75%	16	14	19	27	84	85	81	73	0	1	0	0
STPV 30% 75%	8	3	8	15	92	97	92	85	0	0	0	0
STPV 10% 50%	3	2	3	6	97	97	97	94	0	1	0	0
STPV 20% 50%	2	0	2	4	98	99	98	96	0	1	0	0
STPV 30% 50%	1	0	1	2	99	99	99	98	0	1	0	0

Table 16: UDI thresholds in cardinal orientations under CEI clear sky condition (Algiers city).

Orientation (Algiers)	South	East	North	West	South	East	North	West	South	East	North	West
Configuration (STPV)	UDI <100				UDI 100–2000				UDI >2000			
R. model	1	1	1	1	66	78	99	82	33	11	0	17
STPV 10%	100	100	100	100	0	0	0	0	0	0	0	0
STPV 20%	85	89	100	92	15	10	0	8	0	1	0	0
STPV 30%	54	69	97	75	46	30	3	25	0	1	0	0
STPV 10% 75%	24	53	94	58	76	47	6	42	0	0	0	0
STPV 20% 75%	15	46	84	50	85	53	16	50	0	1	0	0
STPV 30% 75%	7	30	50	30	93	69	50	70	0	1	0	0
STPV 10% 50%	4	11	13	13	93	87	86	86	3	2	0	1
STPV 20% 50%	3	9	14	10	93	89	86	89	4	2	0	1
STPV 30% 50%	3	5	8	5	93	93	92	93	4	2	0	1

Table 17: DGP in cardinal orientation of reference model open-office buildings in different cities.

Reference model	Annual DGP east facade (Riyadh)	Annual DGP south facade (Riyadh)	Annual DGP west facade (Riyadh)
	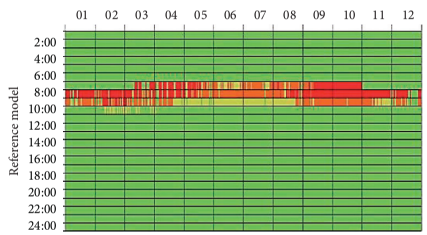	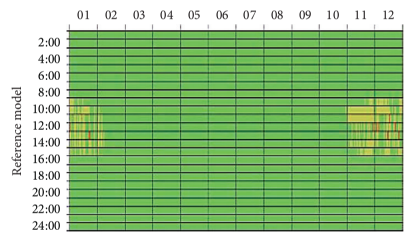	
Optimum model	Annual DGP east facade (Riyadh)	Annual DGP south facade (Riyadh)	Annual DGP west facade (Riyadh)
	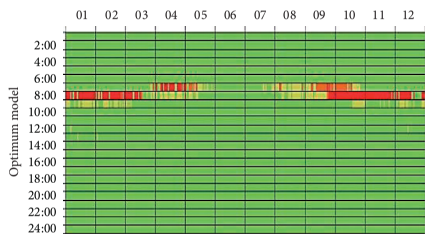	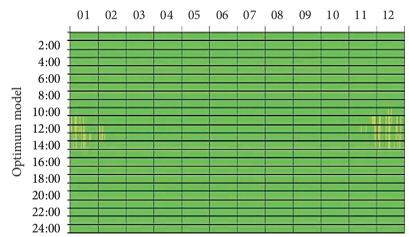	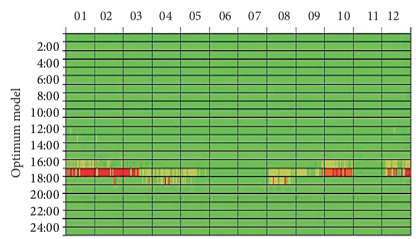
Reference model	Annual DGP east facade (London)	Annual DGP south facade (London)	Annual DGP west facade (London)
	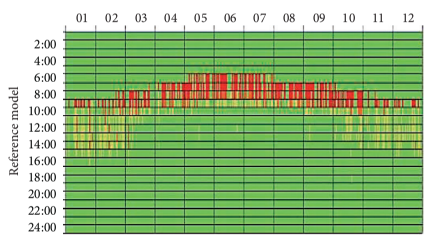	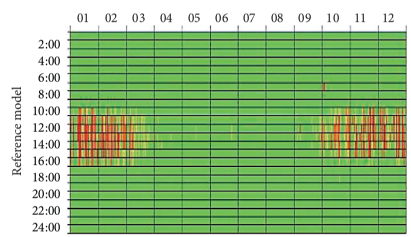	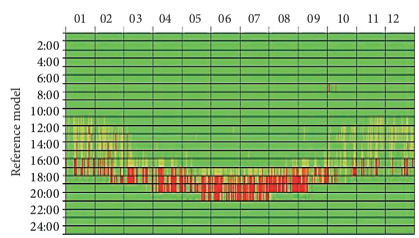
Optimum model	Annual DGP east facade (London)	Annual DGP south facade (London)	Annual DGP west facade (London)
	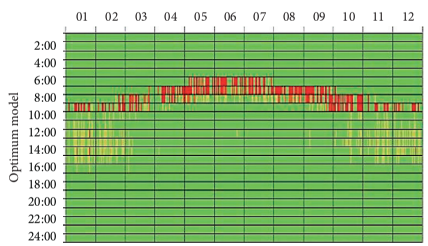	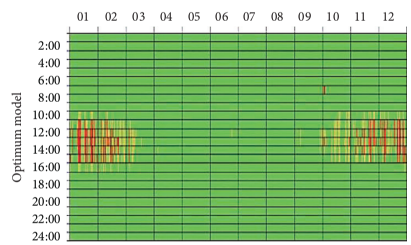	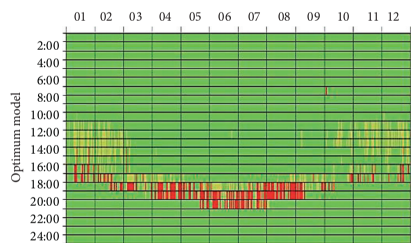

Table 17: Continued.

Reference model	Annual DGP east facade (KL)	Annual DGP south facade (KL)	Annual DGP west facade (KL)
	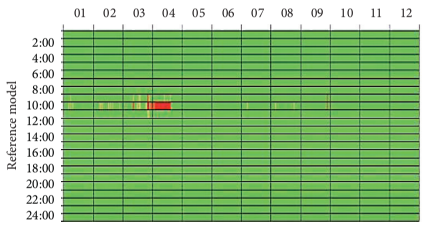	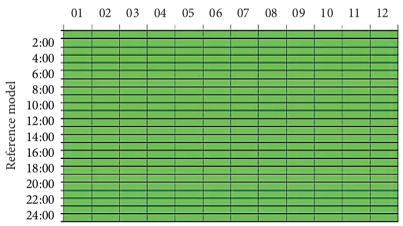	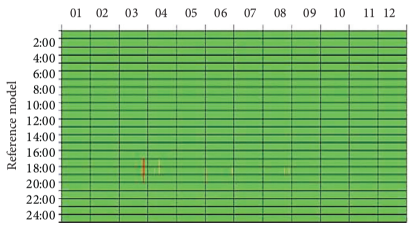
Optimum model	Annual DGP east facade (KL)	Annual DGP south façade (KL)	Annual DGP west façade (KL)
	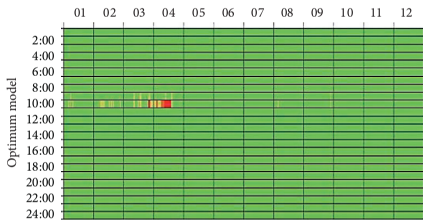	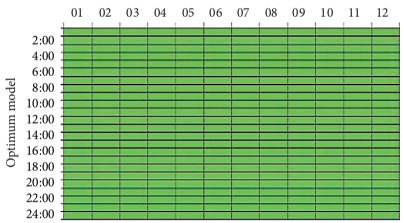	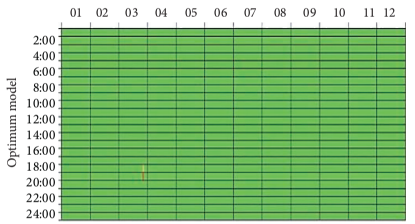
Reference model	Annual DGP east facade (Algiers)	Annual DGP south facade (Algiers)	Annual DGP west facade (Algiers)
	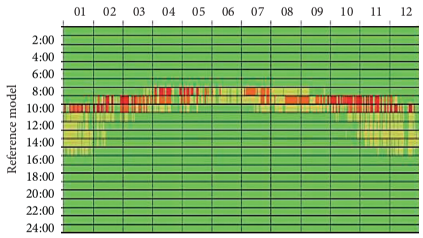	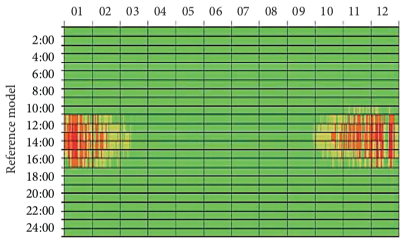	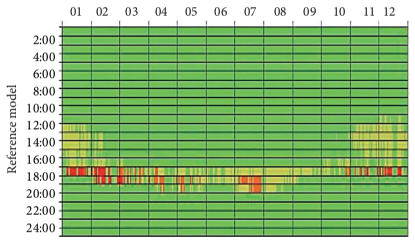
Optimum model	Annual DGP east facade (Algiers)	Annual DGP south facade (Algiers)	Annual DGP west facade (Algiers)
		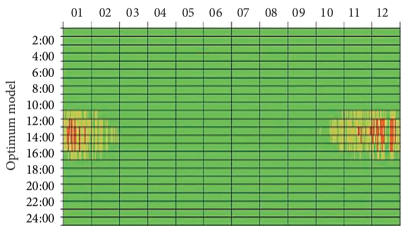	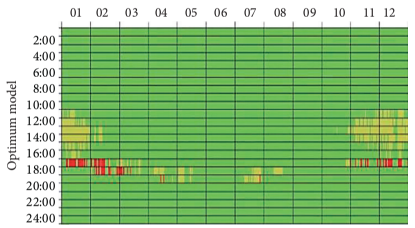
Legend		Intolerable glare, DGP > 0.45 Disturbing glare, 0.45 > DGP > 0.4	Perceptible glare, 0.45 > DGP > 0.4 Imperceptible glare 0.45 > DGP > 0.4

Table 18: The maximum and optimum energy saving percentages of STPV combined with ILS configurations in different climates regions.

Configurations	Riyadh city				London city				Kuala Lumpur city				Algiers city			
	South	East	North	West	South	East	North	West	South	East	North	West	South	East	North	West
STPV 10%	0.53	0.69	0.15	**0.52**	−0.14	0.67	−0.24	0.50	0.30	**0.53**	0.22	**0.50**	0.62	**0.74**	0.12	**0.69**
STPV 20%	0.49	0.64	0.13	0.45	−0.15	0.64	−0.25	0.41	0.27	0.49	0.20	0.44	0.56	0.72	0.08	0.60
STPV 30%	0.46	0.63	0.11	0.40	−0.10	0.72	−0.23	0.35	0.24	0.45	0.18	0.36	0.52	0.59	0.06	0.53
STPV 10% 75%	**0.85**	**0.69**	0.72	0.23	**0.93**	**0.83**	0.74	**0.54**	**0.72**	0.46	**0.67**	0.40	**0.87**	0.76	**0.64**	0.64
STPV 20% 75%	0.83	0.63	**0.72**	0.20	0.89	0.77	0.76	0.51	0.70	0.43	0.66	0.37	0.83	0.71	0.64	0.59
STPV 30% 75%	0.78	0.55	0.70	0.18	0.83	0.68	0.75	0.44	0.67	0.36	0.63	0.32	0.75	0.52	0.63	0.52
STPV 10% 50%	**0.76**	**0.49**	0.68	**0.35**	**0.83**	**0.62**	0.76	0.41	**0.65**	**0.30**	**0.61**	**0.26**	**0.70**	**0.53**	0.58	**0.46**
STPV 20% 50%	0.74	0.44	0.68	0.31	0.80	0.57	0.76	0.39	0.64	0.28	0.61	0.25	0.66	0.49	0.59	0.43
STPV 30% 50%	0.71	0.38	**0.68**	0.27	0.77	0.50	**0.79**	0.37	0.62	0.24	0.60	0.22	0.61	0.38	**0.60**	0.39

Optimum performance of STPV configurations (maximum energy saving + visual comfort)
Maximum energy saving of STPV configurations

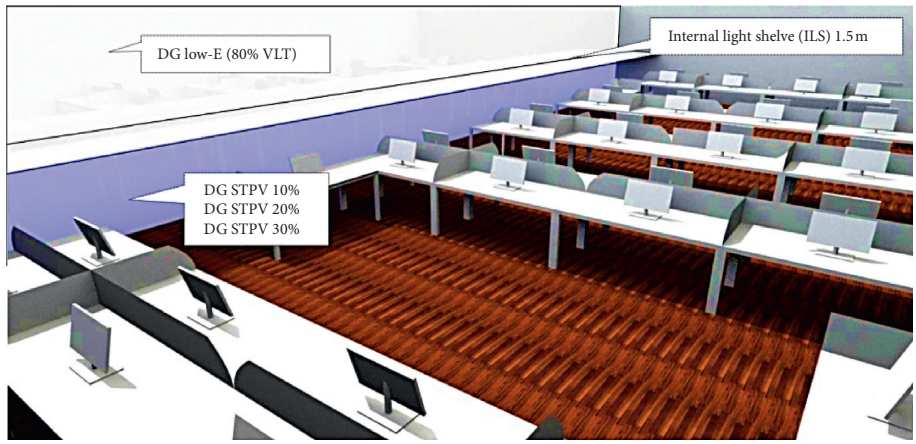

Figure 3: Optimum STPV and ILS configurations.

optimum configuration eliminates intolerable glare from an imperceptible glare state in the summer season in cardinal orientation due to the usage of ILS that reflects the direct sunlight to the center and back area of the office. Furthermore, it provides a significant improvement of reducing glare states, in particular in southern orientations.

3.4. Energy Saving Evaluation. The largest potential of maximum and optimum percentage savings that can be attained by integrating nine STPV glazing combined with and without ILS compared of employing the reference model (see the base model) in cardinal alignments within four different cities can be seen in Table 18. The table showcases inconsistent savings in an approximate range of 6% to 93%, and, in some cases, the result was negative (no-savings) compared to the base model. A significant percentage of savings was achieved in the southern orientation by using STPV10 75%, whose maximum energy savings were estimated to be 85%, 93%, 72%, and 87%, due to receiving the maximum solar energy, high conversion efficiency compared with other STPV modules and the important role of ILS that reduce the control the distribution of light in deep office which offers reduction in lighting and cooling energy. Nevertheless, the lowest saving achieved in the northern orientation by using the first group (fully STPV) had a negative percentage in London city. The integration of STPV10% in east-west axis shows the highest saving percentages because of the low performance of ILS in these orientations. The optimum performance of both axes obtained with the third group (STPV10 75%) is explained by the failure to fulfil the visual comfort conditions in particular the first group.

4. Conclusions

A comprehensive investigation was carried out in this study to evaluate the net energy and visual comfort of STPV configurations combined with and without ILS compared to a reference model of an open-office building in different climate regions. The key findings of this study are as follows:

(i) In hot regions, the integration of DG-STPV (first group) instead of DG-clear glazing can effectively reduce cooling energy consumption. Conversely, it increases the heating energy in a temperate climate region (London) mainly due to the thermal properties of DG-STPV, especially in south-north axis.

(ii) The first and second group configurations did not provide sufficient daylight to the office. But the third group configurations meet the visual comfort requirements (DA300 lux, UDI100 lux–2000 lux) and eliminate a significant portion of glare in all climates

because of the adoption of ILS that reflects and balances the quantity of illuminance in the centre and back daylit areas.

(iii) The maximum performance in terms of overall energy is achieved by means of the second group in the south-north axis, with the first group in the east-west axis including all transparencies. As depicted in Table 17, the optimum performance of both axes obtained with the third group is explained by the failure to fulfil the conditions for visual comfort for the first group, as presented in Figure 3. The energy produced by a-Si modules with 50% of the total glazing area can compensate the lighting energy consumption. Thus, a significant percentage of saving was achieved by the south-north axis: 76% to 68%, 83% to 79%, 65% to 61%, and 70% to 60%. This is higher than the east-west axis: 49% to 35%, 62% to 54%, 30% to 26%, and 53% to 46% in Riyadh, London, Kuala Lumpur, and Algiers, respectively.

Overall, these outcomes give a vision of the correlation between the net energy visual comforts related to the spatial distribution of STPVs and clear glazing configurations combined with ILS in various climates. Also its adoption offers a range of benefits for the carbon footprint within buildings and develops design strategies that seek to balance implemention of STPV window and ILS with the improvements in energy efficiency and luminous environment aspects. Further studies need to evaluate the impact of internal dynamic shading devices and any STPV technology in terms of thermooptical properties and high conversion efficiency with various sizing. Eventually, the potential of applying STPVs combined with ILS has a substantial influence to provide better visual comfort and save energy in open-office buildings.

Data Availability

The data used in the study can be made available upon sending request to the corresponding author.

Conflicts of Interest

The authors declare that there are no conflicts of interest regarding the publication of this paper.

Acknowledgments

This research has been funded from Research Deanship in University of Ha'il, Saudi Arabia, through Project no. RG-20 105.

References

[1] Y. Cheng, M. Gao, J. Dong, J. Jia, X. Zhao, and G. Li, "Investigation on the daylight and overall energy performance of semi-transparent photovoltaic facades in cold climatic regions of China," *Applied Energy*, vol. 232, pp. 517–526, 2018.

[2] K. Konis, "Evaluating daylighting effectiveness and occupant visual comfort in a side-lit open-plan office building in San Francisco, California," *Building and Environment*, vol. 59, pp. 662–677, 2013.

[3] A. Ghosh and B. Norton, "Advances in switchable and highly insulating autonomous (self-powered) glazing systems for adaptive low energy buildings," *Renewable Energy*, vol. 126, pp. 1003–1031, 2018.

[4] I. L. Wong, "A review of daylighting design and implementation in buildings," *Renewable and Sustainable Energy Reviews*, vol. 74, pp. 959–968, 2017.

[5] A. A. Y. Freewan and J. A. Al Dalala, "Assessment of daylight performance of advanced daylighting strategies in large University classrooms; case study classrooms at JUST," *Alexandria Engineering Journal*, vol. 59, no. 2, pp. 791–802, 2020.

[6] A. Mesloub and A. Ghosh, "Daylighting performance of light shelf photovoltaics (LSPV) for office buildings in hot desert-like regions," *Applied Sciences*, vol. 10, no. 22, p. 7959, 2020.

[7] A. Kontadakis, A. Tsangrassoulis, L. Doulos, and S. C. Zerefos, "A review of light shelf designs for daylit environments," *Sustainability*, vol. 10, no. 1, p. 71, 2018.

[8] H. Lee, S. Park, and J. Seo, "Development and performance evaluation of light shelves using width-adjustable reflectors," *Advances in Civil Engineering*, vol. 2018, Article ID 2028065, 9 pages, 2018.

[9] A. Ghosh, "Potential of building integrated and attached/applied photovoltaic (BIPV/BAPV) for adaptive less energy-hungry building's skin: a comprehensive review," *Journal of Cleaner Production*, vol. 276, Article ID 123343, 2020.

[10] B. Joseph, T. Pogrebnaya, and B. Kichonge, "Semitransparent building-integrated photovoltaic: review on energy performance, challenges, and future potential," *International Journal of Photoenergy*, vol. 2019, Article ID 5214150, 17 pages, 2019.

[11] H. Alrashidi, W. Issa, N. Sellami, A. Ghosh, T. K. Mallick, and S. Sundaram, "Performance assessment of cadmium telluride-based semi-transparent glazing for power saving in façade buildings," *Energy and Buildings*, vol. 215, Article ID 109585, 2020.

[12] Y. Hamakawa, *Thin-Film Solar Cells: Next Generation Photovoltaics and Its Applications*, Vol. 13, Springer Science & Business Media, Berlin, Germany, 2013.

[13] A. Shah, "Thin-film silicon solar cells," in *McEvoy's Handbook of Photovoltaics*, pp. 235–307, Elsevier, Amsterdam, Netherlands, 3rd edition, 2017.

[14] A. Roy, A. Ghosh, S. Bhandari, P. Selvaraj, S. Sundaram, and T. K. Mallick, "Color comfort evaluation of dye-sensitized solar cell (DSSC) based building-integrated photovoltaic (BIPV) glazing after 2 years of ambient exposure," *The Journal of Physical Chemistry C*, vol. 123, no. 39, pp. 23834–23837, 2019.

[15] S. Bhandari, A. Roy, and A. Ghosh, T. K. Mallick, S. Sundaram, "Perceiving the temperature coefficient of carbonased perovskite solar cells," *Sustainable Energy & Fuels*, vol. 4, 2020.

[16] A. Ghosh, S. Bhandari, S. Sundaram, and T. K. Mallick, "Carbon counter electrode mesoscopic ambient processed & characterised perovskite for adaptive BIPV fenestration," *Renewable Energy*, vol. 145, pp. 2151–2158, 2020.

[17] Laboratory NREL, *Champion Photovoltaic Module Efficiency Chart*, NREL, Washington, D.C, USA, 2020.

[18] A. N. Özakın, S. Karsli, F. Kaya, and H. Güllüce, "The heat recovery with heat transfer methods from solar photovoltaic systems," in *Journal of Physics: Conference Series*vol. 707, no. 1, IOP Publishing, Article ID 012050, 2016.

[19] C. Kurayama, "Development of a measurement system for SHGC and U-value: study on SHGC and U-value for fenestration and shading system part 1," *Journal of Environmental Engineering (Transactions of AIJ)*, vol. 71, no. 604, pp. 15–22, 2006.

[20] P. Orouji, A. Vakili, M. K. Behrouz et al., "Methodology of standardizing the energy labeling and rating of window fenestration in Iran," *Sustainable Energy Technologies and Assessments*, vol. 33, pp. 24–33, 2019.

[21] T. Y. Y. Fung and H. Yang, "Study on thermal performance of semi-transparent building-integrated photovoltaic glazings," *Energy and Buildings*, vol. 40, no. 3, pp. 341–350, 2008.

[22] W. He, Y. X. Zhang, W. Sun, J. X. Hou, Q. Y. Jiang, and J. Ji, "Experimental and numerical investigation on the performance of amorphous silicon photovoltaics window in East China," *Building and Environment*, vol. 46, no. 2, pp. 363–369, 2011.

[23] E. L. Didoné and A. Wagner, "Semi-transparent PV windows: a study for office buildings in Brazil," *Energy and Buildings*, vol. 67, pp. 136–142, 2013.

[24] P. K. Ng, N. Mithraratne, and H. W. Kua, "Energy analysis of semi-transparent BIPV in Singapore buildings," *Energy and Buildings*, vol. 66, pp. 274–281, 2013.

[25] A. Mesloub, G. A. Albaqawy, and M. Z. Kandar, "The optimum performance of building integrated photovoltaic (BIPV) windows under a semi-arid climate in Algerian office buildings," *Sustainability*, vol. 12, no. 4, p. 1654, 2020.

[26] L. Olivieri, E. Caamaño-Martin, F. Olivieri, and J. Neila, "Integral energy performance characterization of semi-transparent photovoltaic elements for building integration under real operation conditions," *Energy and Buildings*, vol. 68, pp. 280–291, 2014.

[27] Y. Huang, J.-L. Niu, and T.-M. Chung, "Comprehensive analysis on thermal and daylighting performance of glazing and shading designs on office building envelope in cooling-dominant climates," *Applied Energy*, vol. 134, pp. 215–228, 2014.

[28] K. Kapsis, V. Dermardiros, and A. K. Athienitis, "Daylight performance of perimeter office façades utilizing semi-transparent photovoltaic windows: a simulation study," *Energy Procedia*, vol. 78, pp. 334–339, 2015.

[29] K. Kapsis and A. K. Athienitis, "Building integrated semi-transparent photovoltaics: energy and daylighting performance," in *Photonics North 2011*SPIE, Bellingham, USA, 2011.

[30] Z. Li, L. Wang, and H. Zhang, "Research on the lighting environment using photovoltaic glass in office space—a case study in Tianjin," *China Illuminating Engineering Journal*, vol. 1, pp. 23–28, 2015.

[31] M. Abdelhakim, Y.-W. Lim, and M. Z. Kandar, "Optimum glazing configurations for visual performance in Algerian classrooms under mediterranean climate," *Journal of Daylighting*, vol. 6, no. 1, pp. 11–22, 2019.

[32] G. Chinazzo, A. Legrain, G. Peronato, J. Wienold, and M. Andersen, "Energy performance and occupancy-based analysis of visual and thermal comfort for transmittance level and layout variations of semi-transparent photovoltaics," in *Proceedings of the 16th IBPSA International Conference and Exhibition*, Rome, Italy, September 2019.

[33] Y. Sun, K. Shanks, H. Baig et al., "Integrated semi-transparent cadmium telluride photovoltaic glazing into windows: energy and daylight performance for different architecture designs," *Applied Energy*, vol. 231, pp. 972–984, 2018.

[34] A. McNeil, E. S. Lee, and J. C. Jonsson, "Daylight performance of a microstructured prismatic window film in deep open plan offices," *Building and Environment*, vol. 113, pp. 280–297, 2017.

[35] W. Zhang and L. Lu, "Overall energy assessment of semi-transparent photovoltaic insulated glass units for building integration under different climate conditions," *Renewable Energy*, vol. 134, pp. 818–827, 2019.

[36] M. Abdelhakim, M. Z. Kandar, M. Zin Kandar, and Y.-W. Lim, "Experimental investigation of overall energy performance in Algerian office building integrated photovoltaic window under semi-arid climate," *Journal of Daylighting*, vol. 6, no. 1, pp. 23–41, 2019.

[37] K. R. Wagiman, M. N. Abdullah, M. Y. Hassan, and N. H. M. Radzi, "A new optimal light sensor placement method of an indoor lighting control system for improving energy performance and visual comfort," *Journal of Building Engineering*, vol. 30, Article ID 101295, 2020.

[38] C. Reinhart and P.-F. Breton, "Experimental validation of autodesk® 3ds max® design 2009 and daysim 3.0," *LEUKOS The Journal of the Illuminating Engineering Society of North America*, vol. 6, pp. 7–35, 2009.

[39] A. F. Alajmi, F. Abaalkhail, and A. Alanezi, "Climate-based daylighting metrics assessment to select among optimum energy efficient windows' shading devices solutions: a case study of an office in a hot climate," in *Proceedings of the 16th IBPSA International Conference and Exhibition*.

[40] S. Nundy and A. Ghosh, "Thermal and visual comfort analysis of adaptive vacuum integrated switchable suspended particle device window for temperate climate," *Renewable Energy*, vol. 156, pp. 1361–1372, 2020.

[41] Y. Sun, X. Liu, W. Qu, G. Cao, and N. Zou, "Analysis of daylight glare and optimal lighting design for comfortable office lighting," *Optik*, vol. 206, Article ID 164291, 2020.